The use of single foraminiferal shells for recording seasonal temperatures and water column stratification and its applicability to the fossil record

Dissertation zur Erlangung des akademischen Grades eines Doktors der Naturwissenschaften

Dr. rer. nat.

am Fachbereich 5 (Geowissenschaften) der Universität Bremen

Tim Haarmann

Bremen, 2012

Gutachter der Dissertation:

Prof. Dr. Gerold Wefer

Prof. Dr. Geert-Jan Brummer

Tag des Dissertationskolloquiums:

19. Dezember 2012 um 16 Uhr c.t. im MARUM, Raum 2070

ERKLÄRUNG

Name: Tim Haarmann **Datum**: 02. April 2012

Anschrift: Moselstraße 18, 28199 Bremen

Hiermit versichere ich an Eides statt, dass ich

1. Die Arbeit ohne unerlaubte fremde Hilfe angefertigt habe
2. keine anderen als die von mir angegebenen Quellen und Hilfsmittel benutzt habe und
3. die den benutzten Werken wörtlich oder inhaltlich entnommenen Stellen als solche kenntlich gemacht habe

---

Bremen, 02. April 2012

Tim Haarmann
(Unterschrift)

ACKNOWLEDGEMENTS

First of all, I wish to thank Prof. Dr. Gerold Wefer and Dr. Torsten Bickert who gave me the chance to carry out this PhD project. They have constantly been interested in the progress of my PhD project and shared their great scientific knowledge with me. They encouraged me to participate in several conferences, from which I benefited a lot. I am very grateful to Torsten for always taking the time for discussions and advice.

A great thank you goes to my co-supervisor Dr. Gerald Ganssen, head of the cluster Earth & Climate at the Faculty of Earth Sciences of the Vrije Universiteit Amsterdam. During my abroad stay in Amsterdam, Gerald and Dr. Frank Peeters took a lot of time for discussions and advice and introduced me to the analysis of oxygen isotopes from single foraminiferal shells. For her laboratory assistance during my time in Amsterdam, I wish to thank Suzanne Verdegaal a lot.

It is almost impossible to thank all the people that helped me in the daily work and who shared their expertise with me during these years. I am especially grateful to Dr. Ed Hathorne, who introduced me into the *Marum flow-through* cleaning device and who was a great help in tackling all problems that had to be overcome in order to get the system properly running. For their technical support, I acknowledge Matthias Lange and Wolfgang Schunn. Dr. Mahyar Mohtadi, Dr. Jeroen Groeneveld and Dr. Stephan Steinke took a lot of time for discussions, assisted me with writing and introduced me into many aspects of foraminiferal analysis. Their help was absolutely priceless. For laboratory assistance, I want to express my gratitude to Heike Anders and Petra Witte.

My family, friends and office mates have constantly encouraged me during these years. I especially want to thank Anna Kloss, Francesca Vallé and Rony Küchler for the great time in the office.

I thank the Center for Marine Environmental Sciences (MARUM) for the sample collection and technical support. The Deutsche Forschungsgemeinschaft (DFG) is gratefully acknowledged for supporting me with a scholarship within the International Graduate College EUROPROX. For organizing regular EUROPROX “coffee & science” meetings, I wish to thank Dr. Dorothee Wilhelms-Dick and Dr. Cletus Itambi.

ABSTRACT

Mg/Ca- and oxygen isotope ratios in the shells of planktic foraminifera are widely used in paleoceanographic studies for the reconstruction of water temperatures. Standard investigations analyze multiple shells of a species at once. However, when single shells are analyzed, substantial differences of the Mg/Ca- and oxygen isotope ratios are found. These are explained by seasonality and natural variability, and are increasingly used for the reconstruction of past environmental conditions. The present thesis analyzes the differences of the Mg/Ca- and oxygen isotope ratios between individual shells in the upwelling region off Northwest-Africa. The aim of this thesis is to quantify natural variability, to improve the applicability of single shells for the reconstruction of temperature seasonality and to show the potential of single specimens for recording past ocean stratification.

In the present thesis, calcification temperatures are calculated from the Mg/Ca ratios in single shells of the surface-dwelling planktic foraminifera *Globigerinoides ruber* (pink), *Globigerinoides ruber* (white) and the deep-dwelling species *Globorotalia inflata*, collected from a sediment trap off Northwest-Africa at 20°45.6'N, 18°41.9'W (**Manuscript I**). Single shells of *G. ruber* (pink) showed substantially different Mg/Ca temperatures linked to the seasonal temperature cycle at the sea surface, whereas the Mg/Ca temperatures from *G. ruber* (white) did not. Mg/Ca temperatures from single shells of *G. inflata* did not show seasonal differences and correspond to water depths between the sea surface and about 400 m. Changes in the Mg/Ca range are significant when they are larger than 0.80 mmol/mol (*G. ruber* (pink)) or 0.34 mmol/mol (*G. inflata*). For *G. ruber* (pink), this corresponds to a change in the temperature amplitude of >4°C and >1.7°C for *G. inflata*.

In order to verify the calculated temperature amplitudes and to test them for their paleoceanographic applicability, these were compared to single specimen calcification temperature ranges of *G. inflata*, for selected time slices throughout the past 22,000 years in the study area (**Manuscript II**). The temperature range reconstructed from near present (570 years before present) samples is in good agreement with the one reconstructed from the sediment trap samples. However, in samples from the last deglaciation, the range was significantly reduced. Comparison to water temperatures predicted by a climate model

suggests that the reduction is due to a stronger thermal stratification off Northwest-Africa during the deglaciation and a smaller depth habitat range of *G. inflata*.

Previous studies found high sea surface temperatures in the study area during the Last Glacial Maximum (23,000 - 19,000 years before present), which were explained by weaker upwelling of deeper, colder subsurface water. In this thesis, upwelling strength and water temperatures at the sea surface and ~150 m water depth were reconstructed for the past 24,000 years, using the relative abundance of *Globigerina bulloides* and Mg/Ca analyses of *G. ruber* (pink), *G. bulloides* and *G. inflata* (**Manuscript III**). The results contradict previous assumptions and suggest high upwelling intensities between 24,000 and 16,000 years before present. Further, a high Mg/Ca temperature variability of the surface dwelling species *G. ruber* (pink) and *G. bulloides* was found, in contrast to the subsurface dwelling species *G. inflata*. An inspection of daily satellite data between 1982 and 2008 shows a high degree of temperature variability in the study area and high temperatures, likely through the advection of warm surface waters during times of high wind strength. It is presumed that in the past this mechanism might have also caused higher SSTs at the study site during generally cold climatic states.

ZUSAMMENFASSUNG

Mg/Ca- und Sauerstoffisotopenverhältnisse in Schalen planktischer Foraminiferen werden in vielen paläozeanographischen Studien zur Rekonstruktion von Wassertemperaturen verwendet. Bei der herkömmlichen Methode werden mehrere Schalen einer Art gleichzeitig analysiert. Werden jedoch einzelne Schalen analysiert zeigt sich, dass erhebliche Unterschiede in Mg/Ca- und Sauerstoffisotopenverhältnissen einzelner Individuen bestehen. Diese werden durch Saisonalität und natürliche Variabilität erklärt und zunehmend zur Rekonstruktion vergangener Umweltbedingungen genutzt. Die vorliegende Arbeit erfasst die Unterschiede der Mg/Ca- und Sauerstoffisotopenverhältnisse zwischen einzelnen Individuen planktischer Foraminiferen im Auftriebsgebiet vor Nordwest-Afrika. Ziel der Arbeit ist es, natürliche Variabilität zu quantifizieren, die Nutzbarkeit von Einzelschalen für die Rekonstruktion von Temperatursaisonalität zu verbessern und die Anwendbarkeit von Einzelschalen für die Rekonstruktion der thermischen Ozeanstratifizierung aufzuzeigen.

In der vorliegenden Arbeit werden Kalzifizierungstemperaturen aus den Mg/Ca Verhältnissen in Einzelschalen der an der Wasseroberfläche lebenden planktischen Foraminiferenarten *Globigerinoides ruber* (pink), *Globigerinoides ruber* (white) und der tieflebenden Art *Globorotalia inflata* berechnet, welche in einer Sedimentfalle vor Nordwest-Afrika (20°45.6'N, 18°41.9'W) gesammelt wurden (**Manuskript I**). Einzelschalen von *G. ruber* (pink) wiesen deutlich unterschiedliche Mg/Ca-Temperaturen auf, welche dem saisonalen Temperaturverlauf an der Wasseroberfläche folgten, wohingegen die Mg/Ca-Temperaturen von *G. ruber* (white) keinen Zusammenhang mit saisonalen Wasseroberflächentemperaturen zeigten. Mg/Ca-Temperaturen in Einzelschalen von *G. inflata* zeigten keine saisonalen Unterschiede und entsprachen Wassertemperaturen zwischen der Meeresoberfläche und etwa 400 m Wassertiefe. Änderungen in der Mg/Ca Spannbreite zwischen einzelnen Individuen sind dann signifikant, wenn sie 0,80 mmol/mol (*G. ruber* (pink)) bzw. 0,34 mmol/mol (*G. inflata*) überschreiten. Im Fall von *G. ruber* (pink) entspricht dies einer Temperaturschwankung von >4°C und im Fall von *G. inflata* von >1,7°C.

Um die zuvor berechneten Temperaturspannen zu verifizieren und auf ihre paläozeanographische Anwendbarkeit hin zu überprüfen wurden diese für *G. inflata* mit rekonstruierten Temperaturspannen aus ausgewählte Zeitabschnitten innerhalb der vergangenen 22.000 Jahre im gleichen Arbeitsgebiet verglichen (**Manuskript II**). Es zeigte sich, dass Proben der jüngeren Vergangenheit (570 Jahre vor heute) gut mit der in der Sedimentfallenstudie rekonstruierten Temperaturspanne übereinstimmen. In Proben aus der letzten Abschmelzphase war diese jedoch signifikant reduziert. Der Vergleich mit berechneten Wassertemperaturen eines Klimamodels deutet darauf hin, dass diese Reduktion auf eine ausgeprägtere thermische Stratifizierung vor Nordwest-Afrika und ein schmaleres Tiefenhabitat von *G. inflata* während der letzten Abschmelzphase zurückzuführen ist.

Frühere Untersuchungen erklären hohe Wasseroberflächentemperaturen im Arbeitsgebiet während des letzten glazialen Maximums (23.000 – 19.000 Jahre vor heute) mit geringerem Auftrieb des tieferen und kälteren Wassers. In der vorliegenden Arbeit wurden Auftriebsintensitäten im Arbeitsgebiet und Temperaturen der letzten 24.000 Jahre für die Wasseroberfläche und eine Wassertiefe von ~150 m anhand der relativen Häufigkeit von *Globigerina bulloides* sowie Mg/Ca Analysen an *G. ruber* (pink), *G. bulloides* und *G. inflata* rekonstruiert (**Manuskript III**). Die Ergebnisse stehen im Widerspruch zu früheren Annahmen und weisen auf hohe Auftriebsintensität zwischen 24.000 und 16.000 Jahren vor heute hin. Zudem zeigte sich eine hohe Mg/Ca-Temperaturvariabilität der oberflächenlebenden Arten *G. ruber* (pink) und *G. bulloides* im Vergleich zur tieflebenden Art *G. inflata*. Die Auswertung täglicher Satellitendaten zwischen 1982 und 2008 belegt eine hohe Temperaturvariabilität im Arbeitsgebiet und deutet darauf hin, dass hohe Temperaturen im Arbeitsgebiet insbesondere in Verbindung mit hoher Windintensität auftreten und vermutlich durch die Advektion warmen südlichen Oberflächenwassers bedingt werden. Dieser Mechanismus könnte auch in der Vergangenheit zum Teil hohe Wasseroberflächentemperaturen während grundsätzlich kalter Klimazustände bedingt haben.

TABLE OF CONTENTS

I. INTRODUCTION

1.1 Planktic foraminifera as carriers for geochemical temperature proxies

Planktic foraminifera are short-lived heterotrophic protists that live in the marine upper ocean environment. In their adult stage, their shells range in sizes between 100 µm and 2 mm formed of calcium carbonate precipitated from the seawater carbonate. They either live in the shallow mixed layer or in the subsurface water column close to or below the thermocline. About fifty species are known [*Kucera*, 2007] that occur in all oceans from the tropics to the high latitudes and from surface waters to water depths of several hundred meters [e.g.; *Fairbanks et al.*, 1982]. Each species has different ecological and temperature preferences that determine their geographical distribution, their seasonal succession, and their vertical distribution in the water column [e.g.; *Žarić et al.*, 2005].

Temperature information can be extracted from the chemical composition of their calcitic shells, given that these were precipitated in equilibrium with the ambient seawater. The classical approach stems from the work of *Cesare Emiliani* [1955], who used the foraminiferal shell stable oxygen isotopic composition ($\delta^{18}O_c$) to deduce Pleistocene sea surface temperatures (SST). The use of foraminiferal oxygen isotopes as a paleothermometer is based on the ratio of the heavy (^{18}O) to the light (^{16}O) isotope in their shells, which is a function of both, temperature and the $\delta^{18}O$ of the ambient seawater ($\delta^{18}O_w$), from which the shells are precipitated. As has been shown in the following decades, variability of $\delta^{18}O_w$ substantially influences the use of oxygen isotopes in foraminiferal calcite for determining temperatures. During cold periods within the Pleistocene for instance, the ocean was enriched by ~1.2 to 1.5 ‰, as a result of the preferential removal of ^{16}O during evaporation from the sea surface and its storage on the continental ice sheets, also termed as ice-volume effect [e.g.; *Shackleton*, 1967]. Likewise, locally differing evaporation rates change the $\delta^{18}O_w$, thereby impairing the accuracy of the oxygen isotope thermometer.

In recent years, many efforts have been made to develop a paleothermometer independent of the hydrological influences and in particular ice volume changes. Although it was known from the pioneering work by *Clarke and Wheeler* [1922], investigated in invertebrates, that the substitution of calcium by magnesium in calcite is favored at higher temperatures, it lasted until the work of *Nürnberg et al.* [1996] to implement the Mg/Ca as proxy for paleotemperatures in the tiny tests of planktic

foraminifera. Thermodynamic considerations [*Lea et al.*, 1999] dictate that Mg/Ca ratios increase in an exponential manner with increasing temperature during precipitation. Foraminiferal calcite however deviates from pure thermodynamics in that it (1) contains substantially less magnesium and (2) responds to an increase of temperature with an about three times larger increase than thermodynamically expected [*Lea et al.*, 1999]. Today, many studies confirm the positive correlation between water temperature during calcification and foraminiferal Mg/Ca ratios [e.g. *Nürnberg et al.*, 1996; *Lea*, 1999; *Elderfield and Ganssen*, 2000; *Anand et al.*, 2003; *Cléroux et al.*, 2007; *Dekens et al.*, 2008]. For the calculation of temperatures during calcification, a large number of Mg/Ca-temperature calibrations are now available that are based on laboratory experiments [e.g. *Nürnberg et al.*, 1996], core top calibrations [e.g. *Elderfield and Ganssen*, 2000; *Cléroux et al.*, 2007; *Groeneveld and Chiessi*, 2011] or sediment trap studies [*Anand et al.*, 2003; *McConnell and Thunell*, 2005]. However, standard geochemical analyses measure multiple (10 to 30) shells at once, in order to have sufficient material for analysis and to derive an average value that is considered representative for the measured population of individual shells. This results in the loss of a lot of information on seasonal-, inter-annual- or living depth- related temperatures as recorded by individual shells.

1.2 Short-term environmental changes recorded by planktic foraminifera

Planktic foraminifera have short lifespans of mostly a few weeks to months [*Bé and Spero*, 1981; *Hemleben et al.*, 1989], and individual shells form their tests at different seasons [*Hemleben et al.*, 1989] or water depths [e.g.; *Fairbanks et al.*, 1980; *Fairbanks et al.*, 1982; *Wilke et al.*, 2009]. The reproduction of most shallow-water species appears to be triggered by the synodic lunar cycle, while some deep-dwelling species can have longer reproductive cycles [*Kučera*, 2007 and references therein]. Short reproduction cycles imply that short-term environmental changes are recorded in their shell chemistry and can potentially be used to reconstruct these. Substantial interest therefore exists in the analysis of individual shells, with the aim to assess short term environmental information both from $\delta^{18}O_c$ [e.g.; *Killingley et al.*, 1981; *Spero and Williams*, 1990; *Tang and Stott*, 1993; *Billups and Spero*, 1996; *Koutavas et al.*, 2006; *Leduc et al.*, 2009; *Wit et al.*, 2010; *Ganssen et al.*, 2011] and Mg/Ca [e.g.; *Anand and Elderfield*, 2005; *Sadekov et al.*, 2008; *Haarmann et al.*, 2011]. For interpreting single shell $\delta^{18}O_c$ and Mg/Ca, surface- and subsurface-dwelling species must be considered separately.

1.2.1 Surface-dwelling species

A good example for the behaviour in the shell chemistry of surface-dwelling foraminifera related to seasonality comes from an early study of *Williams et al.* [1979]. It shows that the $\delta^{18}O_c$ of living surface-dwelling foraminifera follows the seasonal temperature cycle (Figure 1.2-1a), which was later confirmed in many studies [e.g.; *Deuser et al.*, 1981; *Erez and Honjo*, 1981; *Curry et al.*, 1983; *King and Howard*, 2005]. *Williams et al.* [1979] already suggested that the "*seasonal occurrence as well as depth habitat are determining factors in the oxygen isotopic composition of planktic foraminifera* [and that] *these relationships may be used to determine the seasonal temperature contrast of oceans in the past*". Recent studies further show that such seasonality is not limited to the $\delta^{18}O_c$ of foraminiferal shells, but also applies to the Mg/Ca temperature proxy [*Anand et al.*, 2003; *McConnell and Thunell*, 2005; *Mohtadi et al.*, 2009] (Figure 1.2-1b).

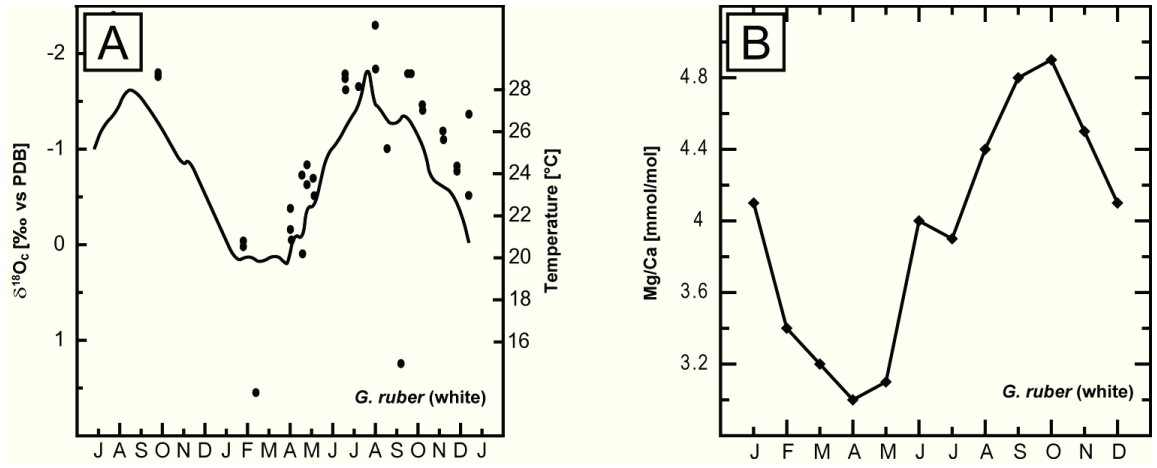

Figure 1.2-1. Seasonal chemical variability recorded in the shells of *Globigerinoides ruber* (white) for two different proxies a) Seasonal variation of $\delta^{18}O_c$ of living planktic *G. ruber* (white) collected off Bermuda. Line indicates surface water temperature measured at the time of plankton collection. Collection period was July 1975 to January 1977 [redrawn and modified after *Williams et al.*, 1979] b) Average intra-annual variation in Mg/Ca of *G. ruber* (white) collected off Bermuda. Each point represents the mean of bimonthly samples from a 6-year time series [redrawn after *Anand et al.*, 2003].

Given that a surface-dwelling species occurs throughout the year, the $\delta^{18}O_c$ and Mg/Ca range of individual specimens collected from the sediment should hence provide information on the annual seasonal cycle. Earlier studies have analyzed $\delta^{18}O_c$ of individual shells with the aim to identify seasonal meltwater pulses during the last deglaciation in the Gulf of Mexico [*Spero and Williams*, 1990], seasonal salinity variations in the Mediterranean Sea during sapropel formation [*Tang and Stott*, 1993], and seasonal temperature maxima in the western and eastern Atlantic throughout the past 150.000 years [*Billups and Spero*, 1996].

A recent study uses single specimen analysis in order to quantify El Niño-Southern Oscillation (ENSO) activity [*Koutavas et al.*, 2006]. During periods of strong ENSO, water at the sea surface is warmer and less saline in the Galapagos region. As a result, $\delta^{18}O_c$ of surface-dwelling *G. ruber* is depleted during strong ENSO and vice versa. From a smaller inter-specimen $\delta^{18}O_c$ range during the Mid- Holocene, as compared to the late Holocene, *Koutavas et al*. [2006] consequently concluded a reduced frequency of El Niño and La Niña events (Figure 1.2-2). They further suggested that a decreased ENSO activity is expressed by a reduced $\delta^{18}O_c$ standard deviation during this time interval.

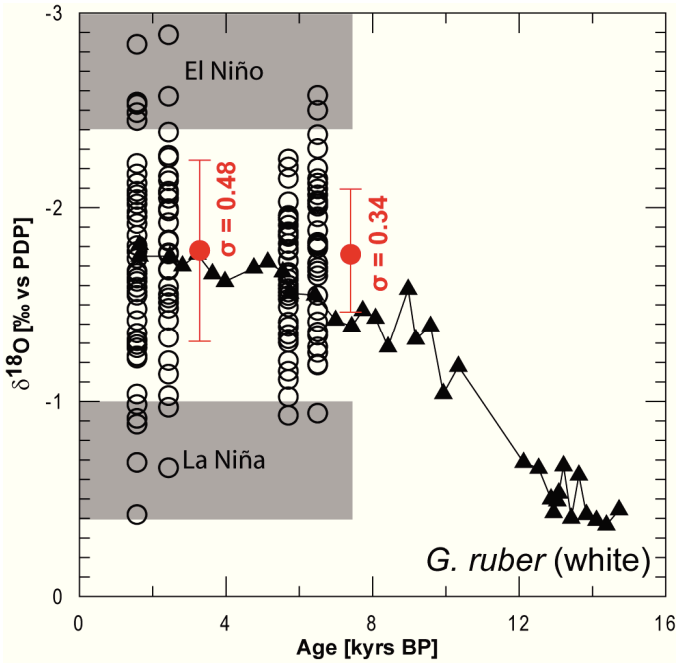

Figure 1.2-2. $\delta^{18}O_c$ measurements on individual planktic foraminifer specimens from the eastern tropical Pacific, used to infer past El Niño-Southern Oscillation activity. $\delta^{18}O_c$ of individual *G. ruber* are shown by open circles. Downcore multispecimen $\delta^{18}O_c$ from the same species are shown by triangles and a solid line. Red circles with error bars show the mean and the standard deviation of pooled individuals from the late- and mid-Holocene. Grey shaded bars show predicted $\delta^{18}O_c$ ranges due to El Niño and La Niña Southern Oscillation. The white area in between is the expected seasonal $\delta^{18}O_c$ range [*Koutavas et al.*, 2006].

New findings show that also inter-specimen Mg/Ca variability in surface-dwelling foraminifera is related to seasonal and inter-annual changes of the SST range [*Sadekov et al.*, 2010]. However, the observed inter-specimen differences are partly larger than can be explained by seasonal variations alone [*Anand and Elderfield*, 2005; *Sadekov et al.*, 2008]. Therefore, the use of individual specimens for the reconstructions of seasonality requires constraining the part of the variability not linked to environmental change, an investigation which has been a major focus of the first part of the given thesis (Manuscript I: *Haarmann et al.*, 2011).

As temperatures cannot be extracted from $\delta^{18}O_c$ alone, and single specimen Mg/Ca analyses of large shell numbers are as yet elaborate (conf. Manuscript I and chapter V), a new approach was recently introduced in a single specimen analysis [*Ganssen et al.*, 2011] which combines conventional, multispecimen Mg/Ca analyses with $\delta^{18}O_c$ single specimen analysis (Figure 1.2-3). With this technique single specimen calcification temperatures can be assessed (a detailed description of the methodology is given in Manuscript II, which applies this approach to subsurface-dwelling specimens), which allowed *Ganssen et al.* [2011] to identify reduced seasonal temperature ranges in the Arabian Sea during the Last Glacial Maximum (LGM). This approach is helpful, as it allows reconstructing calcification temperature ranges exhibited by species which occur during different seasons of the annual cycle. Thereby, seasonal temperature extrema can be assessed, and potential biases introduced by a seasonally-confined occurrence [e.g.; *Bé*, 1960; *Thunell et al.*, 1983; *Sautter and Thunell*, 1991; *Sautter and Sancetta*, 1992; *Žarić et al.*, 2005] of certain species can be resolved, which is not possible when multiple specimens are analyzed at once.

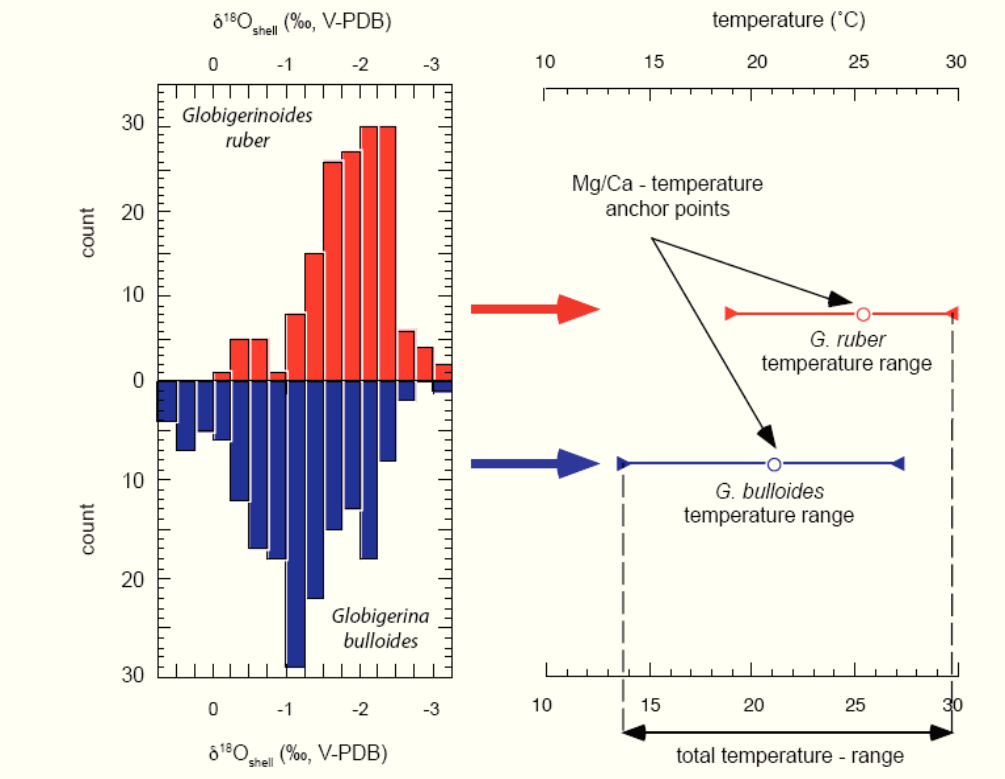

Figure 1.2-3. $\delta^{18}O_c$ of single specimen *G. ruber* and *Globigerina bulloides* from boxcores off the coast of Somalia. Open dots in the right panel show conventional multi-specimen Mg/Ca temperatures, which are used as anchor points for the single specimen analysis [*Ganssen et al.*, 2011].

An example of seasonally variable fluxes of *G. bulloides* and *G. ruber* (pink) is shown in Figure 1.2-4a for a site off Cape Blanc (NW Africa). *G. bulloides* is clearly most abundant when *G. ruber* (pink) fluxes are low and vice versa [data: *Barbara Donner, MARUM, Univ. Bremen*]. Analysis of multiple shells that are ultimately deposited on the seafloor will hence record mainly the prevailing temperatures during the time of their highest abundances. For example, most of *G. bulloides* shells will reflect the temperatures around June/July, while most of *G. ruber* (pink) shells will reflect the temperatures of November/December. *G. ruber* (pink) prefers temperatures between 24.2 and 29.7°C and usually exhibits highest fluxes at these temperatures [*Žarić et al.*, 2005]. This means that, due to seasonally different fluxes, average isotopic temperatures are biased towards summer temperatures (Figure 1.2-4b) when average SSTs are colder than the optimum temperature range of *G. ruber* (pink) [e.g.; *Mulitza et al.*, 1998]. Important is, however, that temperatures derived from the analysis of multiple shells of this species must not necessarily reflect the seasonally warmest temperatures. Off Cape Blanc for instance, flux maxima are offset from the temperature maxima and minima, though *G. ruber* (pink) and *G. bulloides* are species considered to be indicative for warm and cold SSTs [*Hemleben et al.*, 1989], respectively. Although individual specimens reflect seasonal temperatures, the flux-weighted temperature approaches the average annual SST in the case of *G. ruber* (pink) off Cape Blanc (Manuscript I: *Haarmann et al.* 2011). This means that when multiple shells are analyzed, an average value is derived that does not truly reflect the seasonal temperature extrema (conf. Figure 1.2-3).

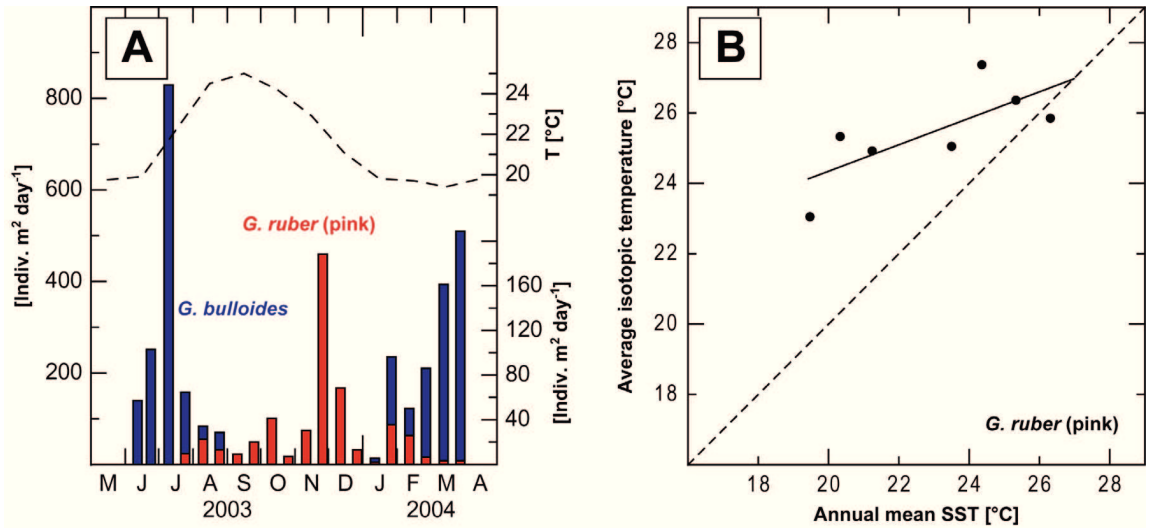

Figure 1.2-4 (previous page). Seasonal variability in the shell flux of *G. ruber* (pink) and *G. bulloides* and its effect on the geochemical signal extracted from the sedimentary record. a) *G. bulloides and G. ruber* fluxes to sediment trap CBi3-o off Cape Blanc at 20°45'N, 18°41'W [data: *Barbara Donner*] and monthly average SST [*Locarnini et al.*, 2006] b) Average *G. ruber* (pink) isotopic temperatures (dots) from classes of samples throughout different latitudes of the Atlantic Ocean versus average annual temperatures within these classes. The solid line shows the regression through the isotopic temperatures [redrawn from *Mulitza et al.*, 1998].

Using single specimen analyses, also specimens are included in the analysis which lived during the season of warmest/coldest temperatures, so that temperature extrema can be assessed, both in specimens collected from the water column by means of a sediment trap (Manuscript I: *Haarmann et al.* 2011) as well as in specimens from the sedimentary record [*Ganssen et al.*, 2011].

1.2.2 Subsurface-dwelling species

Previous studies demonstrate that single specimen analysis of subsurface-dwelling species can be used to asses thermal changes at the depth of the upper thermocline [*Billups and Spero*, 1996] and to reconstruct the past thermocline structure [*Leduc et al.*, 2009]. In analogy to single specimen analysis of surface-dwelling species, changes of the $\delta^{18}O_c$ standard deviation between individual specimens are invoked to identify changes in the paleoceanographic past. From a reduced $\delta^{18}O_c$ standard deviation between individual

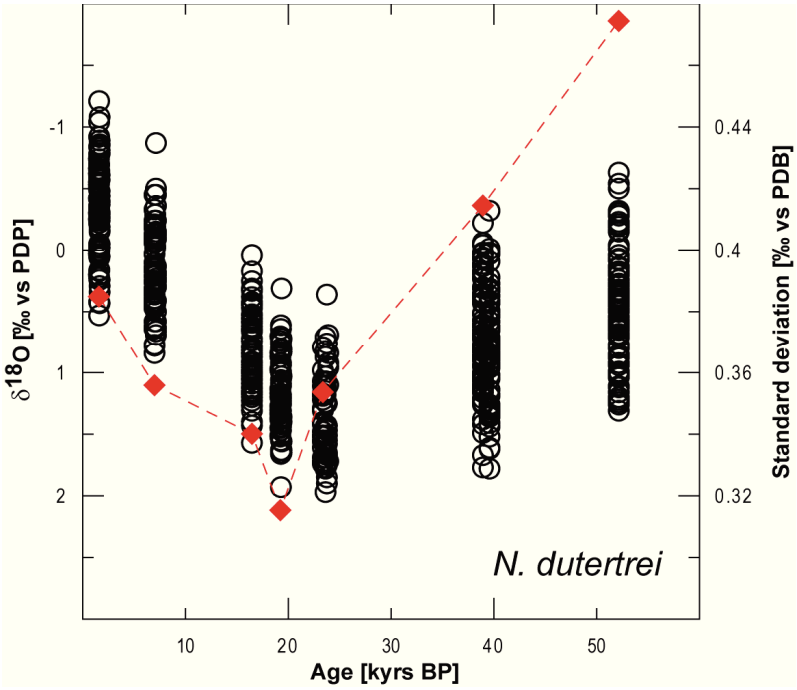

Figure 1.2-5. $\delta^{18}O$ measurements on individual planktic foraminifer specimens from the eastern tropical Pacific, used to infer past El Niño Southern Ocean activity. $\delta^{18}O_c$ of individual *N.dutertrei* are shown by open circles. Red diamonds show standard deviation of pooled individuals [*Leduc et al.*, 2009].

shells of *Neogloboquadrina dutertrei*, *Leduc et al.* [2009] concluded reduced thermocline variability and ENSO activity during the LGM as compared to the preceding glacial (Figure 1.2-5). The interpretation of single subsurface-dwelling species is less straightforward than for surface dwelling species, since the former migrate vertically through the water column during their life cycle [*Lončarić et al.*, 2006; *Wilke et al.*, 2006]. Therefore, despite little temperature changes throughout the year at subsurface depths, large $\delta^{18}O_c$ and Mg/Ca differences are documented between individual specimens [e.g.; *Billups and Spero*, 1996; *Leduc et al.*, 2009; *Haarmann et al.*, 2011]. In this thesis, single specimens of the species *Globorotalia inflata* were investigated (Manuscript II). Typical studies analyze multiple shells in order to derive an average calcification depth considered representative of the whole population. These however vary between 100 and 600 m for *G. inflata* [*Erez and Honjo*, 1981; *Elderfield and Ganssen*, 2000; *Ganssen and Kroon*, 2000; *Anand et al.* 2003; *Chiessi et al.*, 2007; *Groeneveld and Chiessi*, 2011], resulting from different depth habitats and/or the addition of secondary crust calcite [*Groeneveld and Chiessi*, 2011]. As subsurface-dwelling species - in comparison to surface-dwelling species - are valuable for the reconstruction of past ocean stratification [e.g.; *Mulitza et al.*, 1997; *Rashid and Boyle*, 2007], it is important to precisely constrain their habitat (Manuscript I: *Haarmann et al.*, 2011). In order to identify changes of the $\delta^{18}O_c$ standard deviation in the past, these are commonly compared to core top samples [*Leduc et al.*, 2009]. When calcification temperatures are assessed from individual fossil shells, it is ideal to compare these to temperatures derived from specimens collected from the water column, as is demonstrated in Manuscript II.

1.3 Assessing temperature extrema

As has been cited above, *Ganssen et al.* [2011] have recently combined $\delta^{18}O_c$ measurements of individual surface-dwelling specimens with multispecimen Mg/Ca measurements in order to reconstruct surface temperature extrema for the paleoceanographic past. In the present thesis, this approach was used to assess calcification temperatures of subsurface-dwelling *G. inflata* for the past 22,000 years (Manuscript II). Using this technique, single specimen temperatures are calculated as follows.

(1) Multiple specimens (~30) collected from a sedimentary sample are analyzed for their Mg/Ca ratios, using standard cleaning techniques [*Barker et al.*, 2003] and calcification temperatures are calculated [e.g.; *Elderfield and Ganssen*, 2000; *Anand et al.*, 2003].

(2) From the same sedimentary sample, individual specimens are collected and analyzed for their $\delta^{18}O_c$.

(3) The mean value of the individual $\delta^{18}O_c$ measurements is calculated. This value is considered to reflect the mean of the whole fossil population. This is also considered true for the value derived previously from the multiple-shell Mg/Ca analysis.

(4) Consequently, the calculated Mg/Ca temperature is used to assign a calcification temperature to the average $\delta^{18}O_c$.

(5) Temperature extrema around this mean are then calculated using $\delta^{18}O_c$:temperature relationships [e.g.; *Bemis et al.*, 1998].

For the interpretation of temperature extrema as well as for the assumption that the average $\delta^{18}O_c$ value truly represents the population mean, it is important that no bias is introduced by potential outliers. The approach of *Ganssen et al.* [2011] uses the inter-quartile range in order to identify outliers (Figure 1.3-1). An outlier is then defined as being outside of the range (equation 1.3-1)

$$[Q1-1.5*(Q3-Q1), Q3+1.5*(Q3-Q1)] \quad (1.3\text{-}1)$$

with Q3 and Q1 being the third and first quartile.

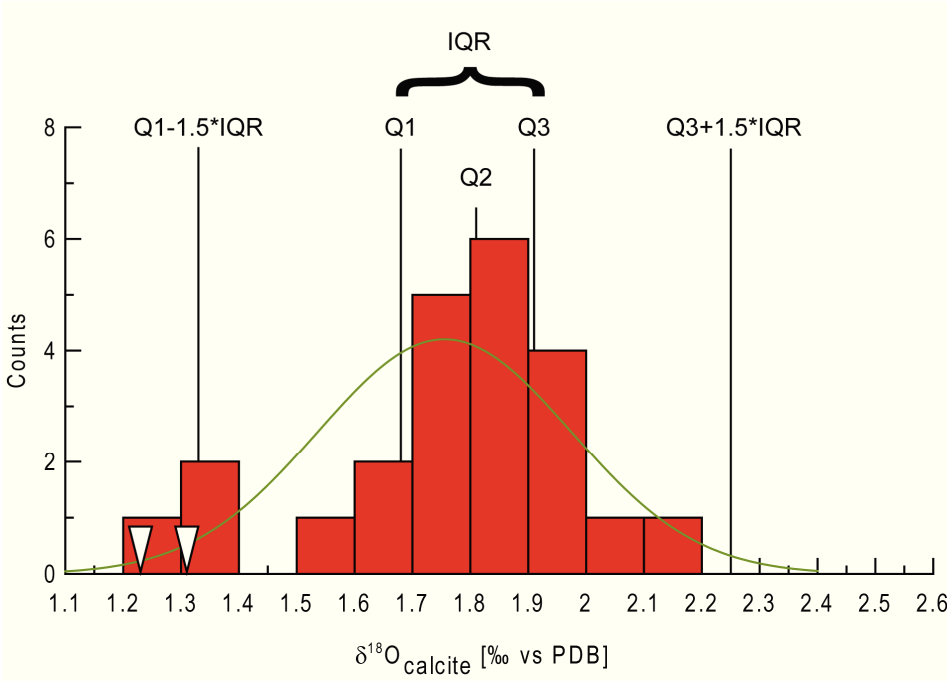

Figure 1.3-1. Example of outlier definition based on the interquartile range. Data is from single *G. inflata* specimen oxygen isotope measurements sampled from sediment core GeoB7926-2, sediment depth 273 cm (conf. Manuscript II). Q1 is the first quartile (25th percentile), Q2 the second quartile (equal to the median), Q3 the third quartile (75th percentile). IQR is the inter-quartile range. Bars show a histogram of the distribution of the samples with a Gaussian fit to the dataset. Triangles show individual data points that were identified as outliers using this method.

1.4 Cleaning and measurement of individual shells

The determination of Mg/Ca ratios in individual foraminifer shells requires a special cleaning technique in order to remove organic matter, clay minerals, Mn-Fe coatings and potentially barite [*Barker et al.*, 2003] from the pristine foraminiferal calcite. During the standard cleaning procedure, however, a substantial amount of material is lost [*Boyle*, 1981; *Lea and Boyle*, 1991; *Barker et al.*, 2003]. Routine analyses therefore need to analyze about 20-30 specimens at once, in order to achieve sufficient material for analysis. For analyzing single shells, the standard cleaning is hence not feasible and a different cleaning technique needed to be used in this thesis to minimize sample loss.

This was achieved through the use and further development of the *MARUM flow-through system* for cleaning and dissolving foraminifer shells. This system was installed by Dr. Ed Hathorne (postdoc at MARUM during the years 2006-2009), is similar to the one developed by *Haley and Klinkhammer* [2002] and was modified and tested during this PhD project to allow for a cleaning of freshly sedimented single foraminiferal shells. As the foraminifera analyzed for Mg/Ca were collected from a sediment trap located well

above the seafloor, only oxidative cleaning was performed, since only organic matter can contaminate Mg/Ca measurements in the water column.

Figure 1.4-1 shows a schematic and photograph of the flow-through. In the system, foraminiferal samples are placed in between two PTFE filters (Whatman International Ltd.), kept in a filter holder that is arranged in the middle of a cleaning line (for reasons of presentability, only one cleaning line is shown; in fact five cleaning lines are used). The computer is then programmed to run a predefined cleaning procedure, so that the samples in the filter holders are consecutively exposed to a constant flow of cleaning and rinsing reagents. First, valve 1 (V1; Neptune Research Inc. 6xGradient Manifold Isolation Valves) is used to select the needed reagent. The reagent is then pumped at a defined speed using pump 1 (Knauer Advanced Scientific Instruments HPLC-pump K-120) and passes a water bath (100°C), where it is heated up to ~60°C. Further downstream, V2 is used to select one of the five cleaning lines. After passing the filter on which the sample is located, V3 and V4 are used to direct the reagent towards waste. After a predefined time, V1 is programmed to disconnect the first reagent (e.g.; H_2O_2) from the cleaning line and connect the next reagent (e.g.; H_2O for rinsing) to it. These steps are repeated for every sample. The reagents used consecutively in this thesis were: Suprapure H_2O_2 (30%) diluted to 1% in 0.1 M analytical grade NaOH (heated to ~60°C) for >20 min (pump speed: 2 ml/min) followed by suprapure water (>18 MΩ cm) for 46 min (pump speed: 6 min at 4 ml min^{-1}, then 40 min at 1 ml min^{-1}). To avoid dissolution during rinsing, the *pH* of the deionised water was kept above 7 by adding a few drops of suprapure NH_3 solution. After cleaning the single specimens were taken off the filter and examined under a binocular microscope to determine if they remained intact during cleaning. They were then transferred to clean vials, dissolved in 500 µL thermally distilled 0.075 M HNO_3 and centrifuged for 10 min at 6000 rpm prior to trace metal analysis. This cleaning procedure produced good results for the cleaning of freshly deposited foraminifer shells. Quick and efficient cleaning procedure for sedimentary shells is also desirable for sedimentary shells. This requires a different approach that also includes dissolution of the foraminiferal shells in the flow-through system. Therefore, a second, acid-resistant pump (pump 2) is attached to the system. Through this pump, dissolution reagent (HNO_3) can be mixed to the stream of solution. After passing the sample, V3 and V4 are then switched to a configuration that directs the solution to collecting vials. A summary of the efforts and results for developing a cleaning procedure for sedimentary shells is given in chapter V.

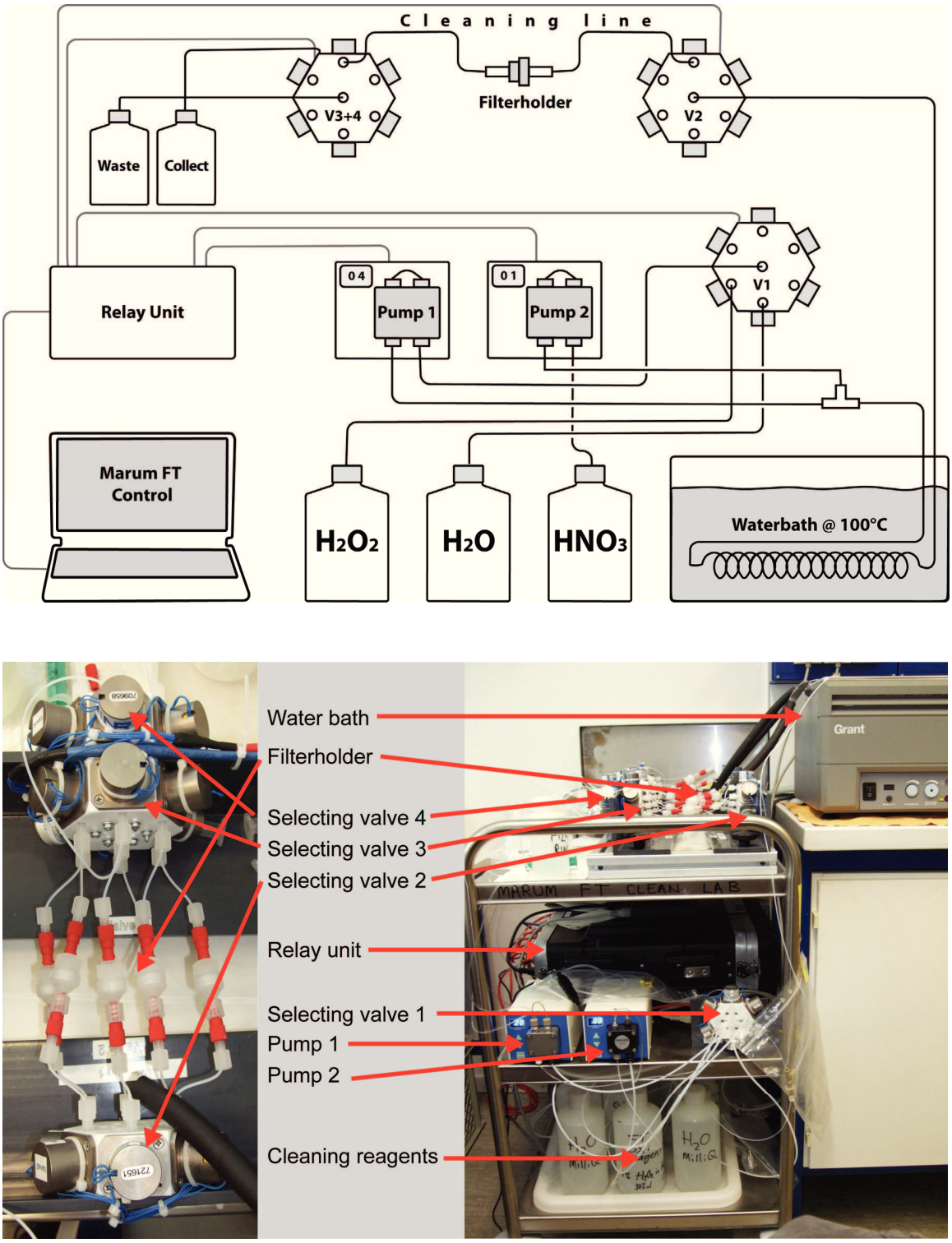

Figure 1.4-1. Schematic and photograph of the flow-through system used for cleaning of the foraminiferal shells in this study. H_2O_2 and H_2O are used for cleaning and rinsing, HNO_3 can be used for dissolution if required. V1-V4 denotes computer controlled Neptune Research Inc. 6xGradient Manifold Isolation Valves. Pump 1 and pump 2 (Knauer Advanced Scientific Instruments HPLC-pumps) are also computer controlled and can be set to variable speeds; pump 2 is acid resistant. Note that between V2 and V3+4, for reasons of better presentability, only one cleaning line is shown in the schematic, while in fact five cleaning lines are attached.

As the thin shells of *G. ruber* (pink) and *G. ruber* (white) analyzed in this thesis produce solutions with low Ca concentrations, determination of Mg/Ca ratios was achieved using inductively coupled plasma mass spectrometry (ICP-MS), following the method of *Rosenthal et al.* [1999]. Sample Ca concentrations were first measured on a Perkin-Elmer Optima 3300R inductively coupled plasma-optical emission spectrometer (ICP-OES) and then diluted to have Ca concentrations of 2 and 5 ppm. Standard solutions having the same Ca concentrations were prepared gravimetrically from single element solutions to have a Mg/Ca ratio of 4.90 mmol/mol (as expected for *G. ruber* (pink) and *G. ruber* (white)). Mg and Ca intensities of the standards and the samples were measured on a Thermo-Finnigan Element 2 sector field ICP-MS and corrected for intensities measured in blank solutions. Mg/Ca ratios were then assessed directly from intensity ratios. In contrast to determination of Mg/Ca ratios from concentrations, this approach has the advantage that different sample dilutions have no effect on the accuracy of the measurement [*Rosenthal et al.*, 1999]. The sample Mg/Ca ratio is calculated as

$$(Mg/Ca)_{sample} = C*(Mg/Ca)_{measured} \quad (1.4\text{-}1)$$

where C is a correction factor that accounts for deviations of the measured ratio from the true ratio (here 4.90 mmol/mol).

$$C = (Mg/Ca)_{standard}/(Mg/Ca)_{measured} \quad (1.4\text{-}2)$$

II. THESIS OUTLINE

The goal of this thesis is to advance recent developments for the reconstruction of past ocean temperature seasonality and thermal water column stratification, using single foraminiferal shell Magnesium to Calcium ratios and oxygen isotope ratios. The results of the thesis are presented in three separate manuscripts, as summarized below.

Manuscript 1: Mg/Ca ratios of single planktonic foraminifer shells and the potential to reconstruct the thermal seasonality of the water column

Tim Haarmann, Ed C. Hathorne, Mahyar Mohtadi, Jeroen Groeneveld, Martin Kölling, Torsten Bickert

Paleoceanography, 26 (doi: 10.1029/2010PA002091)

This article addresses inter-specimen Mg/Ca variability in two surface- (*Globigerinoides ruber* (white) and *Globigerinoides ruber* (pink)) and one intermediate-depth dwelling (*Globorotalia inflata*) foraminiferal species collected from a sediment trap off NW Africa. For *G. ruber* (pink) we could confirm recent hypotheses [*Sadekov et al.*, 2008; *Wit et al.*, 2010] that single shell Mg/Ca ratios are related to seasonal sea surface temperature (SST). For *G. inflata* we show that this species exhibits little Mg/Ca seasonality and that single shells reflect temperatures between the sea surface and ~400 m water depth. The sediment trap time series suggests that for specimens collected from the sedimentary record detectable changes in the past temperature range under which these species calcified correspond to changes of the Mg/Ca ratios ≥0.80 mmol/mol (*G. ruber* (pink)) and ≥0.34 mmol/mol (*G. inflata*). This study was enabled by the further development of the *Marum flow-through system* (chapter 1.4) for cleaning and dissolving foraminiferal shells.

Manuscript 2: Subsurface thermal stratification off NW Africa during the past 24,000 years – inferences from single planktic foraminifer shells

Tim Haarmann, Frank Peeters, Gerald Ganssen, Ute Merkel, Torsten Bickert
For submission to *Paleoceanography*

This study is a continuation of the preceding study and tests the suggested potential of single specimens of *G. inflata* for reconstructing the past thermal ocean stratification at the study site. Conventional multi-specimen Mg/Ca analysis was combined with single specimen $\delta^{18}O_c$ analysis (chapter 1.3) in order to assess past subsurface calcification temperatures of single specimens of this species off NW Africa for the past 22,000 years. The selection of a sediment core at the same site as the sediment trap allowed for excellent comparability to the present day observations and showed that near present (570 years before present) single sedimentary *G. inflata* shells reflect present day calcification temperature ranges of this species well. However, during the last deglaciation, the calcification temperature range of *G. inflata* was significantly reduced. Statistical analysis and comparison to past subsurface water column stratification derived from the Community Climate System Model Version 3 (CCSM3) suggests that *G. inflata* inhabited a substantially reduced habitat range during the deglaciation, as a result of stronger water column stratification. Single specimen $\delta^{18}O_c$ analyses were carried out in collaboration with the project partners at the Vrije Universiteit Amsterdam.

Manuscript 3: Upwelling strength off Cape Blanc (NW Africa) during the past 24,000 BP – Effects on the surface and subsurface Mg/Ca temperature records

Tim Haarmann, Mahyar Mohtadi, Jeroen Groeneveld, Torsten Bickert
In preparation for *Biogeosciences*

In this manuscript, the previously investigated surface- and subsurface dwelling species are used in a conventional, multispecimen Mg/Ca temperature analysis at the study site for the past 24,000 years. At this site, previous studies suggest unexpectedly warm SSTs during generally cold climatic states as a result of decreased upwelling of cold subsurface waters [*Romero et al.*, 2008]. The present thesis contradicts this suggestion and reconstructed strong upwelling from high relative abundances of *G. bulloides* between 24,000 and 16,000 years

before present. Mg/Ca temperatures reconstructed from the surface-dwelling species *G. ruber* (pink) and *G. bulloides* are generally highly variable, in contrast to those of subsurface-dwelling *G. inflata*. Concluded by modern analogy, we explain the high SST variability at the study site during strong upwelling with substantial temperature differences at the sea surface, likely through the advection of warm tropical surface waters towards the study area.

Future studies are needed to test this hypothesis and could be done by analyzing single shells of *G. ruber* (pink) and *G. bulloides* in order to work out temperature extrema at the study site. This could be achieved through a combined approach of multi-specimen Mg/Ca and single specimen $\delta^{18}O_c$ analysis, as used in Manuscript II. More directly, Mg/Ca ratios would be analyzed from single sedimentary shells. This requires a further development of the cleaning technique for single foraminiferal shells. An outlook for such future developments is given in chapter V.

III. MATERIAL AND STUDY SITE

3.1 Samples

This thesis aims to compare recent single foraminiferal specimens from the water column to their fossil, sedimentary counterparts. For this reason, recent samples were collected from a sediment trap and compared to fossil samples collected from a sediment core as close as possible to the sediment trap location. The sediment trap (CBi3-o) was moored ~170 km off Cape Blanc, NW Africa (20°45.6'N, 18°41.9'W) at 1277 meters below sea level, 1416 meters above sea floor. The gravity core GeoB7926-2 was recovered at 20°12.8'N, 18°27.1'W at 2500 m water depth. Coretop samples were obtained from the top centimeter of multicorer GeoB7408-2 at 20°17.4'N, 18°15.0'W from a water depth of 1935 m. Details on the recovery and sampling procedure are provided in Manuscripts I (sediment trap and coretop samples) and II (sediment core). A revised age model for the previously dated sediment core GeoB7926-2 [*Romero et al.*, 2008] is presented in Manuscript II. The sediment trap, sediment core and top centimeter of the multicorer were sampled for *G. ruber* (pink) and *G. inflata*. In addition, the sediment trap was sampled for *G. ruber* (white) and the sediment core for *G. bulloides*.

3.2 Study site

The study site off Cape Blanc is dominated by the seasonal migration of the Inter Tropical Convergence Zone (ITCZ) between ~5° and 20°N and the seasonal migration of the northeast trade winds (Figure 3.2-1), accompanied by a strong seasonal SST contrast and a pronounced seasonal thermocline. The amplitude of the annual temperature cycle at the surface is 5.3°C, and at the depth of the seasonal thermocline (~75 m) about 0.8°C, whereas at 300 m the seasonal temperature range is only 0.3°C [*Locarnini et al.*, 2006]. The surface temperature range can, however, be significantly larger, if daily temperatures are considered (Figure 3.2-1). The trade winds modulate the southward flowing Canary Current and the northward flowing Mauritania current (Figure 3.2-2a). During winter, the Canary Current reaches furthest south. In summer, when the southern boundary of the trade winds has its northernmost position, the coastal northward flowing current advects warm waters up to the latitude of Cape Blanc [*Mittelstaedt*, 1983].

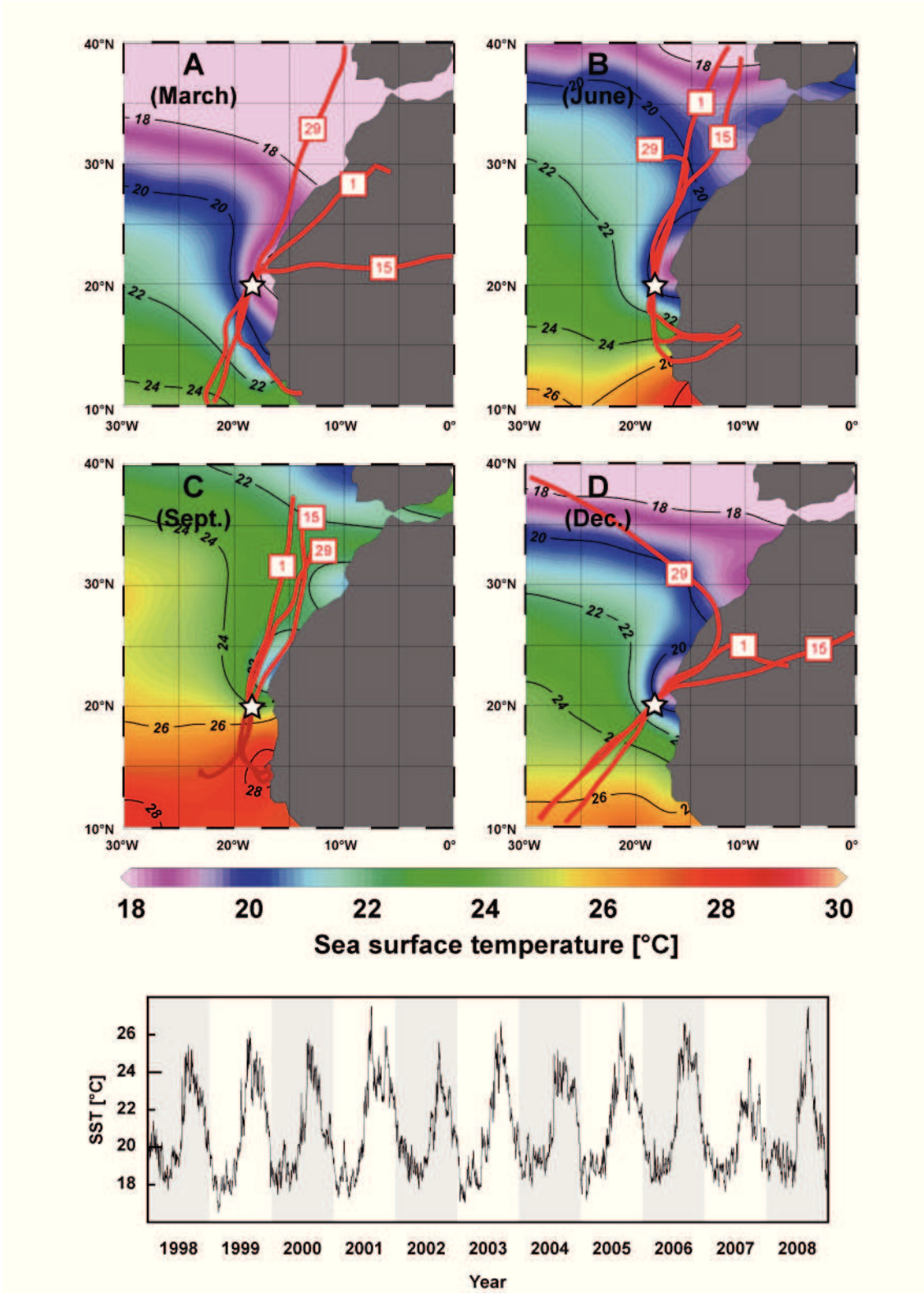

Figure 3.2-1. Sea surface temperatures and winds off NW Africa. (Upper panel) Color shading shows sea surface temperatures [*Locarnini et al.*, 2006]. Red lines show 72h backward (to the north) and forward (to the south) wind trajectories moving at 100 m above the study site during the year 2000 (Calculated using the Hybrid single particle Lagrangian Trajectory Model of the National Oceanic and Atmospheric Administration Air resources laboratory; http://ready.arl.noaa.gov/hysplit-bin/trajtype.pl?runtype=archive). Red numbers in boxes indicate respective day of the month. (lower panel) Daily sea surface temperatures between the years 1998 and 2008 at 20°22.5'N, 18°22.5'W. Temperatures were derived from the Advanced Very High Resolution Radiometer of the National Oceanographic and Atmospheric Administration (http://www.ncdc.noaa.gov).

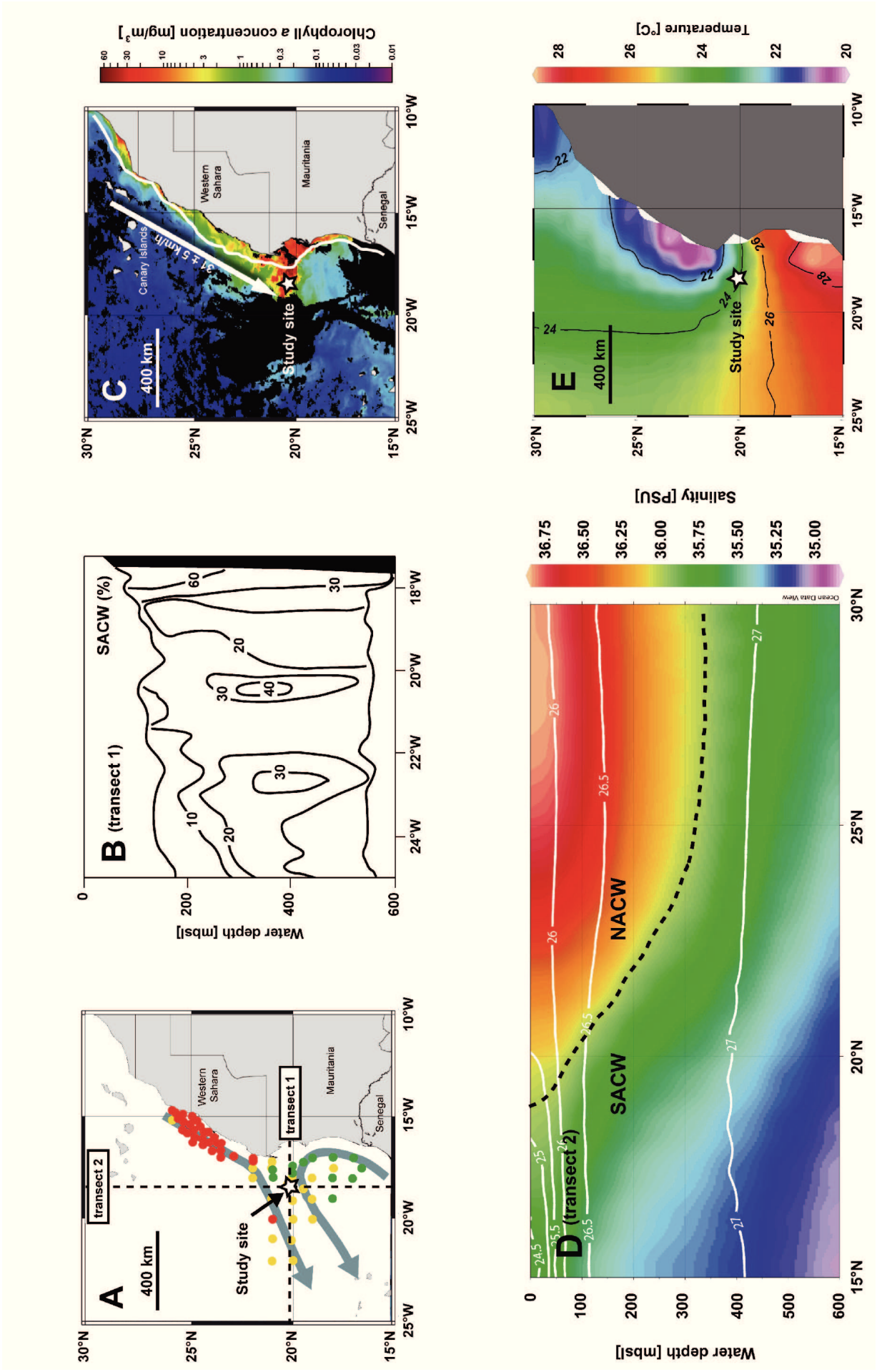
A
400 km
transect 2
transect 1
Study site
Western Sahara
Mauritania
Senegal
30°N
25°N
20°N
15°N
25°W
20°W
15°W
10°W
B (transect 1)
SACW (%)
Water depth [mbsl]
0
200
400
600
24°W
22°W
20°W
18°W
C
400 km
Study site
Canary Islands
21 ± 5 km/h
Chlorophyll a concentration [mg/m³]
E
400 km
Study site
Temperature [°C]
D (transect 2)
NACW
SACW
Salinity [PSU]
Water depth [mbsl]

Figure 3.2-2 (previous page). Main oceanographic features at the study site off Cape Blanc (NW Africa). a) Location of the study site is indicated by a star. Red dots indicate sites that exhibit salinity and temperature properties of the North Atlantic Central Water, green dots indicate sites that exhibit salinity and temperature properties of the South Atlantic Central Water, and yellow dots those sites that represent a mixture of both water masses [*Pastor et al.*, 2008]. Transects shown in the panels B and D are indicated by dashed lines. Arrows indicate the flow path of the Canary Current (north) and the Mauritania Current (south) b) Meridional transect at 20°10'N, modified from *Hagen* and *Schemainda* [1987]. Lines indicate the percentage of the South Atlantic Central Water as compared to the North Atlantic Central Water in April 1983 c) Chlorophyll *a* concentration during the period from 22 to 29 September 2005 (http://oceancolor.gsfc.nasa.gov); white line is the isoline of the ocean floor at 120 m water depth; arrow indicates the average wind direction between 22 and 29 September 2005 (http://ready.arl.noaa.gov/HYSPLIT.php) d) Longitudinal transect at 18.5°W. Colors show salinity, isolines show potential density [World Ocean Atlas, 2005; *Antonov et al.*, 2006; *Locarnini et al.*, 2006]. Dashed line shows the 36 psu isoline, used to exemplify the boundary between higher saline North Atlantic Central Waters and the lower saline South Atlantic Central Waters [*Mittelstaedt*, 1983] e) Average monthly sea surface temperatures during September [*Locarnini et al.*, 2006].

As a result of the trade winds and Ekman-pumping, surface waters are transported offshore and replaced by upwelled waters along the entire NW African margin (Figure 3.2-3). The seasonal movement of the trade winds determines that south of 20°N upwelling is limited to winter and north of ~25°N to summer. Between 20 and 25°N it is perennial [*Schemainda et al.*, 1975]. At the study site, large filaments develop that transport upwelled waters up to 500 km offshore [*Pérez-Rodríguez et al.*, 2001; *Pelegrí et al.*, 2005], also extending over the study site (Figure 3.2-2c).

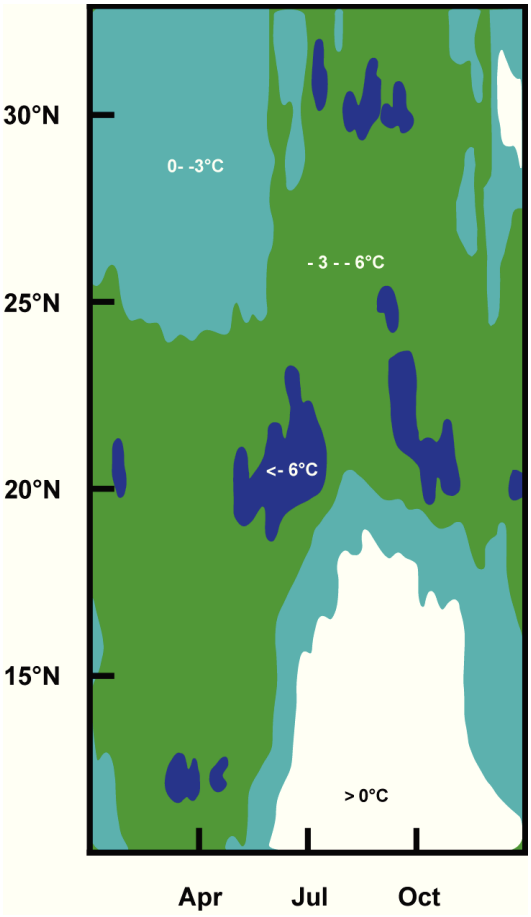

Figure 3.2.-3. Mean temperature differences between NW African coastal areas and mid-Atlantic between 1969 and 1976. Negative values indicate coastal temperatures colder than mid-ocean, indicative of upwelling of cold subsurface waters [modified after *Speth et al.*, 1978].

Upwelled water off NW Africa consists of two distinct water masses: the North Atlantic Central Water (NACW) and the South Atlantic Central Water (SACW) (Figure 3.2-2a, b and d). Upwelled water south of ~24°N is dominated by low salinity (35.6 - 35.9‰) and high nutrient SACW [*Mittelstaedt*, 1983] which are transported by a northward flowing undercurrent at a depth between 200 m and 400 m [*Hagen*, 2001]. Further north, upwelled water consists of higher salinity (36.1 – 36.4‰), but lower nutrient North Atlantic Central

Water (NACW) [*Mittelstaedt*, 1983]. At the study site, both water masses converge and the upwelled water is a mix of NACW and SACW. Because NACW and SACW have the same density (Figure 3.2-2d), mixing and interleaving is facilitated (Figure 3.2-2b).

IV. MANUSCRIPTS

4.1 Manuscript 1

Mg/Ca ratios of single planktonic foraminifer shells and the potential to reconstruct the thermal seasonality of the water column

Tim Haarmann[1], Ed C. Hathorne[2], Mahyar Mohtadi[1], Jeroen Groeneveld[1, 3], Martin Kölling[4], Torsten Bickert[1]

[1]Marum – Center for Marine Environmental Sciences, Leobener Straße, 28359 Bremen, Germany

[2]IFM-GEOMAR, Leibniz Institute for Marine Sciences at the University of Kiel, Wischhofstraße 1-3, 24148 Kiel, Germany

[3]Alfred Wegener Institute, Am Handelshafen 12, 27570 Bremerhaven, Germany

[4]University of Bremen, Department of Geosciences, Klagenfurter Straße 2, 28334 Bremen, Germany

Published in Paleoceanography, 26 (doi: 10.1029/2010PA002091) as editor's highlight and summarized as research spotlight in *Eos*, 92 (43), 25 October 2011

Mg/Ca ratios of surface- and subsurface dwelling foraminifera provide valuable information about the past temperature of the water column. Planktonic foraminifera calcify over a period of weeks to months. Therefore, the range of Mg/Ca temperatures obtained from single specimens potentially records seasonal temperature changes. We present solution derived Mg/Ca ratios for single specimens of the planktonic foraminifera species *Globigerinoides ruber* (pink), *Globigerinoides ruber* (white), and *Globorotalia inflata*, from a sediment trap off NW Africa (20°45.6'N, 18°41.9'W). Cleaning of single specimens was achieved using a flow-through system in order to prevent sample loss. Mg/Ca ratios of surface dwelling *G. ruber* (pink) show strong seasonality linked to sea surface temperature. Mg/Ca ratios of *G. ruber* (white) do not show such seasonality. Subsurface dwelling *G. inflata* flux is largest during the main upwelling season but Mg/Ca ratios reflect annual temperatures at intermediate water depths.

The sediment trap time-series suggests that changes in the range of Mg/Ca ratios exhibited by single specimens of *G. ruber* (pink) and *G. inflata* from the sedimentary record should provide information on the past temperature range under which these species calcified. Statistical analysis suggests detectable changes in the Mg/Ca range are ≥0.80 mmol/mol (*G. ruber* (pink)) and ≥0.34 mmol/mol (*G. inflata*). For *G. ruber* (pink), such changes would

indicate changes in the seasonal sea surface temperature range >4°C or a shift in the main calcification and reproductive period. For *G. inflata*, such changes would indicate >1.7°C changes in the thermocline temperature or a change in the depth habitat.

4.1.1 Introduction

Planktonic foraminifer Mg/Ca ratios are important for reconstructing changes in sea surface temperature (SST) [e.g. *Elderfield and Ganssen*, 2000; *Dekens et al.*, 2008] and water column temperatures [e.g. *Cléroux et al.*, 2007; 2008] related to climatic change. Numerous studies have shown that the Mg content of the shells of foraminifera correlates positively with the water temperature during calcification [e.g. *Nürnberg et al.*, 1996; *Lea*, 1999; *Elderfield and Ganssen*, 2000; *Anand et al.*, 2003; *Cléroux et al.*, 2007; *Dekens et al.*, 2008]. Mg/Ca-temperature calibrations are based on laboratory experiments [e.g. *Nürnberg et al.*, 1996], core top calibrations [e.g. *Elderfield and Ganssen*, 2000; *Cléroux et al.*, 2007; *Groeneveld and Chiessi*, 2011] or sediment trap studies [*Anand et al.*, 2003; *McConnell and Thunell*, 2005]. As such the Mg/Ca ratio of planktonic foraminifera shells is commonly used as a proxy for reconstructing the temperature at the depth in which the utilized species preferentially calcify. The calcification depth of planktonic foraminifera differs for various species. Therefore, a thorough understanding of foraminifer ecology and species specific calibration is needed in order to reconstruct past ocean temperatures with confidence.

Globigerinoides ruber (pink) is a tropical to subtropical species [*Hemleben et al.*, 1989] and lives predominantly in the upper 50 m of the water column [e.g. *Bé*, 1977] preferentially calcifying in the upper 25 m [e.g. *Ravelo et al.*, 1990; *Anand et al.*, 2003; *Tedesco et al.*, 2007; *Steph et al.*, 2009]. *Ganssen and Kroon* [2000] suggest *G. ruber* (pink) is restricted to temperatures above 20°C, while *Žarić et al.* [2005] report a wider tolerance range of 16.4 - 29.6°C. *G. ruber* (pink)

Globigerinoides ruber (white) is a tropical to transitional, mixed layer dwelling species [e.g. *Bé*, 1977; *Ganssen and Kroon*, 2000; *Mohtadi et al.*, 2009] and has a slightly wider temperature tolerance range than *G. ruber* (pink). It possesses photosynthetic algal symbionts and favors a life in the photic zone, where it is found in significant numbers [*Fairbanks et al., 1982*], migrating between the upper photic zone and the chlorophyll maximum [*Wilke et al.*, 2009].

Globorotalia inflata is a transitional to subpolar species [*Hemleben et al.*, 1989], and lives in waters with a temperature

range between 8 and 18°C [e.g. *Bé and Hamlin,* 1967; *Farmer et al.*, 2010]. It is very abundant in the upwelling region off NW Africa, where it constitutes 25% of the recent sedimentary planktonic foraminifers [*Diester-Haass et al.*, 1973]. The apparent calcification depth of *G. inflata* is suggested to vary between 100 and 600 m [*Erez and Honjo*, 1981; *Elderfield and Ganssen*, 2000; *Ganssen and Kroon*, 2000; *Anand et al.*, 2003; *Chiessi et al.*, 2007; *Groeneveld and Chiessi*, 2011]. Like many species, *G. inflata* adds crust calcite to its primary calcite test at greater depth and colder temperatures [*e.g. Caron et al.*, 1990]. This can bias geochemical signals to a deeper apparent calcification depth [*Groeneveld and Chiessi*, 2011; *van Raden et al.,* 2011], although the difference in Mg/Ca between crust and primary calcite cannot be explained entirely by depth migration [*Hathorne et al., 2009*]. *G. inflata* abundance has been found in the subsurface seasonal thermocline and the mixed layer, coincident with the maximum chlorophyll *a* concentration [*Ravelo et al.*, 1990; *Wilke et al.*, 2006]. As such, *G. inflata* has been used to reconstruct water temperatures around the seasonal thermocline [*Cléroux et al.*, 2007, 2008]. *G. inflata* has small symbiotic algae [*Gastrich*, 1987], restricting it to the photic zone during at least part of its life cycle.

Planktonic foraminifera calcify over a period of a couple of weeks to months [e.g. *Bé and Spero*, 1981; *Hemleben et al.*, 1989], with the reproductive cycle often triggered by the synodic lunar cycle [e.g. *Spindler et al.*, 1979; *Bijma and Hemleben*, 1990]. Single specimens thus potentially record short-term temperature variations. However, in standard geochemical analyses, this potential is not exploited, as traditionally, multiple (about 10 to 30) specimens are analysed at once. This is necessary in order to obtain a representative average temperature, and to achieve sufficient material for a reliable analysis since a substantial amount of material can be lost during standard cleaning procedures [*Boyle*, 1981; *Lea and Boyle*, 1991; *Barker et al.*, 2003]. Analyses using standard cleaning techniques can therefore only provide average temperatures, which may additionally be biased towards the main reproductive period of the species.

The importance of single shell $\delta^{18}O$ analyses of planktonic foraminifera for paleoceanographic questions is becoming increasingly recognized [*Spero and Williams*, 1989] and such analyses have been applied to quantify past El Niño-Southern Oscillation (ENSO) and thermocline variance [*Koutavas at al.*, 2006; *Leduc et al.*, 2009]. Recently, laser ablation inductively coupled plasma-mass spectrometry (LA-ICP-MS) has been used

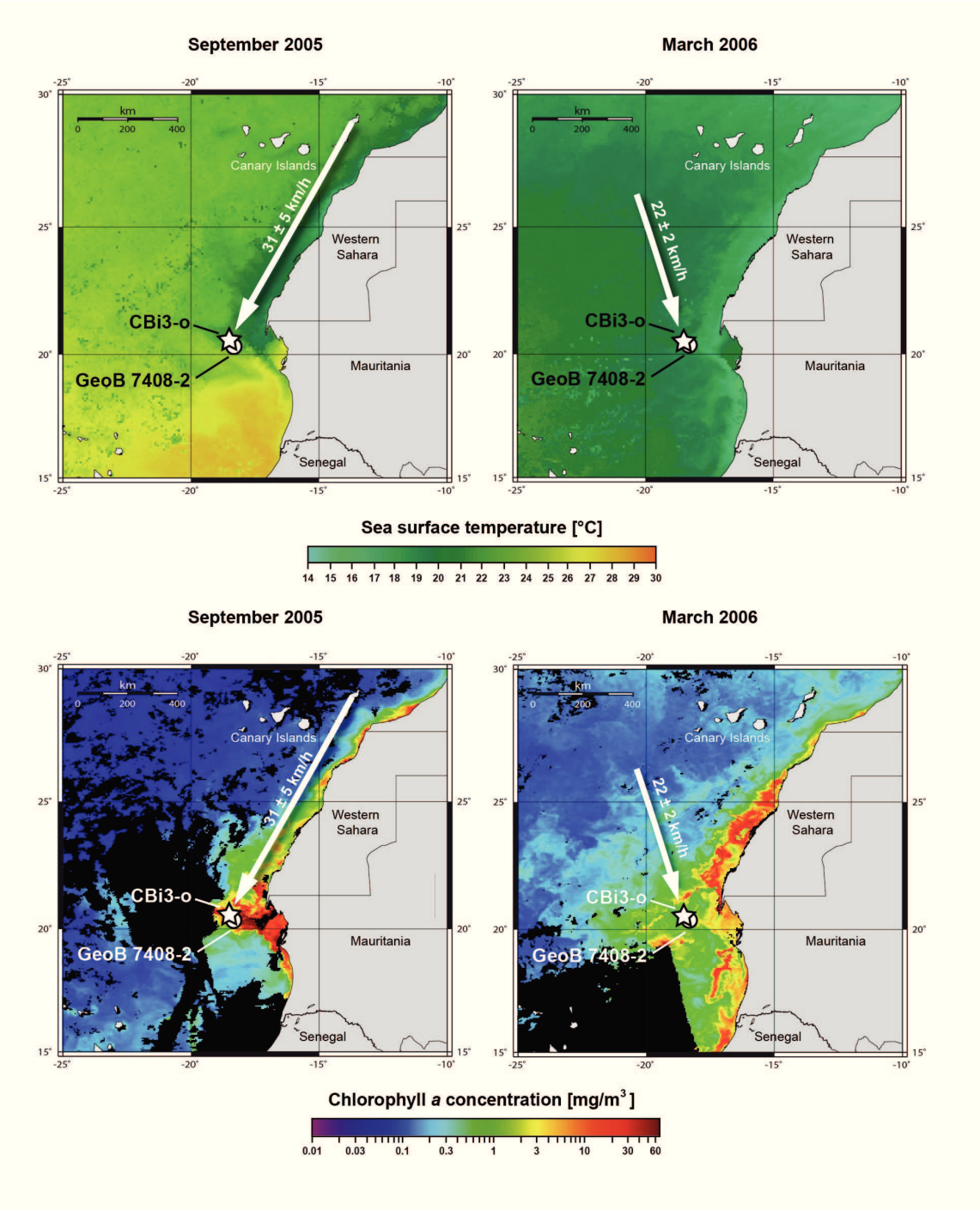

Figure 4.1-1. Map of the study area with SST, chlorophyll *a* concentrations, and surface winds. The sediment trap (indicated by a star) is located at 20°45.6'N, 18°41.9'W off Cape Blanc, NW-Africa. The location of coretop GeoB7408-2 is indicated by a circle. SSTs and chlorophyll *a* concentrations reflect the period from 22-29 September 2005, and 14-21 March 2006, respectively. Arrows indicate average wind direction during the respective period and the average wind speed and standard deviation (1 σ) are given.

to investigate interspecimen Mg/Ca variability in surface dwelling foraminifera [*Sadekov et al.*, 2008; *Wit et al.*, 2010, *Marr et al.*, 2011]. These studies suggest the variability is partly related to seasonal and interannual changes in sea surface temperature and that it resembles the seasonal range of temperatures at the sea surface. However, the interpretation of changes

of the Mg/Ca variability for paleoceanographic reconstructions requires natural Mg/Ca variability, not linked to environmental change, to be well defined. Here we constrain this natural Mg/Ca variability for *G. ruber* (pink), *G. ruber* (white) and *G. inflata* from a sediment trap time series.

In this study, we utilized a flow-through system [*Haley and Klinkhammer*, 2002], enabling Mg/Ca measurements on single shells of planktonic foraminifera from a sediment trap off Cape Blanc, Mauritania, NW Africa, (20°45.6'N, 18°41.9'W). We test several Mg/Ca temperature equations for their applicability to single specimens of three planktonic foraminiferal species (*G. ruber* (white), *G. ruber* (pink), *G. inflata*) and investigate the potential of single tests to assess short term temperature variations. We further evaluate and explain the variability in Mg/Ca temperatures among single specimens of these species, with a focus on their potential applicability in paleoceanographic studies.

4.1.2 Study area

The study area off Cape Blanc (NW-Africa) is dominated by the seasonal migration of the Inter Tropical Convergence Zone (ITCZ), accompanied by a strong seasonal SST contrast (Figure 4.1-1). The amplitude of the annual SST cycle (Figure 4.1-2) derived from the advanced very-high-resolution radiometer at 20°22.5'N and 18°22.5'W (http://www.ncdc.noaa.gov) was 9.6°C during the deployment period with highest temperatures in mid September (27.7°C) and lowest temperatures in mid March (18.1°C). This large annual amplitude of SST is ideal for our study. The main surface current in the study area is the Canary Current, which flows south along the NW African coast as the eastern branch of the North Atlantic Subtropical Gyre. The Canary Current is modulated by south westward directed trade winds (Figure 4.1-1) which blow throughout the year between 20°N and 25°N [*Schemainda et al.*, 1975] and cause perennial upwelling off Cape Blanc. Upwelling is strongest in late spring and autumn [*Ganssen and Sarnthein*, 1983; *Pelegrí et al.*, 2005]. As a result of the steady trade winds and Ekman-pumping, surface waters are transported offshore and replaced by upwelled waters. The upwelled water off NW Africa consists of two distinct water masses: the North Atlantic Central Water (NACW) and the South Atlantic Central Water (SACW). Generally, to the south of 24°N, upwelled water is dominated by low salinity (35.6 - 35.9‰) SACW [*Mittelstaedt*, 1983] transported by a

northward flowing undercurrent at a depth between 200 m and 400 m [*Hagen*, 2001]. To the north, upwelled water consists of the higher salinity (36.1 – 36.4‰) North Atlantic Central Water (NACW) [*Mittelstaedt*, 1983]. The nutrient contrast between NACW and SACW is expressed by nitrate increasing southward from 5 to 20 mmol/m^3 [*Pérez-Rodríguez et al.*, 2001; *Pelegrí et al.*, 2005]. Off Cape Blanc, the Canary Current detaches from the coast, promoting the development of a large filament of upwelled water extending up to 500 km offshore [*Pérez-Rodríguez et al.*, 2001; *Pelegrí et al.*, 2005], which travels over the sediment trap site. Independent of its source, the temperature of the upwelled water ranges between 15°C and 17°C [*Mittelstaedt*, 1983].

4.1.3 Material and methods

Sample collection

Samples were obtained from a sediment trap moored ~170 km off Cape Blanc (20°45.6'N, 18°41.9'W) at 1277 meters below sea level (mbsl), 1416 m above sea floor (Figure 4.1-1). The sediment trap with a surface opening

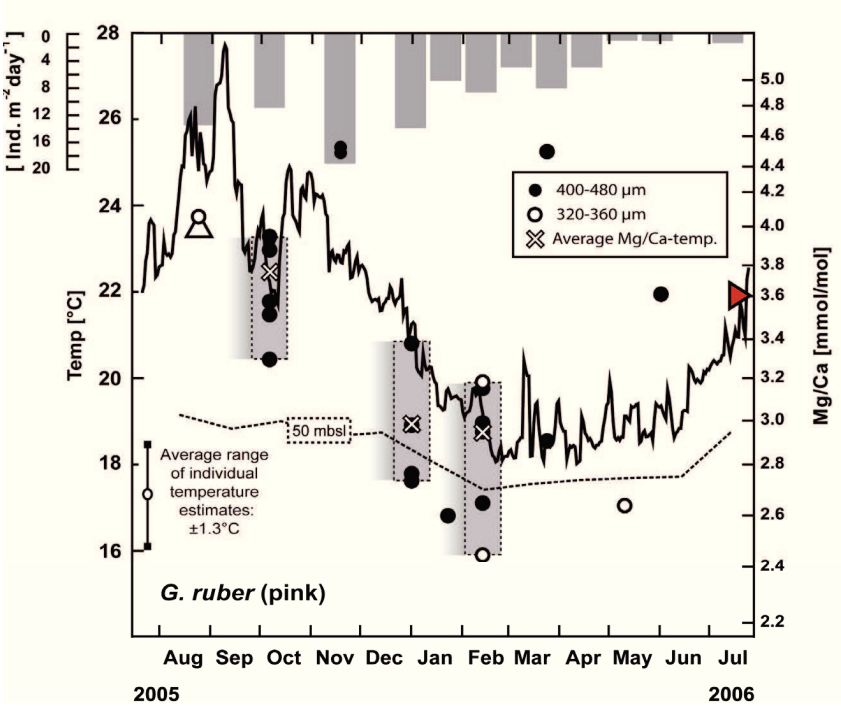

Figure 4.1-2. Single specimen Mg/Ca ratios and Mg/Ca temperatures of *G. ruber* (pink) compared to SST. The black solid line shows the daily SST and is derived from the advanced very-high-resolution radiometer at 20°22.5'N, 18°22.5'W. The dashed line indicates monthly averaged temperatures at a depth of 50 m from the WOA 05. The grey bars indicate the range of individual Mg/Ca temperatures, when the *Regenberg et al.* [2009] calibration after the ACD of *Mulitza et al.* [2004] is used. Shaded grey bars indicate two weeks, which corresponds to the period during which the majority of the shell mass is precipitated**.** All individual data points are calculated after the *Regenberg et al.* [2009] calibration. The grey bars at the top indicate the shell flux of *G. ruber* (pink) to the sediment trap. Where no bars are shown, no *G. ruber* (pink) were collected. The white triangle indicates the Mg/Ca temperature derived from the multi-specimen analysis of 10 specimens. The red triangle on the axis indicates the flux-weighted annual mean Mg/Ca ratio.

of 0.5 m^2 was equipped with 20 collecting cups and poisoned with $HgCl_2$. Samples were collected in intervals of 21.5 days between 25 July 2005 and 28 September 2006. Recovery and redeployment took place during R/V *Poseidon* cruise 344 [*Fischer et al.*, 2008]. Every cup was divided into 5 aliquots using a rotating splitter, of which one was used for this study. When possible, additional aliquots were used to obtain enough specimens for analysis. The shallow depth of the sediment trap precludes any dissolution of the samples. Specimens of ~420 µm size (as used in this study) sink at 1295 m day^{-1} [*Takahashi and Bé*, 1984] and thus reach the sediment trap within about one day. With an approximate eddy kinetic energy of 40 cm^2 s^{-2} at the study site [*Hecht and Hasumi*, 2008] the horizontal averaging scale for a sediment trap at 1000 m depth ranges between 1 and 10 km [*Siegel et al.*, 1990].

The top centimeter of multicore GeoB 7408-2 at 20°17.4'N, 18°15.0'W from a water depth of 1935 m, obtained during R/V *Poseidon* cruise 272 [*Meggers et al.*, 2002] was used to study sedimentary shells.

Individual specimens were picked and their size and morphology noted under the binocular microscope. Most *G. inflata* (d'Orbigny) specimens had four chambers in the last whorl and had moderately thickened walls. All *G. ruber* specimens were strictly from the *G. ruber* sensu stricto morphotype [*Wang*, 2000].

Cleaning procedures

As the foraminifera originate from a sediment trap that was located well above the sea floor, only oxidative cleaning was performed as organic matter can contaminate Mg/Ca measurements [e.g. *Hastings et al.*, 1996; *Barker et al.*, 2003]. We used a flow-through system [*Haley and Klinkhammer*, 2002] run offline to clean single specimens with minimal sample loss. Sample loss is significant using traditional cleaning techniques [*Boyle*, 1981; *Barker et al.*, 2003] especially with small sample sizes. In the flow-through system, we placed single specimens between two PTFE filters and subjected them to a constant flow (2 ml min^{-1}) of suprapure H_2O_2 (30%) diluted to 1% in 0.1 M analytical grade NaOH (heated to ~60°C) for >20 min. The samples were then rinsed for 46 min in a flow (6 min at 4 ml min^{-1}, then 40 min at 1 ml min^{-1}) of pure water (>18 MΩcm). To avoid dissolution during rinsing, the *pH* of the deionised water was kept above 7 by adding a few drops of suprapure NH_3 solution. After cleaning individuals were taken off the filter, examined under the binocular microscope to determine if they remained intact during cleaning, before

being transferred to clean vials and dissolved in 500 µl thermally distilled (TD) 0.075M HNO_3. Samples that broke during cleaning are not considered. After centrifugation for 10 min at 6000 rpm the sample solution was transferred to clean vials for measurement.

For multi-specimen analysis of sediment samples, 10 *G. inflata* specimens were picked from the 400-480 µm size fraction. Cleaning was applied according to *Barker et al.* [2003]. The solution was then centrifuged (10 min at 6000 rpm) and transferred into clean tubes and diluted for measurement.

Data acquisition

Mg/Ca ratios were acquired using two approaches: The thin shells of *G. ruber* (pink and white) produced solutions with low Ca concentrations requiring Mg/Ca ratios to be determined with the more sensitive inductively coupled plasma mass-spectrometry (ICP-MS) technique. The Ca concentrations of the sample solutions were first measured on a Perkin-Elmer Optima 3300R inductively coupled plasma–optical emission spectrometer (ICP-OES) equipped with an ultrasonic nebulizer U-5000 AT (Cetac Technologies Inc.) at the faculty of Geosciences, University of Bremen. Samples for ICP-MS analysis were then diluted to have Ca concentrations of 2 or 5 ppm. Standard solutions with the same Ca concentration were prepared gravimetrically from single element solutions to have Mg/Ca ratios of 4.90 mmol/mol (for measurements of *G. ruber* (pink and white)) and 1.92 mmol/mol (for measurements of *G. inflata*). Mg/Ca ratios were determined using the method of *Rosenthal et al.* [1999] from intensities measured on a Thermo-Finnigan Element 2 sector field ICP-MS at the University of Bremen. During this study the measured Mg/Ca ratios of carbonate reference materials ECRM 752-1 and JCt-1 diluted like the samples, were on average 3.69 mmol/mol (n=19; σ=0.03 mmol/mol), and 1.28 mmol/mol (n=7; σ= 0.01 mmol/mol), respectively. This is in good agreement with the reported Mg/Ca ratios of 3.75 mmol/mol for the ECRM 752-1 [*Greaves et al.*, 2008] and 1.25 mmol/mol for the JCt-1 [*Okai et al.*, 2004]. All blanks analyzed were below the average detection limits of 0.011 ppb Mg and 1.49 ppb Ca.

The relatively thick shells of *G. inflata* contained enough $CaCO_3$ for the determination of Mg/Ca ratios using ICP-OES. Potential drift was monitored by analysis of an in-house standard solution. Values from different ICP-OES analytical sessions were normalized using this standard solution.

Mg/Ca ratios of *G. ruber* (pink), *G. ruber* (white) and *G. inflata* were used to

calculate temperatures during calcification using the calibrations listed in Table 4.1-S1. Shell mass was calculated from the Ca concentration of the sample solution assuming that Ca in the sample solution derives solely from $CaCO_3$ of the dissolved specimen [*Yu et al*. 2008].

Statistics

To approximate the value that would be expected in the sedimentary record, Mg/Ca values of the cups that contained enough specimens for analysis were flux-weighted by multiplying each value by the ratio of the flux of that cup to the total flux, and then summing the respective values to produce a single value. This must be considered a first order approximation since the Mg/Ca ratio could not be measured for foraminifera from every cup so some periods of the year are not considered.

For the interpretation of the average Mg/Ca ratios from 123 specimens of *G. inflata* that were collected throughout the year, it is necessary to calculate if the average is representative and acceptably accurate. The accuracy of the calculation of the average Mg/Ca ratio is given by *e* (equation 4.1-1), at the 95% confidence level, specified by α=0.05. σ^2 is the variance and n the number of samples.

$$e = \sqrt{\frac{z^2\,(1-\frac{\alpha}{2})\,\sigma^2}{n}} \qquad (4.1\text{-}1)$$

We use the quantile $z_{0.975}$=1.96 for a standardized normal distribution, which can be approximately assumed for random samples with n>30. Equation 4.1-1 uses the variance σ^2 of the total statistical population. Since we only have data on a subpopulation, we have to approximate σ^2 using equation 4.1-2, where x_i is the respective sample, $\bar{x}$ is the average of all samples and $E(S^2)$ is the expected value of σ^2.

$$S^2 = \frac{1}{n-1}\sum_{i=1}^{n}(x_i - \bar{x})^2 \qquad (4.1\text{-}2)$$

The 95% confidence interval of the average Mg/Ca ratio is calculated according to equation 4.1-3, where s is the standard deviation of all samples. Again, we use the quantile $z_{0.975}$=1.96, defining the 95% confidence level, with α=0.05.

$$\left[\bar{x} - z\,(1-\frac{\alpha}{2}) - \frac{s}{\sqrt{n}}, \bar{x} + z\,(1-\frac{\alpha}{2})\frac{s}{\sqrt{n}}\right] \qquad (4.1\text{-}3)$$

In order to estimate the change of the variance that would be statistically significant and therefore detectable, we calculate the confidence interval of the variance, according to equation 4.1-4, where S is the standard deviation, n the number of samples and α=0.05 defines the level of confidence of 95%.

Since Mg/Ca ratios lack symmetry, mean values and variance were calculated in

logarithmic space and then reconverted to sample space. To minimize the effects of potential outliers, we do not interpret data lying further than 2σ from the sample mean.

$$\left[\frac{(n-1)*S^2}{\chi^2(n-1,\frac{\alpha}{2})},\frac{(n-1)*S^2}{\chi^2(n-1,1-\frac{\alpha}{2})}\right] \quad (4.1\text{-}4)$$

4.1.4 Results

***G. ruber* (pink)**

Unbroken specimens of *G. ruber* (pink) were analysed from 9 out of 16 cups (Table 4.1-S2). Individual Mg/Ca ratios of *G. ruber* (pink) show strong seasonal differences ranging between 2.45 mmol/mol (November 2005) and 4.53 mmol/mol (February 2006) (Figure 4.1-2).

Mg/Ca ratios of single specimens of the surface dweller *G. ruber* (pink) show strong variability within the sampling intervals, with a maximum intra-cup range of 0.73 mmol/mol during February 2006 (Table 4.1-S2). The mean deviation of individual measurements from the average Mg/Ca ratio within the sampling intervals was 0.27 mmol/mol. Mg/Ca values show no systematic differences between larger and smaller specimens within the limited size range investigated. Two outliers in December 2005 and March 2006 with Mg/Ca ratios corresponding to temperatures more than 4°C different from the measured SST (see section 4.1.5: *G. ruber* (pink)) are not included in the discussion. A multi-specimen analysis from the cup spanning the period 15 August 2005 to 6 September 2005 yields a Mg/Ca ratio of 3.98 mmol/mol.

G. ruber (pink) was collected throughout the year with highest fluxes between August 2005 and December 2005 (max. 19 individuals m^{-2} day^{-1} during November 2005). During the time of highest fluxes, highly variable flux rates were observed and in some cups no *G. ruber* (pink) were found at all. The estimation of flux rates is based on samples collected from splits that contained a substantial amount of plankton and other collected material. Some specimens might therefore have been overlooked and the interpretation of flux rates should be made with some caution. The flux weighted annual Mg/Ca ratio is 3.57 mmol/mol.

***G. ruber* (white)**

Unbroken specimens of *G. ruber* (white) were analysed from 11 out of 16 cups (Table 4.1-S2). The highest Mg/Ca ratio of 4.94 mmol/mol was recorded in January 2006 (Figure 4.1-3) and the lowest Mg/Ca ratio of 2.20 mmol/mol was recorded in June 2006. Within the sampling intervals, Mg/Ca ratios of single specimens of *G. ruber* (white) show pronounced variability, with a maximum intra-cup range of

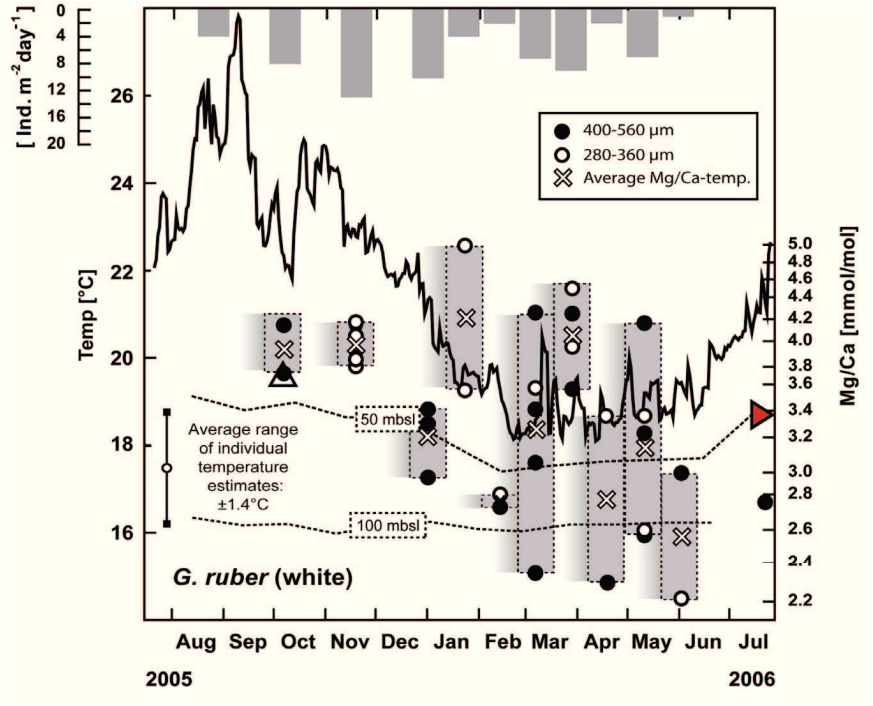

Figure 4.1-3. Single specimen Mg/Ca ratios and Mg/Ca temperatures of *G. ruber* (white) compared to SST. Black line shows the daily SST and is derived from the advanced very-high-resolution radiometer at 20°22.5' N, 18°22.5' W. Shaded grey bars indicate two weeks, which corresponds to the period during which the majority of the shell mass is precipitated. Dashed lines indicate monthly averaged temperatures at depths of 50 m and 100 m from the WOA 05. Mg/Ca temperatures are calculated after the *Elderfield and Ganssen* [2000] calibration. The grey bars at the top indicate the shell flux of *G. ruber* (white) to the sediment trap. Where no bars are shown, no *G. ruber* (white) were collected The white triangle indicates the Mg/Ca temperature derived from the multi-specimen analysis of 10 specimens. The red triangle on the axis indicates the flux-weighted annual mean Mg/Ca ratio.

1.91 mmol/mol in March 2006 (Figure 4.1-3). On average, the deviation of individual measurements from the average Mg/Ca ratio within the sampling intervals was 0.45 mmol/mol. Mg/Ca values show no systematic differences between larger and smaller specimens or between different sampling intervals. A multi-specimen analysis from the cup spanning the period 27 September 2005 to 9 October 2005 yields a Mg/Ca ratio of 3.65 mmol/mol.

G. ruber (white) was collected throughout the year with only moderate annual variability (max. 13 individuals m^{-2} day^{-1} during November 2005). Between August 2005 and November 2005 strong changes in flux rates were observed and in some cups, no *G. ruber* (white) specimens were found at all. As noted above, the interpretation of flux rates should be made with some caution. The flux weighted annual Mg/Ca ratio is 3.38 mmol/mol.

G. inflata

Unbroken specimens of *G. inflata* were analysed from all 16 cups (Table 4.1-S2). The highest Mg/Ca ratio of 3.72 mmol/mol was recorded in January 2006, while the lowest Mg/Ca ratio of 1.53 mmol/mol was recorded in April 2006 (Figure 4.1-1).

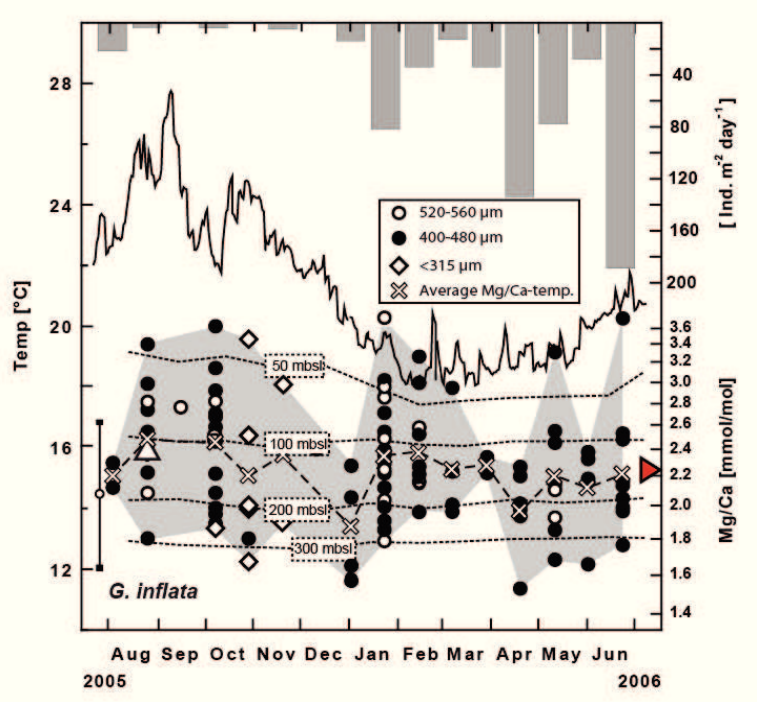

Figure 4.1-4. Single specimen Mg/Ca ratios, Mg/Ca temperatures, and flux rates of *G. inflata* off Cape Blanc. The black line indicates the daily SST and is derived from the advanced very-high-resolution radiometer at 20°22.5' N, 18°22.5'W. The narrow spaced dashed lines indicate monthly averaged temperatures at the shown depths from the WOA 05. Crosses connected with a wide spaced dashed line indicate average Mg/Ca temperatures. The vertical bar indicates the average range of individual temperature estimates of ±2.5°C. Mg/Ca temperatures are calculated after the *Elderfield and Ganssen* [2000] calibration. The grey bars at the top indicate the shell flux of *G. inflata* to the sediment trap. The white triangle indicates the Mg/Ca temperature derived from the multi-specimen analysis of 10 specimens. The red triangle on the axis indicates the flux-weighted annual mean Mg/Ca ratio.

A seasonal trend between different sampling intervals for *G. inflata* is not apparent, however strong variations in the Mg/Ca ratio occur within each of the sampling intervals. The largest intra-cup range in the Mg/Ca ratio of *G. inflata* of 1.95 mmol/mol is recorded during June 2006 (Figure 4.1-1). On average, the deviation of individual values around the average Mg/Ca ratio of a sampling interval is 0.64 mmol/mol. A multi-specimen analysis from the cup spanning the period from 15 August 2005 to 6 September 2005 yields a Mg/Ca ratio of 2.42 mmol/mol.

We found pronounced differences in the flux of *G. inflata* at the study site (Figure 4.1-1). From August 2005 to January 2006, few specimens were collected (max. 21 individuals m^{-2} day^{-1}). From January 2006 to the end of June 2006, fluxes increased to reach a maximum of 188 individuals m^{-2} day^{-1} during June 2006. The flux weighted Mg/Ca ratio is 2.23 mmol/mol. The Mg/Ca ratio of a multi-specimen coretop sample from GeoB 7408-2 is 2.23 mmol/mol.

4.1.5 Discussion

Seasonal shell abundance

G. ruber (pink) and *G. ruber* (white) were collected throughout the year (Figure 4.1-2 and Figure 4.1-3). Fluxes of both species were very variable. Higher fluxes between August 2005 and January 2006 were found for both species, however this is more pronounced for *G. ruber* (pink) than for *G. ruber* (white). Fluxes of *G. inflata* between January 2006 and June 2006 were much higher than and nearly a mirror-image of the fluxes of *G. ruber* (pink). The differences in abundance are assumed to result from the exceptional seasonal changes in the study area. In the upper water column, these changes are controlled by large differences in SST. The large Cape Blanc upwelling filament is also important. In September 2005, the filament moved right over the sediment trap (Figure 4.1-1), with high nutrient concentrations at the surface evident by high chlorophyll *a* concentrations. Conversely, in March 2006, the filament was absent in the study area (Figure 4.1-1). Water temperatures, the thermal stratification of the water column and nutrient availability are likely to act in concert to control shell fluxes at the study site.

G. ruber (pink) was most abundant during summer/fall with warm sea surface temperatures. This is in agreement with the study of *Wilke et al.* [2009] who showed that *G. ruber* (pink) is most abundant when surface mixed layer temperatures are higher than 20°C. Additionally, the strong thermal stratification during the summer has been reported to favor *G. ruber* [*Sautter and Sancetta*, 1992]. High nutrient levels evident by high chlorophyll *a* concentrations (Figure 4.1-1) are also expected to favor the development of *G. ruber* (pink).

In contrast, *G. inflata* flux rates were lowest between August 2005 and January 2006. Since *G. inflata* records very similar Mg/Ca temperatures throughout the year, water temperatures are expected to play a minor, if any, role in controlling flux rates. It is assumed that nutrient availability controls flux rates of *G. inflata* in the study area. CTD casts show that the maximum chlorophyll *a* concentration at different seasons is found above 50 mbsl (Figure 4.1-S1). It is suggested that *G. inflata* cannot make use of the high nutrient concentrations during times of a well stratified water column in summer. Contrastingly, during the main upwelling season in winter/spring, *G. inflata* is more suited to the low nutrient concentrations (Figure 4.1-1) than *G. ruber* (pink and white).

Mg/Ca temperature equations

***G. ruber* (pink)**

We compare measured SSTs to Mg/Ca ratios from individual *G. ruber* (pink) shells and interpret differences as a result of calcification temperature. The exponential fit to our data is remarkably similar to the *Regenberg et al.* [2009] equation (Figure 4.1-5). Mg/Ca temperatures derived from this equation are realistic for *G. ruber* (pink) in the study area (Figure 4.1-2). Using different Mg/Ca temperature equations, Mg/Ca temperatures range between 18.1°C and 27.2°C [*Anand et al.*, 2003] (single species), 20.7°C and 27.5°C [*Anand et al.*, 2003] (multi-species), 15.5°C and 21.6°C [*Elderfield and Ganssen*, 2000], and 15.9°C and 25.4°C [*Regenberg et al.*, 2009].

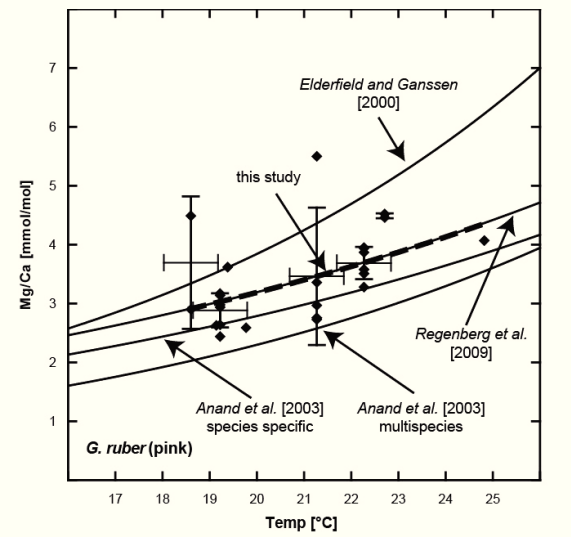

Figure 4.1-5. Comparison of *G. ruber* (pink) Mg/Ca ratios from this study to published Mg/Ca temperature calibrations. The lines represent Mg/Ca temperature calibrations of *Elderfield and Ganssen* [2000], *Anand et al.* [2003], and *Regenberg et al.* [2009] using the ACD of *Mulitza et al.* [2004]. Mg/Ca ratios of *G. ruber* (pink) from this study are shown as diamonds and the exponential fit to these ratios is shown as a dashed line. Vertical error bars show sample standard deviation, horizontal error bars show root mean square error [°C] of the advanced very-high-resolution radiometer derived SST from in situ SST as given by *She et al.* [2007].

It is suggested that the *Regenberg et al.* [2009] equation is best suited for single *G. ruber* (pink) specimens in this study for several reasons: It is species specific, in contrast to the *Elderfield et al.* [2000] equation that does not include *G. ruber* (pink). Moreover, it is based on a larger amount of specimens (20-25) than the *Anand et al.* [2003] calibration (5-15 specimens). It therefore is likely that the Mg/Ca ratios derived from the multi-specimen analysis include a larger range of Mg/Ca ratios and this might be crucial when working with single specimens. In addition, the *Regenberg et al.* [2009] equation was generated solely from samples originating from the tropics, the preferred habitat of *G. ruber* (pink).

Using the *Regenberg et al.* [2009] equation, maximum Mg/Ca temperatures for most individual specimens during one collecting interval closely match the advanced very-high-resolution radiometer derived SST (Figure 4.1-2). We assume that these temperatures correspond to individuals that calcified in the uppermost part of the water column and that highest Mg/Ca ratios represent temperatures near the sea surface during the respective

interval. Our observations are in line with *Tedesco et al.* [2007] who state that *G. ruber* (pink) is capable of accurately estimating SSTs throughout the year.

Mg/Ca temperatures from sediment trap studies [e.g. *McConnell and Thunell*, 2005; *Mohtadi et al.*, 2005] rely on the multi-specimen analyses of at least 10 specimens providing an averaged temperature. We conducted a multi-specimen analysis using 10 specimens from the collecting cup spanning the period from 15 August to 6 September 2005, that produced a Mg/Ca temperature of 23.4°C, similar to one single specimen Mg/Ca temperature of 23.8°C derived from this period. Not enough single specimens could be analysed from this collecting cup to derive an average Mg/Ca temperature. The flux-weighted annual Mg/Ca value of 3.57 mmol/mol of all *G. ruber* (pink) individuals analysed corresponds to a temperature of 21.7, thus slightly lower than the annual average temperature of 22.9°C. This suggests that *G. ruber* (pink) in the study area can be used in sediment archives to reconstruct temperatures that approximate the annual average sea surface temperature.

G. ruber (white)

The range of Mg/Ca ratios measured from the shells of *G. ruber* (white) is large in comparison with the other species. However, the range between the lowest (2.20 mmol/mol) and highest (4.94 mmol/mol) Mg/Ca ratios is similar to that found by *Sadekov et al.* [2008] for *G. ruber* (1.75 mmol/mol to 5.53 mmol/mol at a site exhibiting a SST seasonality of 3.9°C).

Comparison of measured SST with Mg/Ca ratios from individual *G. ruber* (white) shells (Figure 4.1-6) does not fit to any published Mg/Ca temperature equation.

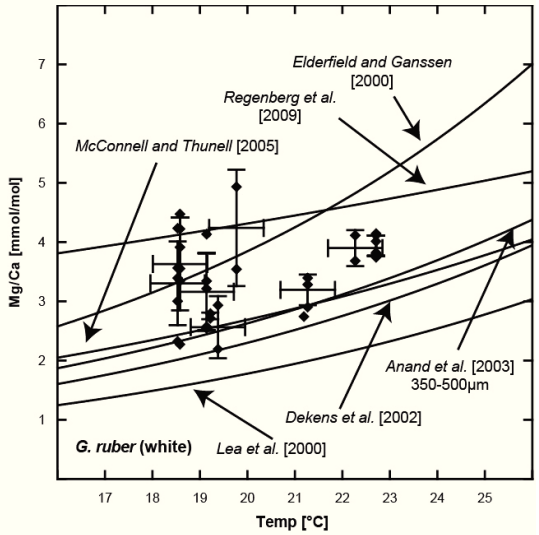

Figure 4.1-6. Comparison of *G. ruber* (white) Mg/Ca ratios from this study to published Mg/Ca temperature calibrations. The lines represent Mg/Ca temperature calibrations of *Elderfield and Ganssen* [2000], *Regenberg et al.* [2009] using the ACD of *Mulitza et al.* [2004], *McConnell and Thunell* [2005], *Anand et al.* [2003], *Dekens et al.* [2002], and *Lea et al.* [2000]. Mg/Ca ratios of *G. ruber* (white) from this study are shown as diamonds. Vertical error bars show sample standard deviation, horizontal error bars show root mean square error [°C] of the advanced very-high-resolution radiometer derived SST from in situ SST as given by *She et al.* [2007].

We can exclude that the mismatch was caused by contamination of the shells

(monitored by analysis of Mn/Ca and Fe/Ca ratios) and the cleaning was identical for *G. ruber* (pink). Most Mg/Ca temperature equations [*Lea et al.*, 2000; *Dekens et al.*, 2002; *Anand et al.*, 2003; *McConnell and Thunell*, 2005] yield temperatures substantially higher than the SST during the sampling interval at the study site and also in the adjacent areas (Figure 4.1-2). Mg/Ca temperature estimations during the time of coldest SSTs are listed in Table 4.1-S3. The equations of *Regenberg et al.* [2009], which are dependent on different apparent calcification depths (ACDs), are an exception to the general overestimation of SSTs. However, the coldest Mg/Ca temperatures derived using the *Regenberg et al.* [2009] equation are unrealistically low during most of the year. The equation of *Elderfield and Ganssen* [2000] yields the most realistic temperatures in this study. The warmest temperatures are however still higher than the SST during the respective collecting intervals (Figure 4.1-3). Lateral advection seems unlikely due to the low horizontal averaging scale at the study site (see section 4.1.3). The coldest temperatures using the *Elderfield and Ganssen* [2000] equation correspond to unrealistically low calcification considering that *G. ruber* (white) is a symbiotic species and thrives to remain in the photic zone.

An additional factor that could explain some of the variability is the pH of the ambient seawater. *Lea et al.* [1999] and *Russell et al.* [2004] have demonstrated that a 0.1 unit pH increase can account for a 6-16% decrease of the Mg/Ca ratio in the shells of *Globigerina bulloides* and *Orbulina universa.* A decreased pH in upwelled waters along the NW African margin of 0.2 units [*Weichart*, 1980] could hence account for a 12-32% increase of the Mg/Ca ratios in our samples. During times of strong upwelling in late spring [e.g. *Pelegrí et al.*, 2005], this could cause an increase in Mg/Ca ratio from 3.14 mmol/mol to 4.14 mmol/mol, in line with the highest Mg/Ca ratio observed between 30 April 2006 and 22 May 2006.

We conducted a multi-specimen analysis consisting of 10 *G. ruber* (white) specimens from the collecting cup spanning the period from 27 September to 19 October 2005, which yielded a Mg/Ca temperature of 19.5°C. This is only 0.6°C lower than the average Mg/Ca temperature of the individual specimen analysis (n=2). The flux-weighted Mg/Ca value of 3.38 mmol/mol corresponds to a temperature of 18.7°C, that is close to winter temperatures (e.g. 17 February 2006: 18.7°C). The flux weighted Mg/Ca ratio of *G. ruber* (white) in this study is however sensitive to a potential sampling bias. For example, a flux of

13 ind. m^{-2} day^{-1} (as determined from 9 November to 1 December) occurring during the time of warmest SST from 25 August to 27 September, would increase the flux weighted Mg/Ca temperature by 2.7°C (using the equation of *Elderfield and Ganssen* [2000]). Any interpretation of the flux weighted average should therefore be made with care.

G. inflata

We found a wide range of Mg/Ca ratios during each sampling interval (Figure 4.1-4) and interpret the varying Mg/Ca ratios as a result of different calcification depths and slight variations in crust calcite thickness. For the approximation of calcification depths, it is important to account for the influence of crust calcite on Mg/Ca ratios, because crust calcite can significantly change the Mg/Ca ratio of planktonic foraminfera [e.g. *Nürnberg et al.*, 1996; *McKenna and Prell*, 2004; *Hathorne et al.*, 2009; *Groeneveld and Chiessi*, 2011]. *Groeneveld and Chiessi* [2011] show that specimens of *G. inflata* with thick crusts yield systematically lower Mg/Ca ratios and emphasize the importance of defining a clear and narrow state of encrustation of the *G. inflata* specimens being used. SEM images show the surface texture of specimens from the sediment trap (Figure 4.1-S2) suggesting moderate crust addition. We calculated the shell weights of *G. inflata*, in order to identify unusually heavy shells, since the addition of crust calcite would lead to heavier shells [*Caron et al.*, 1990; *Lohmann*, 1995]. Shell weights within the respective size fractions range between 9.65 µg and 59.59 µg. Average weights within the respective size fractions are in accordance with smaller and larger shell sizes (Table 4.1-S2 and Figure 4.1-S3).

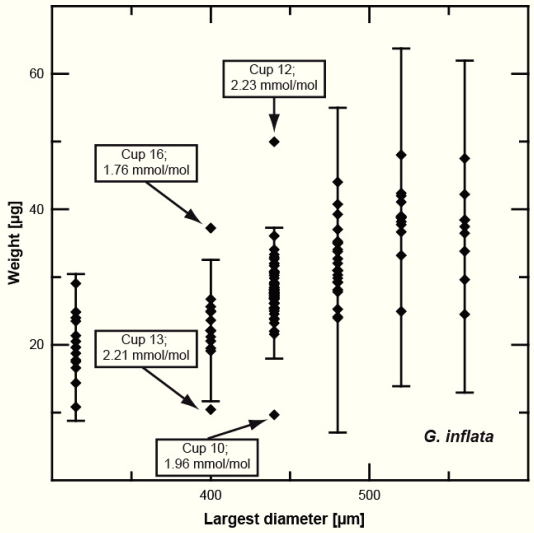

Figure 4.1-7. Size versus single shell weight in the respective size fraction of *G. inflata* from the sediment trap (located at 20°45.6'N, 18°41.9'W). Bars indicate the range between the upper and lower quartile. Outliers and their Mg/Ca ratios are indicated.

Within size fractions, some variability of the mass of individual specimens is found (Figure 4.1-7). We compare shells of the same size to calculated shell mass, in order to identify samples that are potentially thickened by crust calcite. Samples are normally distributed, when the most lightweight and most heavy sample is excluded from the 440 µm size fraction

(Shapiro-Wilk tested at a 95% level of confidence). Four outliers can be identified. The lightest and heaviest samples from the 440 µm size fraction deviate from a normal distribution. Moreover the lightest and heaviest samples from the 400 µm size fraction are outside the upper and lower quartiles. The Mg/Ca ratios of these outliers are however not noticeably different from all other specimens (Figure 4.1-8). We therefore conclude that there is no simple relationship between the amount of crust calcite and the Mg/Ca ratios of *G. inflata* in this study.

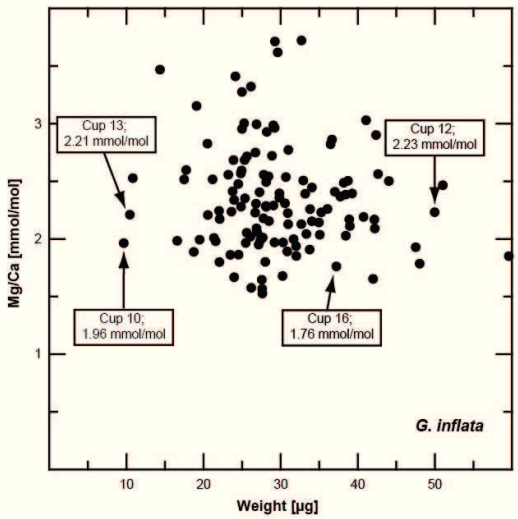

Figure 4.1-8. Weight versus single shell Mg/Ca ratios of *G. inflata* from the sediment trap (located at 20°45.6'N, 18°41.9'W). Outliers and their Mg/Ca ratios are indicated.

Many studies have recognized the potential of *G. inflata* for temperature reconstructions at the base of the seasonal thermocline [e.g. *Thornalley et al.*, 2009] but the existing temperature equations for this species differ substantially from each other [*Elderfield and Ganssen*, 2000; *Anand et al.*, 2003; *Cléroux et al.*, 2008; *Thornalley et al.*, 2009; *Farmer et al.*, 2010; *Groeneveld and Chiessi*, 2011]. Calculation of Mg/Ca temperatures for *G. inflata* using the equations listed in Table 4.1-S1 yields temperature estimates that are either too warm or too cold when compared to World Ocean Atlas temperatures [*Locarnini et al.*, 2006]. In Table 4.1-S4, we compare Mg/Ca temperature estimates from individual *G. inflata* specimens collected between 27 September and 19 October 2005 to monthly average World Ocean Atlas water column temperatures during October [*Locarnini et al.*, 2006]. The equations of *Anand et al.* [2003], *Cléroux et al.* [2008], and *Farmer et al.* [2010] yield warmest temperatures that are 5.4°C, 6.8°C, and 13.0°C above the observed SST in the middle of the collecting period. In contrast, the equations of *Elderfield and Ganssen* [2000], *Thornalley et al.* [2009], and *Groeneveld and Chiessi* [2011] yield temperature estimates that fit with the water column observations.

A multi-specimen analysis of 10 *G. inflata* specimens from the collecting cup spanning the period from 15 August to 6 September 2005, yields a Mg/Ca temperature of 16.0°C, similar to the average Mg/Ca temperature of 16.3°C

from the individual specimen analyses. The close match of the average temperature derived from the multi-specimen analysis and the analyses of single specimens confirms the excellent potential of our approach to measure single specimens, in order to gain information about the overall variability in Mg/Ca temperatures within a population.

The average Mg/Ca temperature of *G. inflata* from the sediment trap samples reflects an annual mean temperature at a depth of about 150 m in the study area (Figure 4.1-1). The largest deviations from the average Mg/Ca temperature are measured in August 2005 (+1.1°C) and December (-1.8°C). As these periods coincide with times of low flux, they are unlikely to lead to a seasonal bias in the sedimentary record. This is supported by the multi-specimen analysis of *G. inflata* from coretop GeoB7408-2, which yields a Mg/Ca ratio of 2.23 mmol/mol. The average Mg/Ca ratio of all *G. inflata* samples from the sediment trap is between 2.23 mmol/mol and 2.38 mmol/mol at a confidence level of 95% and the flux-weighted average is also 2.23 mmol/mol. The good match with the multi-specimen analysis from the sedimentary record supports the assumption that there is no seasonal bias in the Mg/Ca signal of *G. inflata*.

Comparison of inferred calcification depths to reported habitat depths from plankton tows

The Mg/Ca temperature estimates derived using the *Regenberg et al.* [2009] equation mostly correspond to a calcification depth for *G. ruber* (pink) between the surface and ~30 m. This is within the mixed layer at a habitat depth reported in tow studies for this species [e.g. *Wilke et al.,* 2009]. An exception is the lowest temperature (15.9°C) recorded in February 2006 (Figure 4.1-2). Though very low, we assume that this temperature is a realistic record of the calcification temperature at the study site, due to the low horizontal averaging scale at the study site (see section 4.1.3). One possibility could be that the specimen calcified within the upwelled water. Everywhere along the NW African coast, this has a temperature of 15 - 17°C [*Mittelstaedt*, 1983].

Mg/Ca temperatures recorded by *G. ruber* (white) using the *Elderfield and Ganssen* [2000] equation correspond to calcification depths between the surface and ~40 m (October 2005), 0 m (January 2006), ~110 m (February 2006), and ~150 m (May 2006) when compared to World Ocean Atlas data (Figure 4.1-3; *Locarnini et al.*, 2006). It is difficult to reconcile these calcification depths given the fact that *G. ruber* (white) has symbiotic dinoflagellates and should be restricted to

the photic zone. As noted above the calcification depths for *G. ruber* (white) should be treated with caution.

Calculated apparent calcification depths of *G. inflata* mostly correspond to the upper 400 m [*Elderfield and Ganssen*, 2000 equation], 500 m [*Groeneveld and Chiessi*, 2011 equation], and 75 to 500 m [*Thornalley et al.*, 2009 equation] of the water column. In this study, we use the *Elderfield and Ganssen* [2000] equation generated using North Atlantic sediment samples. When compared to World Ocean Atlas data, the majority of our data indicate a shallowest apparent calcification depth between the sea surface and 50 m, hence at the depth of the highest chlorophyll *a* concentration (Figure 4.1-S1), where *G. inflata* can make use of its food source. The mean temperature estimates of the individual sampling intervals are between 16.3°C and 13.4°C, corresponding to calcification depths between about 100 m and 300 m, respectively, hence well below the seasonal thermocline which is at ~ 50 m (Figure 4.1-S1). The interpretation of this large range of calculated calcification depths must account for *G. inflata* calcifying over a wide range of depths, reflected in the depth integrated composition of its shell [*Wilke et al.*, 2006]. It builds part of its shell in the surface mixed layer and the thermocline [*Wilke et al.*, 2006]. The fact that *G. inflata* has small symbiotic algae [*Gastrich et al.*, 1987] suggests that it spends part of the life cycle in the photic zone. However, wall thickening at depth produces crust calcite with a lower Mg/Ca ratio that can constitute a large proportion of the final test mass. This means that apparent calcification depths can be deeper than the depth at which the individuals spent most of their lives.

Implications for paleoceanographic reconstructions

Based on the distribution of single specimen Mg/Ca ratios of *G. ruber* (white), *G. ruber* (pink) and *G. inflata*, it is suggested that in the study area, *G. ruber* (pink) is suitable for investigations of paleo-seasonality. In contrast, *G. ruber* (white) does not appear to be applicable for this purpose in the study area using published Mg/Ca temperature equations. The inferred apparent calcification depth of *G. inflata* below the depth of the seasonal thermocline suggests this species is a recorder of subsurface temperatures. Changes in single specimen maximum and minimum calcification temperatures from sediment core samples could indicate calcification at different subsurface depths in the past.

A study on single specimens of planktonic foraminifera by *Billups and Spero* [1996] demonstrates that the range

of $\delta^{18}O$ values can be used in order to assess seasonal or depth-related calcification temperatures in the paleoceanographic past. *Koutavas et al.* [2006] show that a change in total variance between populations of planktonic foraminifera (*G. ruber* (white)) can provide information on ENSO and seasonal variability. Accordingly, we suggest that a change in Mg/Ca variance and Mg/Ca range can be used as an indicator for environmental variability in the study area when measured on downcore samples.

***G. ruber* (pink)**

The present day difference between highest and lowest Mg/Ca ratios of single *G. ruber* (pink) specimens in the study area over an annual cycle is 2.08 mmol/mol (Table 4.1-S2), corresponding to the difference between warmest and coldest temperatures under which the specimens calcified (Figure 4.1-2). Likewise in the sedimentary record, the difference between highest and lowest Mg/Ca ratios is expected to indicate the range of temperatures under which the specimens calcified. It is suggested that changes in the range between highest and lowest Mg/Ca ratios in the sedimentary record are a measure of interannual changes in the range between highest and lowest SST. A prerequisite for such interpretation is that potential artifacts introduced by variable sedimentation rate and bioturbation can be minimized and natural variability can be confined.

The annual Mg/Ca variance of *G. ruber* (pink) in this study is 1.43 mmol/mol and the 95% confidence interval of this variance ranges from 0.88 mmol/mol to 2.73 mmol/mol. This means that when a different variance measured from sedimentary specimens (with its own confidence interval) falls outside this estimate, it would be significantly different from the variance of the sample investigated here. A hypothetical decrease of variance below this threshold of 0.88 mmol/mol would mean a decrease of variance by 38%. If we assume that the variance relative to the total range of values remains the same (69%) in the past in the study area, a significant decrease of the total variance (below 0.88 mmol/mol) requires a decrease of the Mg/Ca range from 2.08 mmol/mol to 1.28 mmol/mol. Using the equation of *Regenberg et al.* [2009], this would represent a decrease in the temperature range of 4.0°C, from 10.0°C to 6.0°C. We did not calculate what increase in the temperature range would be significant as the modern range is already large (10°C) and a substantial increase is rather unlikely.

G. inflata

The annual variance of *G. inflata* in this study is 1.37 mmol/mol and the 95%

confidence interval of this variance ranges from 1.08 mmol/mol to 1.80 mmol/mol. Again, a variance of sedimentary specimens that falls outside of this confidence interval would be significantly different from the samples investigated here. A decrease of variance beyond the significance threshold of 1.08 mmol/mol would mean a decrease of variance by 21%. If we again hypothesize that the variance relative to the total range of values remains the same (85%) in the study area throughout the past, a significant decrease of the total variance below the significance threshold of 1.08 mmol/mol requires a decrease of the total Mg/Ca range from 1.62 mmol/mol to 1.28 mmol/mol. Using the equation of *Elderfield and Ganssen* [2000], this would represent a decrease in the temperature range of 1.7°C, from 7.6°C to 5.9°C. A reduction of the temperature range of this magnitude was shown by *Billups and Spero* [1996] for the western equatorial Atlantic using individual *Neogloboquadrina dutertrei* shells. *N. dutertrei* is a species that prefers oceanographic conditions similar to *G. inflata*, i.e. upwelling regions and a habitat close to the chlorophyll maximum at the bottom of the mixed layer [*Fairbanks et al.,* 1982]. Between isotopic stage 1 and 2, a decrease of the temperature range of 4.7°C in the western equatorial Atlantic was suggested *Billups and Spero* [1996]. Given the detectable change (1.7°C) of the temperature range suggested in our study, the analysis of single *G. inflata* could prove valuable for detecting changes of thermocline temperatures or calcification depths in the paleoceanographic past.

4.1.6 Conclusions

Mg/Ca thermometry of single specimens of *G. ruber* (pink) is suitable in the upwelling region off Cape Blanc for tracking the seasonal amplitude of SST when applying the Mg/Ca temperature equation of *Regenberg et al.* [2009]. In contrast, Mg/Ca ratios of *G. ruber* (white) do not track seasonal SST using published Mg/Ca temperature equations. The best SST estimate is obtained when using the *Elderfield and Ganssen* [2000] equation. Mg/Ca ratios of single specimens of *G. inflata* do not exhibit any apparent seasonality and are remarkably similar throughout the year. The best SST estimate is also obtained when using the *Elderfield and Ganssen* [2000] equation for *G. inflata*.

Statistical analysis of single specimen Mg/Ca ratios from this study suggests that *G. ruber* (pink) can serve as potential recorder of paleo-seasonality in the sedimentary record. Single specimen Mg/Ca ratios of *G. inflata* are suggested to

track changes of its habitat depth. Changes in the range between highest and lowest Mg/Ca ratios of *G. ruber* (pink) ≥0.80 mmol/mol (4°C) and changes in the range between highest and lowest Mg/Ca ratios of *G. inflata* ≥0.34 mmol/mol (1.7°C) are thought to be indicative of a change of the temperature range in which the specimens calcified.

Acknowledgements

H. Spero made valuable suggestions that greatly improved this manuscript. Sample collection and technical support was provided by The Center for Marine Environmental Sciences (MARUM), University of Bremen. We thank Heike Anders for laboratory assistance and Petra Witte for SEM imaging. Gerald Ganssen and Frank J. C. Peeters are acknowledged for valuable discussions. We thank David Heslop for advice concerning the statistical treatment of the data. ECH and JG were funded by MARUM. We thank Matthias Lange and Wolfgang Schunn for technical support creating the flow-through system funded by MARUM. This study was carried out within the International Graduate College EUROPROX, funded by the Deutsche Forschungsgemeinschaft (DFG).

Appendices to the article are provided below.

Supplement to: Haarmann, T., E. C. Hathorne, M. Mohtadi, J. Groeneveld, M. Kölling, and T. Bickert (2011), Mg/Ca ratios of single planktic foraminifer shells and the potential to reconstruct the thermal seasonality of the water column, Paleoceanography, 26, PA3218, doi:10.1029/2010PA002091.

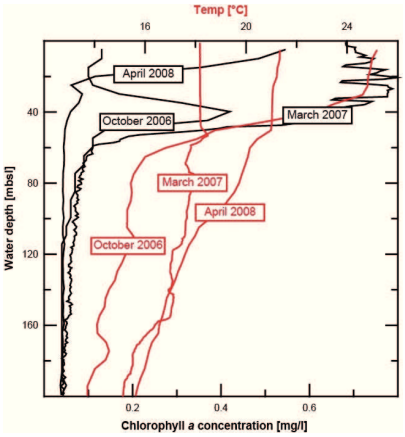

Figure 4.1-S1. Chlorophyll a concentrations and water column temperatures at the location of the sediment trap (located at 20°45.6'N, 18°41.9'W) on 26 October 2006, 25 March 2007, and 24 April 2008.

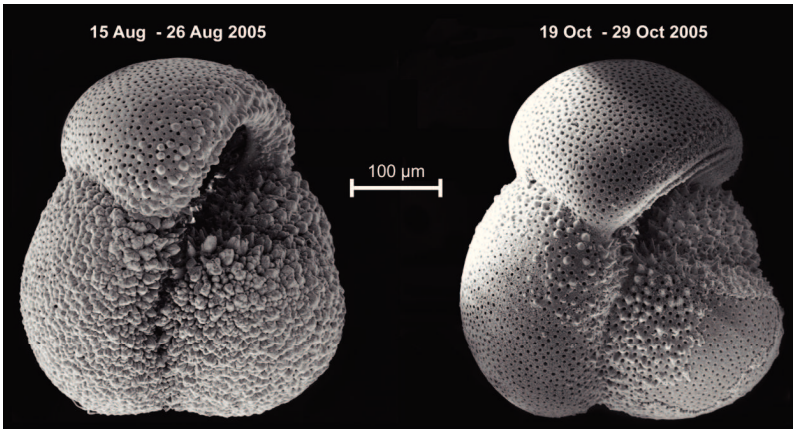

Figure 4.1-S2. SEM images of *G. inflata* specimens collected in between 15 and 26 August 2005 and 19 and 29 October in the sediment trap (located at 20°45.6'N, 18°41.9'W) off Cape Blanc, NW-Africa.

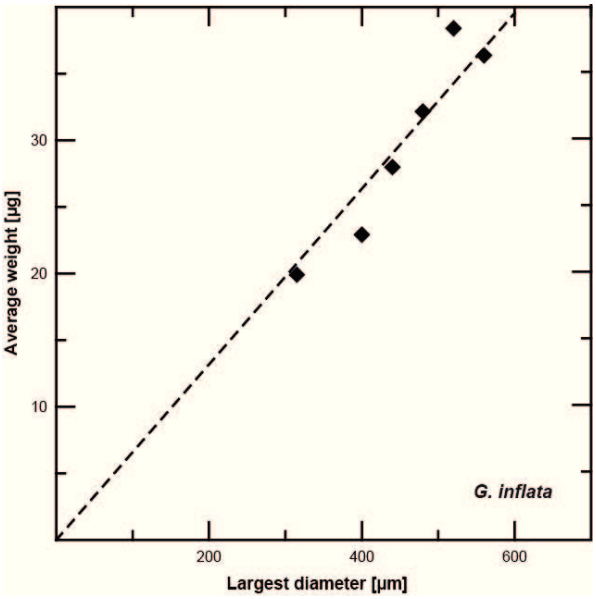

Figure 4.1-S3. Size versus average shell weight in the respective size fraction of *G. inflata* from the sediment trap (located at 20°45.6'N, 18°41.9'W) off Cape Blanc, NW-Africa.

Table 4.1-S1. Calibration equations, where Mg/Ca = A exp(BT)

Species	A	B	Material	Reference	Location
G. ruber (pink) (350-500 µm)	0.73 (±0.17)	0.067 (±0.0.009)	Sediment trap (species specific)	*Anand et al.* [2003]	North Atlantic
G. ruber (pink) (350-500 µm)	0.38 (±0.02)	0.09 (±0.0.003)	Sediment trap (multispecies)	*Anand et al.* [2003]	North Atlantic
G. ruber (pink)	0.52	0.1	Core tops (multispecies)	*Elderfield and Ganssen* [2000]	North Atlantic
G. ruber (pink) (355-400 µm)	0.87	0.065	Core tops	*Regenberg et al*. [2009], ACD after *Mulitza et al.* [2004]	Equatorial Atlantic
G. ruber (white)	0.52	0.1	Core tops (multispecies)	*Elderfield and Ganssen* [2000]	North Atlantic
G. ruber (white) (350-500 µm)	0.48 (±0.07)	0.085 (±0.0.006)	Sediment trap (species specific)	*Anand et al.* [2003]	North Atlantic
G. ruber (white) (212-355 µm)	0.69	0.068	Sediment trap	*McConnell and Thunell* [2005]	Gulf of California
G. ruber (white)	0.30	0.089	Core top	*Lea et al.* [2000]	Equatorial Pacific
G. ruber (white)	2.32	0.031	Core tops	*Regenberg et al.* [2009], ACD after *Mulitza et al.* [2004]	Equatorial Atlantic
G. ruber (white)	1.27	0.051	Core tops	*Regenberg et al.* [2009], ACD after *Bemis et al.* [1998]	Equatorial Atlantic
G. ruber (white)	1.51	0.045	Core tops	*Regenberg et al.* [2009], ACD after *Kim and O'Neil* [1997]	Equatorial Atlantic

Table 4.1-S1 (continued). Calibration equations, where Mg/Ca = A exp(BT)

Species	A	B	Material	Reference	Location
G. ruber (white)	1.28	0.051	Core tops	*Regenberg et al.* [2009], ACD after *Shackleton* [1974]	Equatorial Atlantic
G. ruber (white)	1.87	0.037	Core tops	*Regenberg et al.* [2009], ACD after *Farmer et al.*[2007]	Equatorial Atlantic
G. ruber (white)	2.04	0.034	Core tops	*Regenberg et al.* [2009], ACD after *Thunell et al.* [1999]	Equatorial Atlantic
G. ruber (white)	0.38	0.09	Core tops	*Dekens et al.* [2002]	Equatorial Atlantic and Pacific
G. inflata	0.49	0.1	Core tops	*Elderfield and Ganssen* [2000]	North Atlantic
G. inflata	0.71 (±0.06)	0.056 (±0.006)	Core tops	*Cléroux et al.* [2008]	North Atlantic
G. inflata	0.299 (±0.005)	0.09	Sediment trap	*Anand et al.* [2003]	Sargasso Sea
G. inflata	0.916 (±0.07)	0.039 (±0.006)	Core tops	*Farmer et al.* [2010]	North Atlantic
G. inflata	0.675	0.1	Core tops	*Thornalley et al.* [2009]	North Atlantic
G. inflata	0.72	0.076	Core tops	*Groeneveld and Chiessi* [2011]	South Atlantic

Table 4.1-S2. Sampling dates of sediment trap CBi3-o, duration of opening, Mg/Ca ratios, sizes and weights (calculated from Ca concentrations of the sample solution) of single specimens of *G. ruber* (pink), *G. ruber* (white) and *G. inflata*

Cup	Open	Close	*G. ruber* (pink) Mg/Ca [mmol/mol]	*G. ruber* (pink) size [µm]	*G. ruber* (pink) weight [µg]	*G. ruber* (white) Mg/Ca [mmol/mol]	*G. ruber* (white) size [µm]	*G. ruber* (white) weight [µg]	*G. inflata* Mg/Ca [mmol/mol]	*G. inflata* size [µm]	*G. inflata* weight [µg]
1	25 Jul 2005	15 Aug 2005							2.31	440	30.56
									2.13	400	32.68
2	15 Aug 2005	6 Sep 2005	4.08	360	8.79				2.82	560	36.48
			3.98*	360-400					2.38	560	38.48
									2.09	560	42.21
									3.41	480	24.13
									2.45	480	34.06
									2.99	440	26.87
									2.56	440	23.22
									2.75	400	26.73
									2.41	400	27.26
									2.24	400	23.62
									1.80	400	28.01
									2.42*	440	-
3	6 Sep 2005	27 Sep 2005							2.77	480	31.00
4	27 Sep 2005	19 Oct 2005	3.96	480	16.16	3.69	560	25.40	3.62	560	29.61
			3.88	480	17.92	4.12	480	13.77	2.48	560	24.50
			3.95	440	11.33	3.65*	360-440		3.15	400	19.10
			3.59	440	10.16				2.93	400	28.20
			3.52	440	14.88				2.72	400	25.62
			3.29	440	15.76				2.68	400	23.88
			3.43	320	8.43				2.68	400	25.33
									2.23	400	26.70
									2.09	400	26.87
									1.99	400	27.38
									1.95	400	27.15

Table 4.1-S2.(continued). Sampling dates of sediment trap CBi3-o, duration of opening, Mg/Ca ratios, sizes and weights (calculated from Ca concentrations of the sample solution) of single specimens of *G. ruber* (pink), *G. ruber* (white) and *G. inflata*

Cup	Open	Close	*G. ruber* (pink) Mg/Ca [mmol/mol]	*G. ruber* (pink) size [µm]	*G. ruber* (pink) weight [µg]	*G. ruber* (white) Mg/Ca [mmol/mol]	*G. ruber* (white) size [µm]	*G. ruber* (white) weight [µg]	*G. inflata* Mg/Ca [mmol/mol]	*G. inflata* size [µm]	*G. inflata* weight [µg]
4	27 Sep 2005	19 Oct 2005							1.89	400	30.86
									2.83	<315	20.50
									2.60	<315	17.75
									2.57	<315	24.84
									2.52	<315	17.49
									1.86	<315	23.48
5	19 Oct 2005	9 Nov 2005							2.52	440	21.18
									1.80	440	22.06
									3.47	<315	14.36
									2.53	<315	10.83
									2.01	<315	21.35
									1.98	<315	16.59
									1.67	<315	23.97
6	9 Nov 2005	1 Dec 2005	4.53	440	15.23	3.81	440	17.66	2.99	<315	29.05
			4.47	400	13.43	4.02	400	15.26	1.89	<315	18.73
						4.15	360	13.42			
						4.12	360	12.92			
						3.83	360	13.36			
						3.75	360	11.96			
7	1 Dec 2005	22 Dec 2005							2.41	440	23.78
8	22 Dec 2005	13 Jan 2006	3.37	400	11.38	3.40	400	16.47	2.29	440	29.07
			3.33	400	11.35	3.29	400	17.43	2.29	440	28.09
			2.98	400	11.76	2.91	400	15.04	2.06	440	26.93
			2.77	400	11.11				1.65	440	27.56
			2.74	400	10.06				1.58	440	26.19
			5.51*	360	11.45				1.57	440	27.61

Table 4.1-S2.(continued). Sampling dates of sediment trap CBi3-o, duration of opening, Mg/Ca ratios, sizes and weights (calculated from Ca concentrations of the sample solution) of single specimens of *G. ruber* (pink), *G. ruber* (white) and *G. inflata*

Cup	Open	Close	*G. ruber* (pink) Mg/Ca [mmol/mol]	*G. ruber* (pink) size [µm]	*G. ruber* (pink) weight [µg]	*G. ruber* (white) Mg/Ca [mmol/mol]	*G. ruber* (white) size [µm]	*G. ruber* (white) weight [µg]	*G. inflata* Mg/Ca [mmol/mol]	*G. inflata* size [µm]	*G. inflata* weight [µg]
9	13 Jan 2006	3 Feb 2006	2.60	440	14.51	4.94	360	7.81	2.26	560	33.81
						3.55	360	10.95	2.03	560	38.45
									3.03	520	41.08
									2.90	520	42.38
									2.86	520	36.65
									2.50	520	38.73
									2.50	520	44.03
									2.49	520	38.18
									2.37	520	37.74
									1.79	520	48.03
									3.72	480	32.70
									2.96	480	29.22
									2.56	480	27.81
									2.41	480	37.03
									2.40	480	29.84
									2.39	480	39.26
									2.23	480	35.27
									2.13	480	30.97
									2.04	480	35.08
									1.91	480	33.76
									1.85	480	32.02
									2.72	440	28.88
									2.51	440	32.93
									2.36	440	29.83
									2.31	440	26.80
									2.26	440	36.08

Table 4.1-S2.(continued). Sampling dates of sediment trap CBi3-o, duration of opening, Mg/Ca ratios, sizes and weights (calculated from Ca concentrations of the sample solution) of single specimens of *G. ruber* (pink), *G. ruber* (white) and *G. inflata*

Cup	Open	Close	*G. ruber* (pink) Mg/Ca [mmol/mol]	*G. ruber* (pink) size [µm]	*G. ruber* (pink) weight [µg]	*G. ruber* (white) Mg/Ca [mmol/mol]	*G. ruber* (white) size [µm]	*G. ruber* (white) weight [µg]	*G. inflata* Mg/Ca [mmol/mol]	*G. inflata* size [µm]	*G. inflata* weight [µg]
9	13 Jan 2006	3 Feb 2006							2.04	440	33.33
									2.00	440	31.68
									1.86	440	24.55
10	3 Feb 2006	25 Feb 2006	2.99	480	15.82	2.72	400	8.19	2.59	520	24.93
			2.95	440	14.15	2.80	360	7.92	2.17	520	38.90
			3.15	400	9.42				3.00	480	25.26
			3.18	360	9.03				2.22	480	30.92
			2.65	360	8.02				2.54	440	30.69
			2.45	360	10.27				2.18	440	27.77
									2.16	440	28.49
									1.96	440	9.65
									3.27	400	24.98
									2.28	400	24.87
									2.21	400	20.56
11	25 Feb 2006	18 Mar 2006				3.01	480	13.26	2.24	440	24.99
						4.24	400	7.98	2.24	440	22.01
						3.40	400	7.99	2.01	440	27.68
						2.33	400	16.86	1.97	440	25.48
						3.57	360	7.92			
12	18 Mar 2006	9 Apr 2006	4.50*	400	12.95	3.56	480	14.36	2.35	440	25.37
			2.91	400	11.43	4.23	400	10.12	2.23	440	49.97
						4.48	360	8.80			
						3.92	360	10.31			
13	9 Apr 2006	30 Apr 2006				2.28	400	13.24	2.28	440	28.12
						3.35	360	11.61	2.21	440	10.45
									2.02	400	26.08

Table 4.1-S2.(continued). Sampling dates of sediment trap CBi3-o, duration of opening, Mg/Ca ratios, sizes and weights (calculated from Ca concentrations of the sample solution) of single specimens of *G. ruber* (pink), *G. ruber* (white) and *G. inflata*

Cup	Open	Close	*G. ruber* (pink) Mg/Ca [mmol/mol]	*G. ruber* (pink) size [µm]	*G. ruber* (pink) weight [µg]	*G. ruber* (white) Mg/Ca [mmol/mol]	*G. ruber* (white) size [µm]	*G. ruber* (white) weight [µg]	*G. inflata* Mg/Ca [mmol/mol]	*G. inflata* size [µm]	*G. inflata* weight [µg]
13	9 Apr 2006	30 Apr 2006							1.98	440	21.57
									1.94	440	32.00
									1.53	440	27.63
14	30 Apr 2006	22 May 2006	2.64	360	9.61	3.22	440	10.34	1.93	560	47.51
						2.55	440	9.10	2.11	520	38.98
						4.14	400	9.30	3.32	440	26.15
						2.58	360	9.61	2.15	440	34.05
						3.35	280	7.52	1.68	440	30.25
									2.56	425	42.63
									2.47	425	51.03
									1.85	425	59.59
15	22 May 2006	12 Jun 2006	3.63	400	10.51	2.94	400	14.92	2.39	520	33.19
						2.20	360	9.87	1.65	520	41.99
									2.19	480	40.75
									2.34	480	23.97
									2.17	425	42.15
16	12 Jun 2006	4 Jul 2006				2.75	400	12.11	3.71	480	29.26
									2.49	480	28.12
									2.14	480	34.96
									1.97	480	30.31
									2.54	440	28.42
									2.05	440	25.60
									1.97	440	29.21
									2.17	400	22.10
									1.76	400	37.23
									1.99	400	19.49

Table 4.1-S3. Maximum and minimum Mg/Ca temperatures derived from various equations for *G. ruber* (white) compared to SST on 29 March 2006

Calibration	SST	Min Mg/Ca temp	Max Mg/Ca temp
Anand et al. [2003] 350-500µm	18.61	23.6	26.3
Dekens et al [2002]	18.61	24.9	27.4
Lea et al. [2000]	18.61	27.8	30.4
McConnell and Thunell [2005]	18.61	23.5	29.1
Regenberg et al. [2009], ACD after *Bemis et al.* [1998]	18.61	20.2	24.7
Regenberg et al. [2009], ACD after *Kim and O'Neil* [1997]	18.61	19.1	22.9
Regenberg et al. [2009], ACD after *Shackleton* [1974]	18.61	20.1	24.6
Regenberg et al. [2009], ACD after *Farmer et al.* [2007]	18.61	17.4	23.6
Regenberg et al. [2009], ACD after *Thunell et al.* [1999]	18.61	16.4	23.1
Regenberg et al. [2009], ACD after *Mulitza et al.* [2004]	18.61	13.8	21.2
Elderfield and Ganssen [2000]	18.61	19.2	21.5

Table 4.1-S4. Maximum and minimum Mg/Ca temperatures between 27 September and 19 October 2005 derived from various equations for *G. inflata* and corresponding calcification depth when compared to WAO 05 water column temperatures

Calibration	Min Mg/Ca temp [°C]	Corresponding depth [mbsl]	Max Mg/Ca temp [°C]	Corresponding depth [mbsl]
Anand et al. [2003]	20.32	~40	27.70	Out of range
Cléroux et al. [2008]	17.22	~75	29.08	Out of range
Farmer et al. [2010]	18.19	50-75	35.23	Out of range
Elderfield and Ganssen [2000]	13.35	~250	19.99	30-50
Thornalley et al. [2009]	10.15	~500	16.79	75-100

4.2 Manuscript 2

Subsurface thermal stratification off NW Africa during the past 24,000 years – Inferences from single planktic foraminifer shells

Tim Haarmann[1], Frank Peeters[2], Gerald Ganssen[2], Ute Merkel[1], Torsten Bickert[1]

[1]Marum – Center for Marine Environmental Sciences, Leobener Straße, 28359 Bremen, Germany

[2]Section Marine Biogeology, Faculty of Earth- and Life Sciences,

Vrije Universiteit Amsterdam, de Boelelaan 1085, 1081 HV Amsterdam, The Netherlands

To be submitted to Paleoceanography

Climate models indicate a large scale upper ocean warming of the South Atlantic during Heinrich event 1 that spreads towards the North Atlantic at subsurface depths. Using the Community Climate System Model Version 3 we show that during this short-term deglaciation event the warming reached as far as ~20°N off the coast of NW Africa at depths >100 m. Mg/Ca-based calcification temperatures of the intermediate depth-dwelling planktic foraminifer *Globorotalia inflata* from a sediment core off Cape Blanc (~20°N) document a warming of ~3°C between ~19 and ~10 kyrs BP.

We combine the Mg/Ca analysis with single specimen $\delta^{18}O_c$ measurements in order to derive temperature extrema during seven selected time slices. Near present (570 years before present) temperature ranges of sediment samples (12.7 to 17.8°C) are in good agreement with results from a sediment trap time series at the study site. However, calcification temperatures exhibit a narrower distribution during the deglaciation compared to the Last Glacial Maximum and the Holocene. The reduced calcification temperature ranges are largely due to temperature changes at the cold end of the calcification temperature range and support the view that the temperature change/subsurface warming is most pronounced at the deepest calcification depths of *G. inflata*. Previous studies show that single specimens of *G. inflata* reflect water temperatures between the sea surface and ~400 m at the study site. Sediment single specimen $\delta^{18}O_c$ from 8 cm sediment depth (570 years before present) agree with this estimate and correspond to calcification depths between 0 and 420 m when compared to $\delta^{18}O_{eq}$. Reduced $\delta^{18}O_c$ standard deviation between single specimens during the deglaciation suggests a reduced depth habitat range of *G. inflata* as a response to increased thermal stratification of the water column, congruent with modeled thermal stratification during Heinrich-like conditions.

4.2.1 Introduction

The coastal area off NW Africa is one of the four large global eastern boundary upwelling systems of the subtropics. Located at the eastern boundary of the North Atlantic subtropical gyre, cold and nutrient-rich subsurface waters are upwelled from water depths between 100 and 300 m [*Mittelstaedt*, 1983]. This important process enriches surface waters with nutrients and strongly enhances upper ocean biological productivity [*Fischer et al.*, 1996; *Helmke et al.*, 2005].

At present day, the temperature of upwelled water along the NW African margin ranges between 15 and 17°C [*Mittelstaedt*, 1983]. In a broader geographic sense, there is evidence for a widespread warming of the tropical Atlantic from the surface to ~1000 m [e.g.; *Stouffer et al.*, 2006] and for an increase of subsurface temperatures throughout the Atlantic during the last deglaciation, in response to high latitude meltwater fluxes and a decreased Atlantic Meridional Overturning Circulation [*Liu et al.*, 2009 and references therein]. Among other factors, productivity of coastal upwelling systems depends on light availability and the temperature of the upwelled water [*Lachkar and Gruber*, 2011]. It is therefore important to know, if warming also occurred at subsurface depths in the upwelling system off NW Africa.

An established tool for assessing subsurface temperatures are intermediate depth-dwelling planktic foraminifer Mg/Ca ratios [e.g.; *Mulitza et al.*, 1997; *Farmer et al.*, 2010; *Groeneveld and Chiessi*, 2011]. Intermediate depth-dwelling species migrate vertically several hundred meters through the water column during their life cycle [e.g.; *Wilke et al.*, 2006], thereby recording past subsurface conditions over a large depth range. Off Cape Blanc individual specimens of the intermediate depth-dwelling species *Globorotalia inflata* reflect apparent calcification depths between the sea surface and ~400 m [*Haarmann et al.*, 2011]. They hence cover the full depth range of upwelling source water off NW Africa.

In this study, we explore the thermal evolution of the subsurface water off Cape Blanc over the past 24 kyrs. We have established a Mg/Ca temperature record from multiple shells of *G. inflata* over the past 24 kyrs. We test, if the previously suggested deglacial subsurface warming reaches as far north as 20°N and compare our temperature reconstruction to modeled subsurface temperatures using the Community Climate System Model version 3

(CCSM3).

We further reconstruct temperature ranges in the subsurface recorded by single specimen $\delta^{18}O_c$ measurements of *G. inflata* at seven selected time slices in the past 24 kyrs. We compare the reconstructed temperature ranges to present day observations from a sediment trap above the core location to evaluate if they faithfully reflect sediment trap observations. We then compare reconstructed single specimen temperatures to the modeled subsurface thermal stratification, in order to identify changes of the depth habitat range, possibly linked to changes in water column stratification.

4.2.2 Modern climate

Climatological conditions off Cape Blanc (NW Africa) are dominated by the seasonal migration of the Inter Tropical Convergence Zone (ITCZ), accompanied by a strong seasonal sea surface temperature (SST) contrast and a pronounced seasonal thermocline. The amplitude of the annual temperature cycle at the surface is 5.3°C, and at the depth of the seasonal thermocline (~75 mbsl) this is about 0.8°C, whereas at 300 m the seasonal temperature range is only 0.3°C (World Ocean Atlas 2005). The surface temperature range can, however, be significantly larger, if daily temperatures are considered. As an example, during the year 2006 it was 8.6°C at 20.23°N, 18.23°W, as obtained from the Advanced Very High Resolution radiometer of the National Oceanic and Atmospheric Administration (http://www.ncdc.noaa.gov/oa/ncdc.htm)

The Canary Current is the main surface current in the study area and flows southward along the NW African coast, modulated by southwestward directed trade winds which blow throughout the year between 20° and 25°N [*Schemainda et al.*, 1975]. Off Cape Blanc (~20.5°N), the steady winds cause perennial upwelling, which is strongest in late spring and autumn [*Ganssen and Sarnthein*, 1983; *Pelegrí et al.*, 2005]. South of 24°N (i.e. off Cape Blanc), upwelled water is dominated by low saline (35.6 - 35.9 psu) and relatively cold, nutrient rich SACW [*Mittelstaedt*, 1983] transported by a northward flowing undercurrent at a depth between 200 and 400 m [*Hagen*, 2001]. To the north, upwelled water consists of the higher saline (36.1 – 36.4 psu), nutrient poor North Atlantic Central Water (NACW) [*Mittelstaedt*, 1983], conveyed southward by the Canary Current. The Cape Verde front at ~20°N (off the coast) separates NACW from SACW [*Arhan et al.*, 1994] (Figure 4.2-1a and

c). Since NACW and SACW however occupy the same density range, the front is density-compensated, which results in a multitude of intrusions, filaments and lenses [*Tomczak and Godfrey*, 1994] (Figure 4.2-1b).

Off Cape Blanc, the detachment of the Canary Current from the coast promotes the development of a large filament of upwelled water which spreads in a SW direction up to 500 km offshore [*Pérez-Rodríguez et al.*, 2001; *Pelegrí et al.*, 2005], usually extending over the study site.

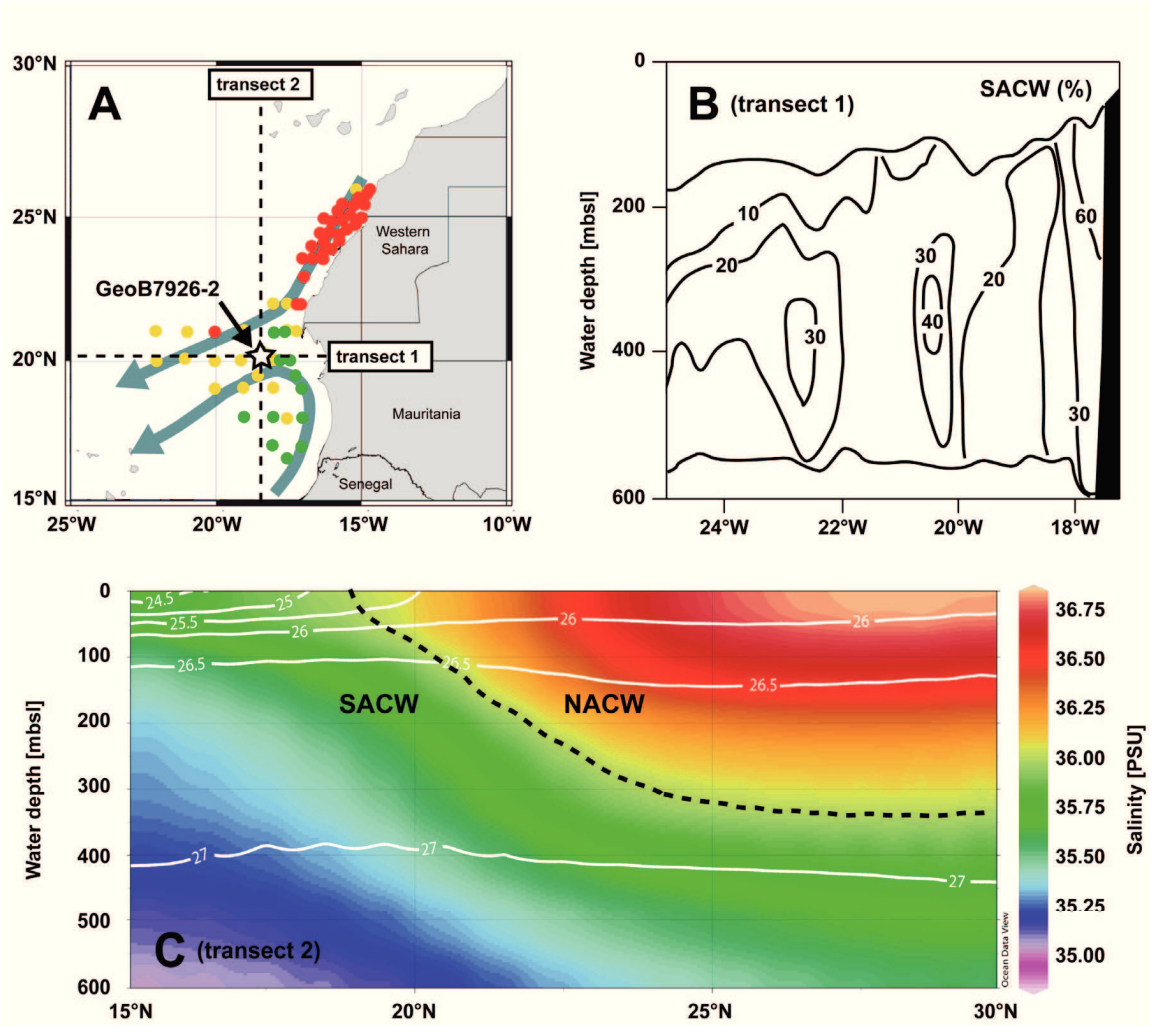

Figure 4.2-1. Schematic map and depth transects showing the main oceanographic features at the study site and the location of sediment core GeoB7926-2. a) Location of sediment core GeoB7926-2 is indicated by a star. Red dots indicate sites that exhibit salinity and temperature properties of the North Atlantic Central Water, green dots indicate sites that exhibit salinity and temperature properties of the South Atlantic Central Water, and yellow dots those sites that represent a mixture of both water masses [*Pastor et al.*, 2008]. Transects shown in the other panels are indicated by dashed lines. Arrows indicate the flow path of the Canary Current (north) and the Mauritania Current (south) b) Meridional transect at 20°10'N in April 1983, modified from *Hagen* and *Schemainda* [1987]. Lines indicate the percentage of the South Atlantic Central Water as compared to the North Atlantic Central Water c) Longitudinal transect along 18.5°W. Colors show salinity, isolines show potential density [World Ocean Atlas, 2005; [*Antonov et al.*, 2006; *Locarnini et al.*, 2006]. Dashed line shows the 36 psu isoline, used to exemplify the boundary between higher saline North Atlantic Central Waters and the lower saline South Atlantic Central Waters [*Mittelstaedt*, 1983].

4.2.3 Material and methods

Sample collection and revised age model

The 1330 cm long gravity core GeoB7926-2 was recovered during R/V *Meteor* Cruise 53/1c [*Meggers and cruise participants*, 2003] at 20°12.8'N, 18°27.1'W at 2500 m water depth. Samples considered representative for present day were collected from the top centimeter of multicore GeoB 7408-2 at 20°17.4'N, 18°15.0'W from a water depth of 1935 m, recovered during R/V

Poseidon cruise 272 [*Meggers et al.*, 2002]. Sediment sample were wet-sieved (>63um) and the residual dry-sieved into two size fractions, 63-150 μm and >150 μm. From the >150 μm size fraction specimens of the planktic foraminifer *G. inflata* were hand-picked under a binocular microscope (largest diameter 400-560 μm; most specimen 400-480 μm). Samples were weighted in three replicates with a microbalance and only specimens strictly between 20 and 50 μg are used in the discussion.

The age model of the upper 820 cm is based on 12 Accelerator Mass Spectrometry (AMS) ^{14}C dates on monospecific samples of the planktonic foraminifera *G. inflata* and covers approximately the last 24 kyrs. Radiocarbon ages have been previously published [*Romero et al.*, 2008]. We revised the age model, converting radiocarbon ages into calendar years using the Calib Rev 6.1.0 program, with the most recent marine calibration dataset marine09.14c [*Reimer et al.*, 2009]. We acknowledge that the dated species *G. inflata* was possibly exposed to water exceeding the global reservoir age of ~400 yrs. We hence calculated the calendar age that would be associated with an additional local reservoir age of 197 yrs. This is the local reservoir age further south, where old South Atlantic Central Water is upwelled (http://www.calib.qub.ac.uk/marine/regioncalc.php), likely exhibiting the oldest reservoir age at the study site. In Table 4.2-1, we show calculated calendar ages assuming no reservoir age and in Table 4.2-2 assuming a reservoir age of 197 yrs, to show the effect this has on the calculated calendar ages.

Table 4.2-1. Revised age model of sediment core GeoB7926-2, using the ^{14}C dates measured by *Romero et al*. [2008] on *Globorotalia inflata*.

Lab number	Interval [cm]	Age [^{14}C]	± Error [yrs]	Age[a] [cal yrs BP](Δ=0yrs)[b]	1σ range [yrs BP][c]
KIA 24287	8	1170	35	712	670-740 (1.0)
KIA 25812	48	4455	35	4640	4557-4707 (1.0)
KIA 25810	98	8970	45	9629	9542-9681 (1.0)
KIA 24286	173	10050	70	11041	10937-10995 (0.20)
					11000-11157 (0.80)
KIA 22417	248	10830	70	12303	12119-12136 (0.05)
					12180-12392 (0.79)
					12469-12520 (0.16)
KIA 24285	378	12220	70	13662	13517-13528 (0.03)
					13578-13777 (0.97)
KIA 29030	418	13050	70	14946	14692-14726 (0.06)
					14786-15152 (0.94)
KIA 27310	483	14220	100	16916	16801-17012 (1.0)
KIA 29029	508	14290	60	16956	16850-17044 (1.0)
KIA 22416	553	14670	80	17350	17171-17532 (1.0)
KIA 27309	688	17100	130	19844	19581-19729 (0.38)
					19774-20051 (0.62)
KIA 29028	803	20450	160	23956	23742-24218 (1.0)
KIA 24283	868	23650	220-230	28091	27857-28357 (1.0)

Table 4.2-2. Same as Table 4.2-1, but with an additional local reservoir age of 197 years

Lab number	Interval [cm]	Age [^{14}C]	± Error [years]	Age[a] [cal yrs BP](Δ=197yrs)[d]	1σ range [yrs BP][c]
KIA 24287	8	1170	35	567	530-603 (1.0)
KIA 25812	48	4455	35	4368	4306-4418(1.0)
KIA 25810	98	8970	45	9449	9412-9491 (1.0)
KIA 24286	173	10050	70	10759	10604-10822 (0.86)
					10837-10883 (0.14)
KIA 22417	248	10830	70	11945	11754-11797 (0.11)
					11840-12092 (0.89)
KIA 24285	378	12220	70	13463	13363-13518 (0.82)
					13528-13576 (0.18)
KIA 29030	418	13050	70	14548	14216-14754 (1.0)
KIA 27310	483	14220	100	16763	16660-16889 (1.0)
KIA 29029	508	14290	60	16827	16742-16911 (1.0)
KIA 22416	553	14670	80	17115	16922-17233 (1.0)
KIA 27309	688	17100	130	19684	19445-19605 (0.54)
					19683-19837 (0.46)
KIA 29028	803	20450	160	23715	23477-23912 (1.0)
KIA 24283	868	23650	220-230	27872	27602-28250 (1.0)

[a] To convert uncorrected ^{14}C ages into calendar ages, the CALIB REV 6.1.0 program was used [*Stuiver and Reimer*, 1993]. The calibration data set used was marine09.14c [*Reimer et al.,*2009].
[b] Global ocean reservoir correction was used as incorporated in the marine 09.14c calibration data set and is about 400 years [*Reimer et al.*, 2009].
[c] Enclosing 68.3% of the probability distribution. Values in parenthesis are the relative area under probability distribution
[d] An additional local ΔR of 197 years was included, based on the weighted mean of samples between 16.05° and 15.65°N off the West African coast, i.e. samples exposed to upwelling of South Atlantic Central Waters (http://www.calib.qub.ac.uk/marine/regioncalc.php)

Analytical approach

Mg/Ca thermometry

For Mg/Ca measurements, about 20 specimens of *G. inflata* were gently crushed and cleaned following the protocol described in *Barker et al.* [2003]. Samples were washed seven times with suprapure water, twice with methanol followed by two oxidation steps of 10 min and a weak acid leach in 0.001M TD HNO_3. Samples were then centrifuged for 10 min at 6000 rpm, transferred into test tubes and diluted. Mg/Ca ratios were measured on a Perkin-Elmer Optima 3300R inductively coupled plasma-optical emission spectrometer (ICP-OES) equipped with an ultrasonic nebulizer U-5000 AT (Cetac Technologies Inc.) and on a Agilent Technologies 700 Series ICP-OES, at the faculty of Geosciences and the Center for Marine Environmental Sciences, University of Bremen. During the analysis, the measured Mg/Ca ratio of carbonate reference material ECRM 752-1 was on average 3.84 mmol/mol ($n = 12$; $\sigma = 0.04$), in good agreement with the reported Mg/Ca ratio of 3.75 mmol/mol [*Greaves et al.*, 2008]. The precision of measurements on *G. inflata* was on average 0.004 mmol/mol, based on mostly three (n=111) and few times (n=17) two replicates. Mg/Ca temperatures were calculated using the equation of *Elderfield and Ganssen* [2000] (equation 4.2-1).

$$T = LN ((Mg/Ca)/0.49)/0.1) \quad (4.2\text{-}1)$$

Single specimen oxygen isotope analysis

Planktic foraminifera calcify over a period of a couple of weeks to months [*Bé and Spero*, 1981; *Hemleben et al.*, 1989]. This short calcification period implies that their shell chemistry records temperatures that prevailed during this particular period. When a large amount of individual shells from the sedimentary record is analyzed, these were likely formed during different periods. By comparison of individual shells of surface dwelling species, seasonal temperature ranges may be assessed [e.g.; *Ganssen et al.*, 2010; *Wit et al.*, 2010; *Haarmann et al.*, 2011].

In contrast shells of intermediate depth-dwelling foraminifera calcify over a large depth range [*Wilke et al.*, 2006], implying that the geochemical signal of an individual shell reflects the environmental conditions throughout this depth range, centered at the depth were the gross of the calcite was formed.

Assuming that a population of intermediate depth-dwelling foraminifera did not change its habitat in the past, individual shells have been used to assess changes at these depths of main calcification [*Leduc et al.*, 2009; *Khider et al.*, 2011].

In this study, temperatures are reconstructed from individual shells of *G. inflata*, assuming that these reflect temperatures over the depth range inhabited by this species at present day. To capture the spread in the calcification temperatures of *G. inflata*, the stable oxygen isotope composition of individual shells was measured. We reconstructed calcification temperature ranges from between 21 and 43 single specimens of *G. inflata*. After weighing in three replicates on a microbalance, oxygen isotopes were determined on a Finnigan MAT 252 mass spectrometer coupled to a Kiel preparation device, housed at the Vrije Universiteit in Amsterdam (VUA), The Netherlands. Reproducibility of VUA standard calibrated against National Bureau of Standards NBS-20 carbonate standard was 0.10 ‰ (1σ) over all analytical sessions. In order to exclude potential outliers, we do not interpret data which fall outside the range

$$\left[Q1 - 1.5 * (Q3 - Q1), Q3 + 1.5 * (Q3 - Q1)\right] \quad (4.2\text{-}2)$$

with Q1 and Q3 being the first and the third quartile of the data, respectively. Potential outliers, identified using this method, are indicated in Table 4.2-S1.

In order to calculate temperatures from oxygen isotopes of individual shells, the previously established Mg/Ca temperatures combined with the average $\delta^{18}O_c$ of the individual oxygen isotope measurements at the respective core depths were used in equation 4.2-3 in order to calculate $\delta^{18}O_{seawater.}$ The equation is reported solved for $\delta^{18}O_{seawater}$ and based on the equation of *Kim and O'Neil* [1997] in its rewritten form [*Bemis et al.*, 1998].

$$\delta^{18}O_{seawater} = \delta^{18}O_{calcite} - \left(\frac{\left(4.64 - \sqrt{(-4.64)^2 - 4 * 0.09 * 16.1 - T}\right)}{2 * 0.09} \right) \quad (4.2\text{-}3)$$

Assuming that both, the Mg/Ca multi specimen and the average $\delta^{18}O_c$ single specimen values mirror the mean calcification temperature, temperatures of every single specimen oxygen isotope measurement around the average Mg/Ca temperature can be used to estimate calcification temperature ranges, applying the equation in its form solved for temperature (equation 4.2-4).

$$T = 16.1 - 4.64 * (\delta^{18}O_{calcite} - \delta^{18}O_{seawater}) + 0.09 * (\delta^{18}O_{calcite} - \delta^{18}O_{seawater})^2$$

(4.2-4)

We calculated expected equilibrium values ($\delta^{18}O_{eq}$) for various water depths and seasons using the rearranged equation of *Kim and O'Neil* [1997] (equation 4.2-5).

$$\delta^{18}O_{eq} = \delta^{18}O_W + 25.778 - 3.333 * \sqrt{T + 43.704}$$

(4.2-5)

$\delta^{18}O_w$ was estimated from salinity data [World Ocean Atlas, 2005; *Antonov et al.*, 2006], used in equation 4.2-6. Equation 4.2-6 is based on the local $\delta^{18}O_w$:salinity relationship between 18.4° and 20.5°N and 18.1° and 21.2°W, calculated from *Pierre et al.* [1994], as provided in the global seawater ^{18}O database [*Schmidt, G.A., G. R. Bigg and E. J. Rohling*, 1999; http://data.giss.nasa.gov/o18data/].

$$\delta^{18}O_w = 0.4664 * \text{salinity} - 16.024$$

(4.2-6)

Statistics

In order to determine, if the standard deviation of the single specimen oxygen isotope measurements in the past differed from the near present day standard deviation, the confidence interval of the 8 cm sediment depth standard deviation was calculated according to equation 4.2-7, where σ is the standard deviation, n the number of samples and α=0.05 defines the 95% confidence level.

$$\left[\sigma * \sqrt{(n-1)/\chi^2(n-1,\frac{\alpha}{2})}, \sigma * \sqrt{(n-1)/\chi^2(n-1,1-\frac{\alpha}{2})}\right]$$

(4.2-7)

Model

In this study, we present model results from simulations using the comprehensive Community Climate System Model Version 3 (CCSM3; see *Collins et al.*, 2006 for an overview) in its coarse-resolution setup [*Yeager et al.*, 2006] to simulate the climates of the Last Glacial Maximum (LGM) and Heinrich event/stadial 1 (HE1). Details on these glacial simulations and on a preindustrial control simulation used as a reference can be found in *Merkel et al.* [2010]. In the glacial simulations, changes of the orbital parameters, greenhouse gas concentrations, ice sheet albedo and topography as well as the lowering of the sea level during the LGM are taken into account. In addition, for the Heinrich simulation, a permanent freshwater anomaly over the Greenland-Iceland-Norwegian Seas is imposed to the glacial ocean, thereby inducing a pronounced

slowdown of the Atlantic Meridional Overturning Circulation [*Merkel et al.*, 2010]. For our study here, results from these simulations are presented as long-term averages of the last 100 years of each simulation.

4.2.4 Results

Mg/Ca ratios

In Figure 4.2-2 the Mg/Ca ratios measured in multiple specimens of *G. inflata* are presented versus age. The Mg/Ca ratios ranged between a minimum of 1.41 mmol/mol at 1.5 kyrs BP and a maximum of 4.08 mmol/mol at 9.9 kyrs BP. Between 23.5 and 22.2 kyrs BP, Mg/Ca ratios sharply decrease from 3.59 mmol/mol to 1.52 mmol/mol. This is followed by a gradual increase to 4.08 mmol/mol (9.9 kyrs BP). Mg/Ca ratios then decrease again to a value of 1.41 mmol/mol at 1.5 kyrs BP, before reaching their present day value of 2.25 mmol/mol.

$\delta^{18}O_c$ values and their distribution

Based on the outlier definition given in equation 4.2-2, two measurements were excluded at core depth 273 cm and three measurements at core depth 733 cm (all raw values including outliers are provided in Table 4.2-S1). Figure 4.2-2 shows the oxygen isotope ratios of single *G. inflata* specimens. These (excluding outliers) range between 3.24 ‰ (563 cm; 17.4 kyrs BP) and 0.20 ‰ (8 cm, 0.57 kyrs BP). The average $\delta^{18}O_c$ for each core depth ranges between 0.80 ‰ (0 cm; 0 kyrs BP) and 2.82 ‰ (563 cm; 17.4 kyrs BP). The maximum oxygen isotope range between single specimens of 1.78 ‰ is measured at 733 cm (22.2 kyrs BP) and the smallest range of 0.86 ‰ at 413 cm (14.4 kyrs BP).

At most core depths single specimen oxygen isotopes appear normally distributed, except for core depth 733 cm. There, Shapiro-Wilk-testing at 95% confidence [*Shapiro and Wilk*, 1965] suggests there is enough evidence that the data are not normally distributed (using the Shapiro-Wilk test implemented in the statistics software 'PAST' [*Hammer et al.*, 2001]). The standard deviation of $\delta^{18}O_c$ between single specimens (Table 4.2-3) ranges from 0.44 (733 cm; 22.2 kyrs) to 0.21 (413 cm; 14.4 kyrs BP).

The core top sample had few specimens between 20 and 50 µg. For the discussion of past changes of the standard deviation between individual specimens, we therefore calculated the 95% confidence interval of the standard deviation for the next youngest sample (8 cm; 0.57 kyrs), which is between 0.25 and 0.48.

Table 4.2-3. Average $\delta^{18}O_c$ values [‰ vs. PDB], standard deviation (underlined when significantly different from the most recent sample) and p value of Shapiro-Wilk test, derived from individual specimens of *G. inflata* from sediment core GeoB7926-2 at selected core depths.

Age (Depth)	n	Average $\delta^{18}O_c$ [‰ vs. PDB]	σ	p(normal)	p(normal)>0.05
0.57 kyrs BP (8 cm)	21	0.86	0.33	0.263	Yes
6.16 kyrs BP (78 cm)	30	0.87	0.41	0.473	Yes
12.26kyrs BP (273 cm)	23	1.76	0.22	0.061	Yes
14.41kyrs BP (413 cm)	41	2.36	0.21	0.860	Yes
16.80 kyrs BP (498 cm)	43	2.31	0.23	0.459	Yes
17.36 kyrs BP (563 cm)	24	2.82	0.32	0.054	Yes
22.18 kyrs BP (733 cm)	39	1.90	0.44	0.026	No

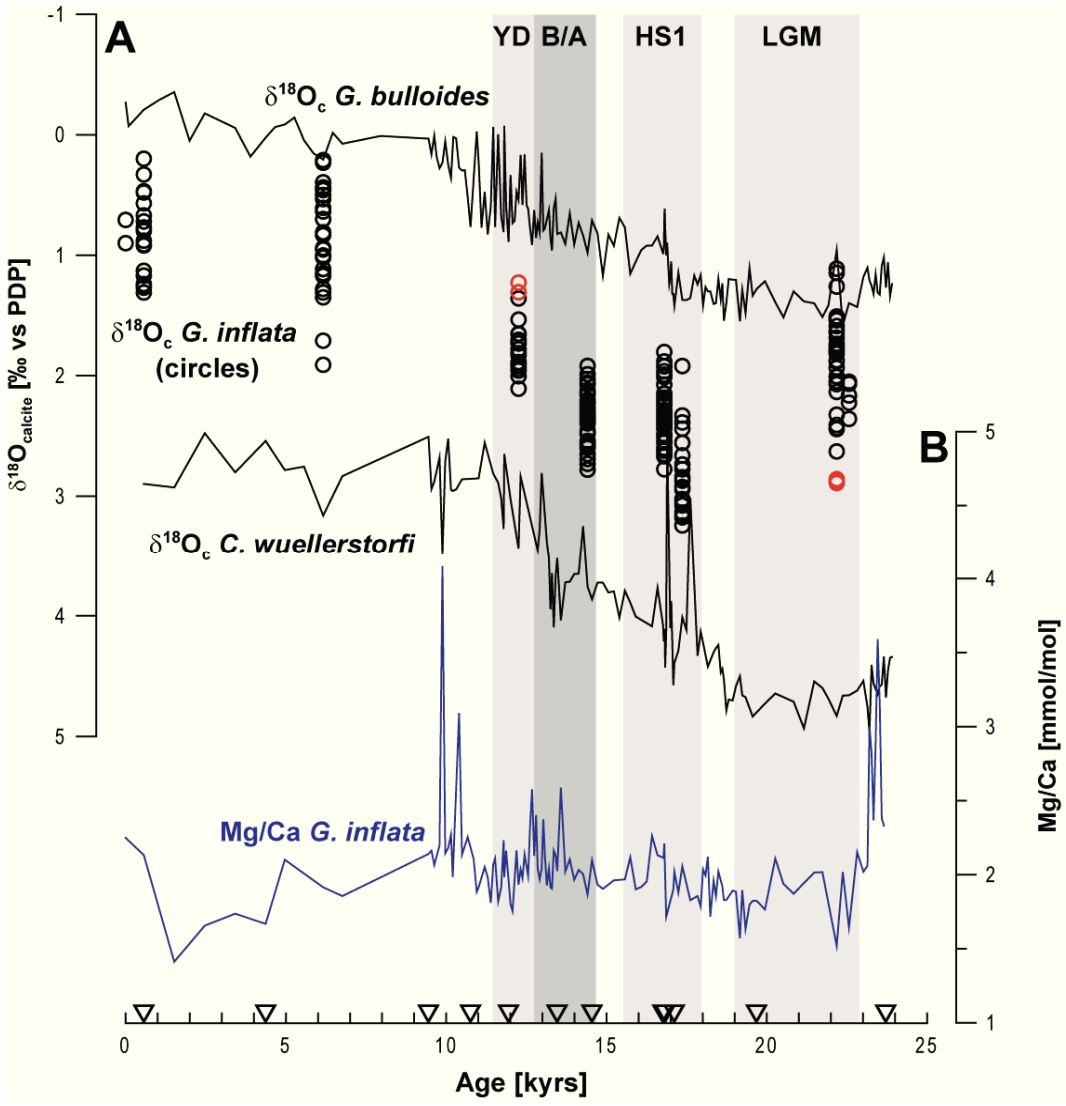

Figure 4.2-2 (previous page). Results of the single specimen $\delta^{18}O_c$ and multi-specimen Mg/Ca measurements in sediment core GeoB7926-2. a) Oxygen isotopes of *G. bulloides* (line) in sediment core GeoB7926-2 [*Romero et al.*, 2008] and single *G. inflata* oxygen isotopes (circles). Youngest sample is from the top centimeter of multicorer GeoB7408-2 [*Meggers et al.*, 2002]. Red circles show measurements that are considered outliers using the definition given in equation 4.2-2. Curve shows $\delta^{18}O_c$ of *Cibicidoides wuellerstorfi* [data: *B. Donner*]. b) Mg/Ca of multi-specimen measurements on *G. inflata*. Triangles on the abscissa show ^{14}C age control points revised from *Romero et al.* [2008]. LGM: Last Glacial Maximum, HS1: Heinrich Stadial 1, B/A: Bølling-Allerød, YD: Younger Dryas.

4.2.5 Discussion

Single specimen temperatures reflect thermal water column stratification

Modern observations show that Mg/Ca ratios in single specimen of *G. inflata* at the study site correspond to calcification depths between the sea surface and ~400 m [*Haarmann et al.*, 2011]. The calcification depth derived from analyzing multiple shells is about 150 m. This means that the analysis of multiple shells will to a limited extend only detect a subsurface warming and stratification changes that occur mostly below 100 m.

It is suggested that the analysis of single specimens provides a more detailed picture. In the case of a potential subsurface warming off NW Africa below 100 m, in particular the deepest (i.e. indicative for the coldest temperatures) individuals are expected to be mostly affected by this warming. Increased water column stratification is expected to result in a decreased $\delta^{18}O_c$ standard deviation of the sampled population, as a result of a narrowed depth habitat.

Single specimen analysis requires that the sampled population captures the full calcification range, as observed in the water column. Also, the single specimen $\delta^{18}O_c$ ranges must be independent of the number of shells which are analyzed (here $r^2 < 0.00$) and $\delta^{18}O_c$ must be independent of shell weights (here r^2 between 0.00 and 0.39, see Figure 4.2-S1). Finally, the calcification range of the used size fraction must be well known. For this, we confined our analysis to the same size fraction (400-560 µm; most specimen 400-480 µm) and weights as in *Haarmann et al.* [2011].

In Figure 4.2-3 and Table 4.2-4, we present calculated seasonal oxygen isotope equilibrium values ($\delta^{18}O_{eq}$) for February (most positive values) and September (most negative values) in order to assess the seasonal $\delta^{18}O_{eq}$ range. The calculation is based on monthly temperature [*Locarnini et al.*, 2006] and salinity [*Antonov et al.*, 2006], used in equations 4.2-5 and 4.2-6, respectively.

Table 4.2-4. Seasonal $\delta^{18}O_{eq}$ at 18.5°W, 20.5°N versus water depth. The calculation is based on atlas temperature [*Locarnini et al.*, 2006] and salinity [*Antonov et al.*, 2006] data, used in equations 4.2-5 and 4.2-6, respectively.

Depth [m]	Jan	Feb	Mrch	Apr	May	Jun	Jul	Aug	Sep	Oct	Nov	Dec
0	0.03	0.19	0.05	0.00	0.02	-0.17	-0.63	-0.91	-0.94	-0.81	-0.52	-0.25
10	0.03	0.20	0.05	0.00	0.02	-0.15	-0.60	-0.88	-0.91	-0.76	-0.50	-0.25
20	0.05	0.22	0.08	0.03	0.05	-0.10	-0.53	-0.82	-0.83	-0.71	-0.45	-0.23
30	0.07	0.23	0.13	0.08	0.09	0.01	-0.37	-0.60	-0.60	-0.53	-0.37	-0.20
50	0.16	0.31	0.25	0.24	0.24	0.24	0.01	-0.08	-0.03	-0.04	0.00	-0.03
75	0.32	0.41	0.38	0.39	0.38	0.40	0.27	0.30	0.32	0.31	0.32	0.28
100	0.47	0.52	0.49	0.48	0.50	0.52	0.43	0.48	0.50	0.46	0.50	0.44
125	0.57	0.61	0.59	0.58	0.57	0.60	0.54	0.59	0.58	0.57	0.60	0.56
150	0.67	0.70	0.69	0.62	0.65	0.67	0.64	0.68	0.65	0.66	0.70	0.64
200	0.83	0.87	0.81	0.77	0.79	0.79	0.83	0.83	0.80	0.80	0.82	0.81
250	0.94	0.97	0.93	0.91	0.88	0.90	0.91	0.93	0.93	0.93	0.93	0.94
300	1.03	1.03	1.01	0.99	0.98	0.97	1.03	1.02	1.01	1.03	1.02	1.05
400	1.00	1.25	1.23	1.21	1.20	1.19	1.23	1.26	1.22	1.23	1.23	1.25
500	1.45	1.47	1.44	1.46	1.46	1.43	1.47	1.50	1.45	1.47	1.44	1.45
600	1.66	1.65	1.63	1.66	1.70	1.67	1.66	1.68	1.66	1.63	1.67	1.65

The $\delta^{18}O_c$ of single shells from 8 cm sediment depth (0.20 to 1.31 ‰) corresponds to $\delta^{18}O_{eq}$ between the sea surface and ~420 m, in excellent agreement with the results of the sediment trap (Figure 4.2-4). The average $\delta^{18}O_c$ corresponds to $\delta^{18}O_{eq}$ at a depth of ~200-225 m, slightly deeper than the depth of 150 m inferred from the sediment trap study.

Notably, lowest $\delta^{18}O_c$ are heavier than $\delta^{18}O_{eq}$ at the sea surface (Figure 4.2-3). *G. inflata* may calcify in the mixed layer [e.g. *Fairbanks et al.*, 1980; *Wilke et al.*, 2006; *Haarmann et al.*, 2011], or spend part of its life cycle in the photic zone, due to the presence of small symbiotic algae [*Gastrich*, 1987]. Isotopically lightest specimens therefore reflect mixed layer conditions, which is corroborated by very similar $\delta^{18}O_c$ of *G. inflata* and *G. bulloides* in the Holocene samples (Figure 4.2-2). This is mostly the case during the cold season, when single *G. inflata* specimens reflect temperatures close to those of the sea surface [*Haarmann et al.*, 2011]. We therefore assume that the heavier $\delta^{18}O_c$ than $\delta^{18}O_{eq}$ at the sea surface result from calcification in the surface mixed layer only during the cold season. This is in agreement with the fact that there is highest shell production in winter [*Haarmann et al.*, 2011].

The good match of the depths concluded from single sedimentary *G. inflata* shells with present day observations suggests that single sedimentary specimens can reliably be used to assess subsurface temperatures throughout a wide depth range.

The distribution of the 0.57 kyrs population is described through its $\delta^{18}O_c$ standard deviation (0.33) and the 95%

confidence interval of the standard deviation, which ranges from 0.25 to 0.48. In the following, we will use this confidence interval in order to investigate, if populations in the past have a different standard deviation, possibly linked to changes in water column stratification.

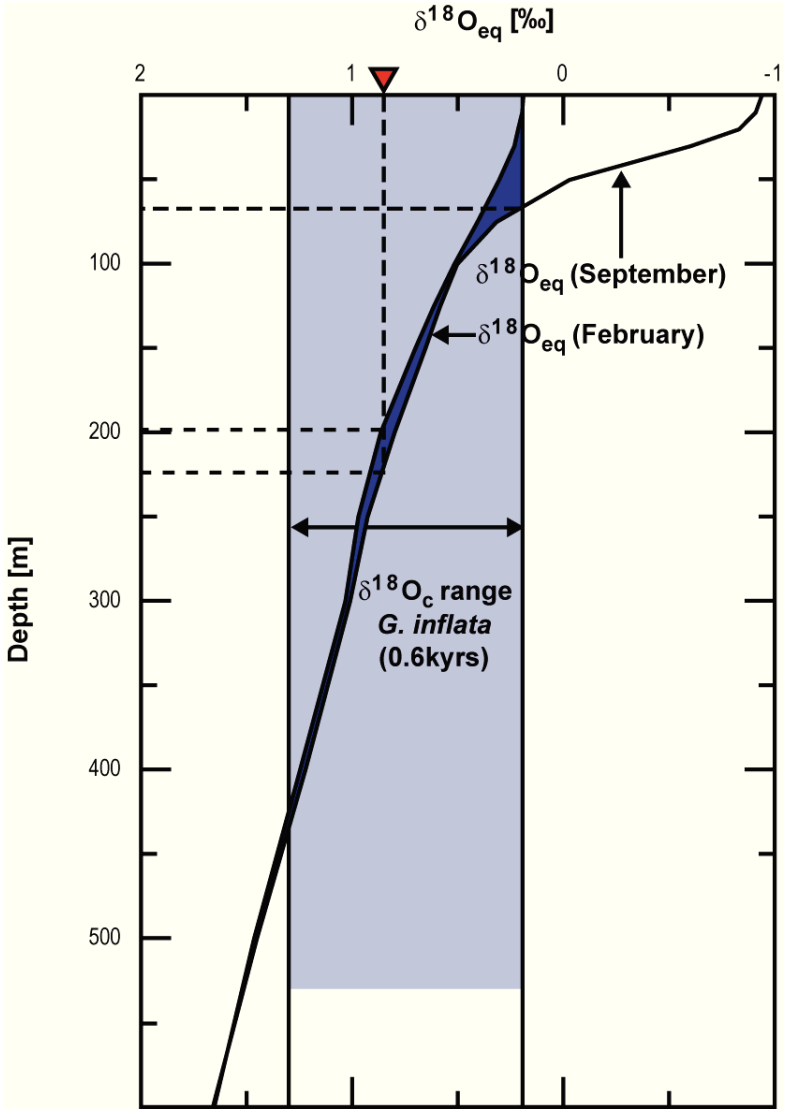

Figure 4.2-3. Comparison of the $\delta^{18}O_c$ range of sediment single *G. inflata* specimens (sediment depth 8 cm) to seasonal maximum and minimum oxygen isotope equilibrium values at the study site. Solid lines indicate highest $\delta^{18}O_{eq}$ (February) and lowest $\delta^{18}O_{eq}$ (September) at 18.5°W, 20.5°N calculated from salinity [*Antonov et al.*, 2006] and temperature [*Locarnini et al.*, 2006] using equations 4.2-5 and 4.2-6, respectively. Light blue shading indicates the $\delta^{18}O_c$ range (0.20 to 1.31‰) measured from individual *G. inflata* specimens from sediment core GeoB7926-2 at the core depth 8 cm (0.57 kyrs BP). Dark blue indicates the expected calcification depths according to the seasonal $\delta^{18}O_{eq}$ range. The red triangle indicates the average $\delta^{18}O_c$ calculated from all individual specimens. The average $\delta^{18}O_c$ corresponds to an equilibrium value of 0.86‰ and hence to an apparent calcification depth of ~200-225 m.

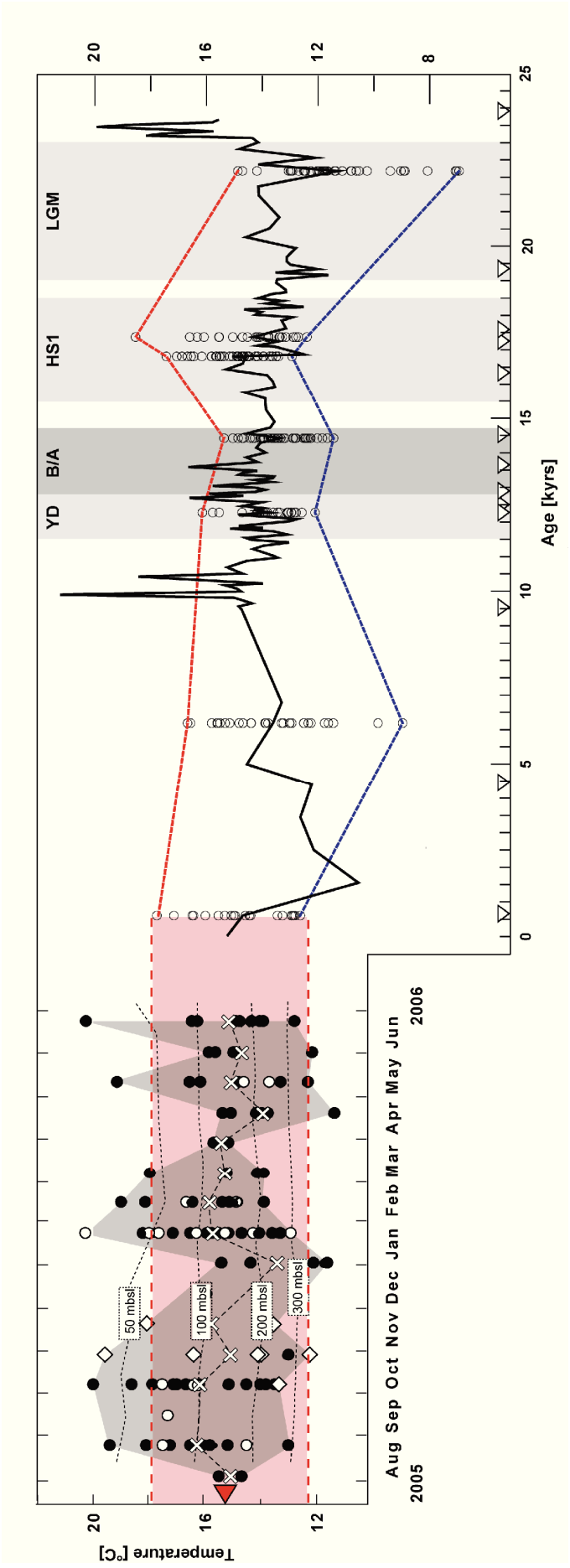

Figure 4.2-4. (Left) Mg/Ca temperatures of single *G. inflata* off Cape Blanc. Open circle indicates size fraction 520-560 µm, close circle 400-480 µm, diamond <315 µm, cross the average Mg/Ca temperature. The narrow spaced dashed lines indicate monthly averaged temperatures at the shown depth from the WAO 05. Crosses connected with a wide-spaced dashed line indicate average Mg/Ca temperatures. The red triangle on the axis indicates the flux-weighted annual mean Mg/Ca ratio (modified after *Haarmann et al.*, 2011). (Right) The black line shows Mg/Ca temperatures derived from multi specimen *G. inflata* analysis. Open circles indicate temperatures calculated from single *G. inflata* specimens (20-50 µg; see methods section). Red and blue dashed lines illustrate warmest and coldest reconstructed temperatures, respectively. Age control points revised from *Romero et al*. [2008] are indicated by triangles. All Mg/Ca temperatures are calculated using the regression equation reported in *Elderfield and Ganssen* [2000]. LGM: Last Glacial Maximum, HS1: Heinrich Stadial 1, B/A: Bølling-Allerød, YD: Younger Dryas

Paleoceanographic applicability of single *G. inflata* specimens

We have demonstrated earlier that the $\delta^{18}O_c$ range of single *G. inflata* shells matches the present day calcification temperature range of the upper water column from near surface values down to about 425 m. It can be expected that a subsurface warming below ~100 m will preferentially raise the lowest calcification temperature.

Furthermore, considering all single specimens of a sampled population, this must consequently result in a reduced $\delta^{18}O_c$ standard deviation. As can be seen in Figure 4.2-5, this indeed is the fact for the deglacial samples between 16.8 and 12.3 kyrs BP all having a standard deviation outside of the 95% confidence interval of the standard deviation of the 0.57 kyrs BP sample (Table 4.2-3).

It is interesting to note that changes of the temperature range between intervals with a large and a small range (i.e. 22.2 to 17.4 kyrs BP and 12.3 to 6.2 kyrs BP; Figure 4.2-5) are largely due to a different number of specimens representing the temperature minima. We interpret this as a result of a subsurface warming and/or changes of water column stratification taking place at the lower habitat depth of *G. inflata*. This observation also suggests that a warming is unlikely to have a surface origin and/or results from a stronger mixing of the water column, since this

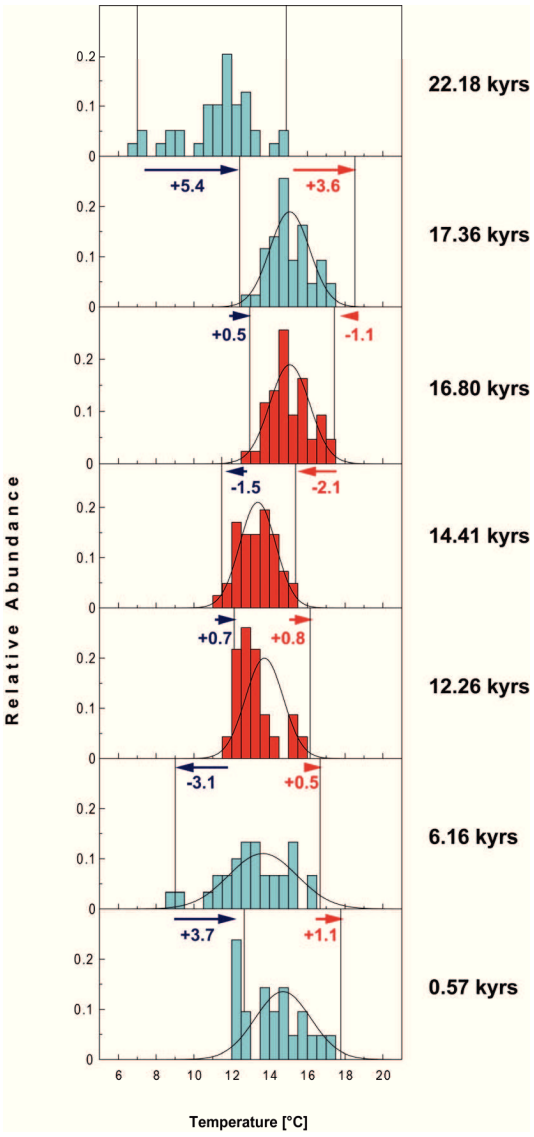

Figure 4.2-5. Distribution of temperatures calculated from the oxygen isotopic composition of single specimens of *G. inflata* in sediment core GeoB7926-2. Calculation of temperatures is explained in the main text. Red histograms have a different $\delta^{18}O_c$ standard deviation from the 0.57 kyrs sample; blue histograms have a statistically identical standard deviation. Temperatures that do not deviate enough from a normal distribution to conclude that they are non-normally distributed (Shapiro-Wilk tested at the 95% confidence level) are shown with a Gaussian fit. Arrows with numbers show temperature difference to the next younger sample.

should affect the shallowest (i.e. warmest) specimens stronger than the deeper ones.

Data-model comparison

Stratification and habitat depth range of *G. inflata*

Figure 4.2-6a shows the modeled thermal stratification for preindustrial conditions in a latitudinal transect between 25° and 15°W. Reconstructed temperature extrema of the 0.57 kyrs BP sample of *G. inflata* (17.8 and 12.7°C) correspond to depths between 75 and 150 m (at 20°N) in the model. These depth ranges are smaller than the previously concluded ones (0-425 m). However, it should be noted that while isotherms in the model deepen north of 20°N, world ocean atlas temperatures [*Locarnini et al.*, 2006] show that this is actually the case some 10° further south. Comparison to these observed temperatures (dashed lines in Figure 4.2-6a) therefore results in a more realistic depth estimation of 100 to 350 m (at 20°N).

Furthermore, comparison of model temperatures to modern atlas temperatures shows that the model underestimates actual temperatures at the average living depth of *G. inflata*. At a depth of 150 m, modeled temperatures are ~12°C, while they are observed to be ~14°C [*Locarnini et al.*, 2006]. This results in a shallower average calcification depth concluded from the Mg/Ca multi-specimen temperature (14.7°C), when compared to the model (~80 m) or to observed temperatures (~180 m) [*Locarnini et al.*, 2006].

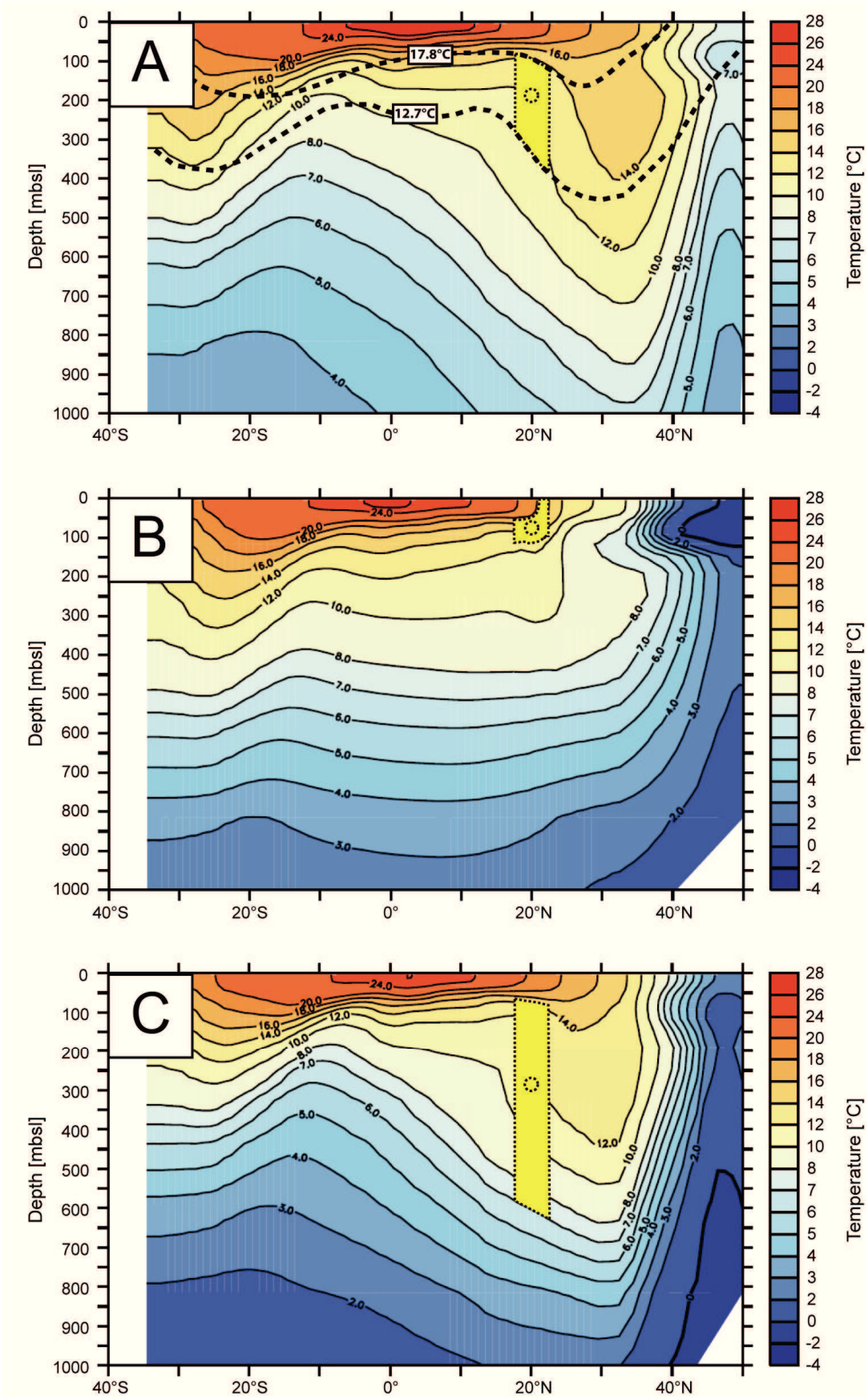
A
B
C
17.8°C
12.7°C
Depth [mbsl]
Temperature [°C]
40°S
20°S
0°
20°N
40°N

Figure 4.2-6 (previous page). Comparison of model vertical thermal stratification and temperatures derived from the single specimen analysis. Annual mean temperatures (°C) are simulated by the CCSM3 model and the results are based on the last 100 years of the model runs and show the zonal average between 25° and 15°W for the upper 1000 m of the water column. a) Preindustrial conditions. Yellow field highlights temperature range between 17.8°C and 12.7°C from 17.5 to 22.5°N. These are the maximum and minimum temperatures derived from the single specimen *G. inflata* analysis of the 0.57 kyrs sample. Dashed yellow circle indicates the multispecimen *G. inflata* Mg/Ca temperature at 20°N (14.7°C). Dashed line shows the annual average 12.7°C and 17.8°C isotherms from atlas data [*Locarnini et al.*, 2006] b) Heinrich-like conditions. Yellow field highlights temperature range between 17.4°C and 12.9°C from 17.5 to 22.5°N. These are the maximum and minimum temperatures derived from the single specimen *G. inflata* analysis at 16.8 kyrs BP. Dashed yellow circle indicates the multispecimen *G. inflata* Mg/Ca temperature (15.1°C) c) LGM conditions. Yellow field highlights temperature range between 14.9 and 7.0°C (22.2 kyrs). These are the maximum and minimum temperatures derived from the single specimen *G. inflata* analysis. Dashed yellow circle indicates the multispecimen *G. inflata* Mg/Ca temperature (11.3°C).

We hence note that, within the given model resolution, the concluded depths must be interpreted with some caution. However, the large scale patterns of a highly stratified water column in the tropics and a weak stratification in the subtropics and mid-latitudes are well reflected by the model.

During Heinrich-like conditions, the model predicts a thermal stratification substantially different from the preindustrial state (Figure 4.2-6b). The most notable difference to the preindustrial (and LGM, see below) thermal stratification is that north of 20°N the isotherms below ~150 m raise, resulting in a stronger stratification of the water column throughout the subtropics and mid-latitudes, including the study site. The reconstruction of temperature ranges of the Heinrich Stadial samples (16.8 kyrs BP) yields temperatures between 17.4 and 12.9°C. Comparison of these temperatures to the modeled subsurface temperatures suggests a substantially reduced calcification depth range during Heinrich-like conditions compared to the preindustrial state. At 17.5°N, the depth range would be 50 to ~100 m and at 22.5°N about 0 to 90 m.

This reduction is well reflected by the single specimen analysis. The $\delta^{18}O_c$ standard deviation (0.23) of the HS1 population (Table 4.2-3) is below the 95% confidence interval of the 570 years BP population (0.25-0.48). From this we conclude that the habitat of *G. inflata* during HS1 was substantially narrower than during the present, due to increased water column stratification. While the model reflects only the situation during Heinrich-like conditions, it is interesting to note that the reduced standard deviation is a persistent feature of all samples between 16.8 and 12.3 kyrs BP (Table 4.2-3 and Figure 4.2-5), suggesting a strong water column stratification after HS1 persisting until at least 12.3 kyrs BP.

As for the preindustrial model, the Mg/Ca multi-specimen temperature record (15.1°C) suggests an average calcification depth somewhat shallower (~70 m) than observed at present. It is assumed that the actual average calcification depth was deeper. This is supported by $\delta^{18}O_c$ of *G. inflata* substantially different from surface mixed layer values throughout the deglaciation (Figure 4.2-2).

Deglacial subsurface warming

A further important aspect predicted by the model is a subsurface warming during Heinrich-like conditions compared to the LGM that reached as far as 20°N (Figure 4.2-7). The warming reached from ~100 to 200 m, hence covering a crucial depth to influence the temperatures recorded by *G. inflata*.

The warming (~0.5°C) is, however, smaller than that suggested by the Mg/Ca record, which shows an average warming of ~1.6°C between the LGM (average value 23-19 kyrs BP) and HS1 (average value 16.8-16 kyrs BP). We therefore assume that further mechanisms must have contributed to the recorded warming. As suggested above, during Heinrich-like conditions (Figure 4.2-6b) and potentially throughout the deglaciation (Figure 4.2-4), *G. inflata* inhabited a reduced vertical depth range as compared to the preceding LGM. This suggests that only relatively warm temperatures of the upper water column are recorded. A further important aspect that may have contributed to the warming could have been the sea level rise by ~120 m [*Waelbroeck et al.*, 2002] during the deglaciation.

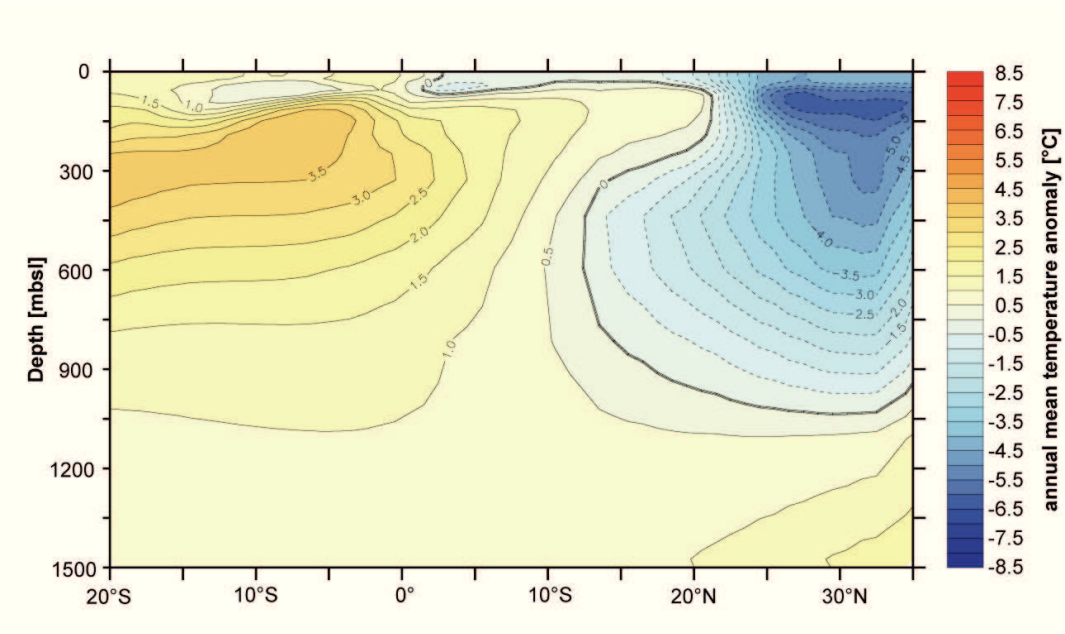

Figure 4.2-7 (previous page). Annual mean temperature anomalies (°C) of Heinrich-like conditions with respect to LGM-like conditions as simulated by the CCSM3 model. Results are based on the last 100 years of the model runs and show the zonal average between 25° and 15°W for the upper 1500 m of the water column.

A lower sealevel during the LGM dictates that the continental shelf extended further seawards. It is assumed that this may have caused a seaward displacement of the rather narrow (~50 km) poleward undercurrent (Figure 4.2-1b), so that the study site was exposed to a larger influence of cold SACW conveyed with this. With rising sealevel, a shoreward retreat of the core of northward flowing SACW would have implied a gradual increase of subsurface temperatures.

4.2.6 Conclusions

Using a combined approach of conventional Mg/Ca temperature reconstruction from the planktic foraminifer *G. inflata*, single specimen temperature reconstruction and modeling, we assess upper water column temperatures and stratification off NW Africa for the past 24 kyrs. Our results show that

1. The near modern $\delta^{18}O_c$ range of single specimens from the sedimentary record matches the $\delta^{18}O_{eq}$ in the water column between 0 and ~420 m, in good agreement with the results of a sediment trap study at the same site
2. Water column stratification was higher during the deglaciation compared to the LGM and Holocene. This reduced the habitat depth range of *G. inflata* during the deglaciation and is seen in a reduced variability of $\delta^{18}O_c$ between individual specimens
3. The calcification temperature of *G. inflata* shows a long term deglacial warming of ~3°C and a cooling between 10 and 1.5 kyrs BP
4. Reduced temperature ranges are mostly due to higher minima of the calcification range of *G. inflata,* suggesting that thermal changes are most pronounced at depth >~200 m.

Acknowledgements

Sample collection and technical support was provided by The Center for Marine Environmental Sciences (MARUM), University of Bremen and the Vrije Universiteit Amsterdam. We thank Suzanne Verdegaal for laboratory assistance. This study was carried out within the International Graduate College EUROPROX, funded by the Deutsche Forschungsgemeinschaft (DFG).

Supplement to: Haarmann, T., F. Peeters, G. Ganssen, U. Merkel, and T. Bickert (for submission to Paleoceanography), Subsurface thermal stratification off NW Africa during the past 24,000 years – inferences from single planktic foraminifer shells

Table 4.2-S1. Single specimen $\delta^{18}O_c$ [‰ vs. PDP] of *G. inflata* at selected depths in sediment core GeoB7926-2. Data that have been identified as outliers and which are not used are shown in brackets. Outliers are defined as falling outside the range [Q1-1.5*(Q3-Q1), Q3+1.5*(Q3-Q1)] with Q1 and Q3 being the first and the third quartile of the data, respectively.

$\delta^{18}O_c$ O cm	$\delta^{18}O_c$ 8 cm	$\delta^{18}O_c$ 78 cm	$\delta^{18}O_c$ 273cm	$\delta^{18}O_c$ 413 cm	$\delta^{18}O_c$ 498 cm	$\delta^{18}O_c$ 563 cm	$\delta^{18}O_c$ 733 cm	$\delta^{18}O_c$ 743 cm
0.71	0.20	0.21	(1.23)	1.92	1.80	1.92	1.11	2.05
0.90	0.33	0.23	(1.31)	1.99	1.88	2.33	1.15	2.07
	0.47	0.40	1.36	2.03	1.92	2.39	1.26	2.16
	0.48	0.44	1.53	2.06	1.92	2.44	1.51	2.22
	0.57	0.44	1.65	2.07	1.96	2.55	1.52	2.36
	0.67	0.46	1.66	2.12	1.99	2.56	1.53	
	0.72	0.50	1.70	2.14	2.01	2.66	1.53	
	0.77	0.53	1.71	2.16	2.07	2.74	1.54	
	0.79	0.61	1.72	2.20	2.15	2.78	1.59	
	0.80	0.64	1.73	2.20	2.15	2.84	1.63	
	0.88	0.70	1.78	2.21	2.15	2.85	1.64	
	0.91	0.70	1.81	2.22	2.18	2.87	1.64	
	0.91	0.81	1.81	2.23	2.19	2.92	1.68	
	0.92	0.81	1.83	2.23	2.21	2.94	1.74	
	1.13	0.82	1.89	2.26	2.21	2.94	1.75	
	1.17	0.83	1.89	2.29	2.23	3.02	1.75	
	1.24	0.94	1.90	2.30	2.25	3.03	1.78	
	1.25	0.95	1.92	2.31	2.29	3.03	1.79	
	1.26	1.00	1.92	2.32	2.31	3.05	1.79	
	1.27	1.02	1.95	2.33	2.34	3.08	1.80	
	1.31	1.11	1.96	2.33	2.35	3.14	1.81	
		1.12	2.00	2.34	2.36	3.16	1.82	
		1.15	2.11	2.36	2.38	3.18	1.87	
		1.17		2.38	2.39	3.24	1.88	
		1.28		2.40	2.39		1.93	
		1.31		2.46	2.40		1.94	
		1.35		2.46	2.40		2.01	
		1.71		2.48	2.42		2.01	
		1.91		2.48	2.43		2.05	
				2.48	2.43		2.07	
				2.54	2.44		2.13	

Table 4.2-S1 (continued). Single specimen $\delta^{18}O_c$ [‰ vs. PDP] of *G. inflata* at selected depths in sediment core GeoB7926-2. Data that have been identified as outliers and which are not used are shown in brackets. Outliers are defined as falling outside the range [Q1-1.5*(Q3-Q1), Q3+1.5*(Q3-Q1)] with Q1 and Q3 being the first and the third quartile of the data, respectively.

$\delta^{18}O_c$ 0 cm	$\delta^{18}O_c$ 8 cm	$\delta^{18}O_c$ 78 cm	$\delta^{18}O_c$ 273cm	$\delta^{18}O_c$ 413 cm	$\delta^{18}O_c$ 498 cm	$\delta^{18}O_c$ 563 cm	$\delta^{18}O_c$ 733 cm	$\delta^{18}O_c$ 743 cm
				2.55	2.44		2.32	
				2.56	2.44		2.41	
				2.57	2.49		2.43	
				2.58	2.51		2.44	
				2.60	2.51		2.63	
				2.60	2.55		(2.86)	
				2.65	2.55		(2.87)	
				2.69	2.60		(2.89)	
				2.73	2.62			
				2.78	2.65			
					2.67			
					2.78			

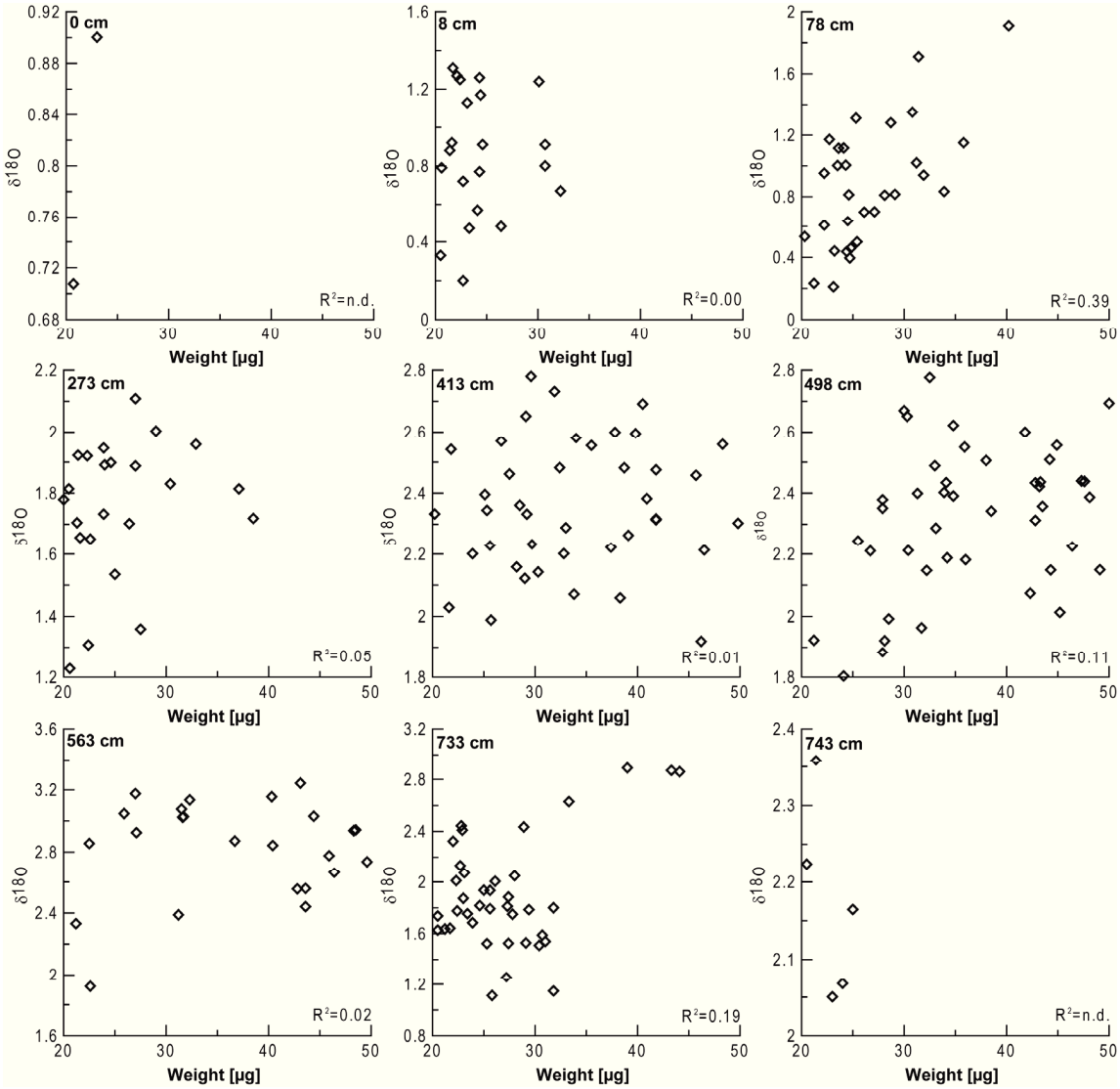

Figure 4.2-S1. Single specimen oxygen isotope ratios [‰ vs. PDB] of *G. inflata* from sediment core GeoB7926-2 versus shell weight (each sample was weighted in three replicates).

4.3 Manuscript 3

Upwelling strength off Cape Blanc (NW Africa) during the past 24,000 years – Effects on the surface and subsurface Mg/Ca temperature records

Tim Haarmann, Mahyar Mohtadi, Jeroen Groeneveld, Torsten Bickert

Marum – Center for Marine Environmental Sciences, Leobener Straße, 28359 Bremen, Germany

In preparation for Biogeosciences

Upwelling of cold, nutrient rich subsurface waters is an important process that strongly fosters productivity in the coastal area off NW Africa. Previous studies suggest increased paleoproductivity along most of the NW African continental margin during the Last Glacial Maximum (LGM), whereas off Cape Blanc (~20°N) decreased productivity was found. This finding has been associated with a decrease of upwelling strength that has also been invoked to explain unexpectedly warm local surface water temperatures during this cold climatic state.

In the present study, we reconstruct upwelling strength off NW Africa for the past 24,000 years from the relative abundance of the planktic foraminifer *Globigerina bulloides*. Sea surface temperatures (SST) were reconstructed using the Mg/Ca temperature proxy in the surface-dwelling foraminifer species *G. bulloides* and *Globigerinoides ruber* (pink) and compared to Mg/Ca temperatures of the subsurface-dwelling species *Globorotalia inflata*.

Despite of previous findings, *G. bulloides* abundances suggest a strong upwelling during the LGM between 24 and 16 kyrs BP followed by a strong decrease afterwards. The decrease in upwelling intensity coincides with a decrease of wind strength reconstructed in other studies off Cape Blanc, suggesting a strong influence of wind strength on upwelling at the study site. Reconstructed Mg/Ca temperature variability is generally high in the surface dwelling species throughout the record. As no such variability is recorded in the intermediate depth dwelling species *G. inflata*, the large temperature differences appear to result from exceptionally large SST variability at the study site. Inspection of daily SSTs between 1982 and 2008 from upwelling and non-upwelling months suggests that increased wind strength has the potential to substantially increase local SSTs, likely through a northward advection of warm southerly surface waters towards the study site. It is presumed that also in the past this mechanism might have caused higher SSTs at the study site during generally cold climatic states

4.3.1 Introduction

The coastal area off NW Africa is one of the four large global eastern boundary upwelling systems of the subtropics. Located at the eastern boundary of the North Atlantic Subtropical Gyre, cold and nutrient-rich subsurface waters are pumped to the surface through Ekman-transport from water depths between 100 and 300 m [*Mittelstaedt*, 1983]. This important process enriches surface waters with nutrients and strongly fosters productivity [*Fischer et al.*, 1996; *Helmke et al.*, 2005], which in turn largely contributes to global primary productivity and the sequestration of carbon.

Considerable interest in the role of this system related to climate change and potential increase of upwelling strength during the 20th century [*Bakun*, 1990] resulted in a multitude of reconstructions of upwelling and productivity for the past [e.g.; *Chapman et al.*, 1996; *Martinez et al.*, 1999; *Zhao et al.*, 2000; *Freudenthal et al.*, 2002; *Kuhlmann et al.*, 2004; *Adkins et al.*, 2006; *Haslett and Smart*, 2006; *Romero et al.*, 2008; *Filipsson et al.*, 2011]. It is now clear that this system is spatially very heterogeneous. In particular off Cape locations, where offshore advected filaments develop [*Pelegrí et al.*, 2005], large uncertainties remain. A good example for this phenomenon is the perennial upwelling off Cape Blanc (~21°N). While highest productivity is reported for most of the NW African continental margin during glacials [e.g.; *Abrantes*, 2000; *Freudenthal et al.*, 2002; *Henderiks et al.*, 2002] or the last deglaciation [*Kuhlmann et al.*, 2004], reconstructions off Cape Blanc are contradictory.

While decreased productivity is attributed to more easterly winds, effectively suppressing Ekman-induced upwelling [*Zhao et al.*, 2000], higher productivity is attributed to stronger northeast trade winds that modified the direction an extent of the upwelling cell [*Chapman et al.*, 1996]. Since upwelling can lower the sea surface temperature (SST) by up to 6°C, a past decrease of upwelling strength was invoked as a possible mechanisms for explaining unexpectedly warm SST off Cape Blanc during the Last Glacial Maximum (LGM) that exceeds those of the preceding older glacial and the following deglaciation [*Zhao et al.*, 2000; *Sicre et al.*, 2001; *Romero et al.*, 2008].

In the present study, we reconstruct the upwelling strength off Cape Blanc for the past 24,000 years based on the relative abundance of the planktic foraminifera *Globigerina bulloides* for

testing the previous hypothesis of decreased upwelling strength at the study site [*Romero et al.*, 2008]. We further reconstruct Mg/Ca temperatures from various species of planktic foraminifera to test if we can reproduce an increase of SST in response to decreased upwelling strength. We carried out our analysis on the typical upwelling species *G. bulloides* [*Fairbanks et al.*, 1982; *Sautter and Sancetta*, 1992; *Mohtadi et al.*, 2009] and compared it with Mg/Ca temperatures from less abundant species during upwelling (*Globigerinoides ruber* (pink)) and from intermediate depths (*Globorotalia inflata*). We discuss the potential influence of interannual SST variability in response to different upwelling intensities on Mg/Ca temperature reconstructions of different planktic foraminifera.

4.3.2 Modern climate

The climatology at the study site is dominated by the seasonal migration of the Inter Tropical Convergence Zone (ITCZ). During boreal winter, the ITCZ is located at ~5°N, while its position in summer is ~15°N. Following the movement of the ITCZ the northeast trade winds move northward in summer to ~32°N and southward in winter to ~12°N. Between 20°N and 25°N, they blow throughout the year [*Schemainda et al.*, 1975]. The trade winds modulate the southward flowing Canary Current, while during summer monsoon winds advect warm (>27°C) surface water northward as far as 20°N [*Nykjær and Van Camp*, 1994 and references therein] in a narrow northward compensation flow along the Mauritanian coast between Cape Vert and Cape Blanc [*Mittelstaedt*, 1983; *Gabric et al.*, 1993].

The wind system provokes upwelling along the whole NW African coast (Figure 4.3-1). Between ~20°N and

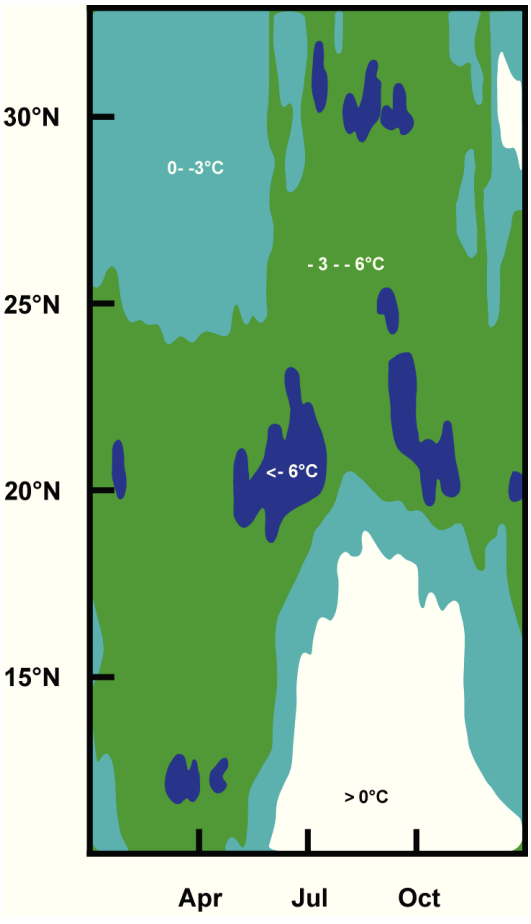

Figure 4.3-1. Mean temperature differences between NW African coastal areas and mid-Atlantic between 1969 and 1976. Negative values indicate coastal temperatures colder than mid-ocean [modified after Speth et al., 1978].

~30°N upwelling is perennial and between 20°N and 12°N it is limited to the winter months [*Barton*, 2001]. Strongest upwelling occurs between ~20°N and ~24°N during summer. Upwelling advects cold subsurface water to the surface and ascends from depths of 200 to 300 m north off Cape Blanc and 100 to 200 m south of Cape Blanc. The upwelled water is frequently transported up to 500 km offshore by large filaments [*Pérez-Rodríguez et al.*, 2001; *Pelegrí et al.*, 2005], which also stretch over the study site (Figure 4.3-2c).

Generally, to the south of 24°N, upwelled water is dominated by the cold, nutrient rich and relatively fresh (35.6 - 35.9‰) South Atlantic Central Waters [*Mittelstaedt*, 1983]. North of 24°N, the upwelled water consists of the relatively nutrient poor, saline (36.1 – 36.4‰) and warmer North Atlantic Central Waters. Off Cape Blanc, the Cape Verde frontal zone stretches southwest from Cape Blanc to the Cape Verde Islands and separates the NACW from the SACW. Due to the similar density of NACW and SACW they are strongly mixed up, forming a melange of both water masses.

Overall, the interplay of upwelling and surface circulation results in a strong annual as well as interannual SST variability. Between 1982 and 2008, the average annual temperature was 20.9°C and the average annual range 8.2°C (σ = 1.5°C). The highest temperature during the period of satellite observation was recorded on 11 September 2005 (27.8°C) and the lowest on 21 February 1999 (16.5°C) (derived from daily SST of the advanced very high resolution radiometer at 20.45°N, 18.41°W; http://www.ncdc.noaa.gov/oa/ncdc.html)

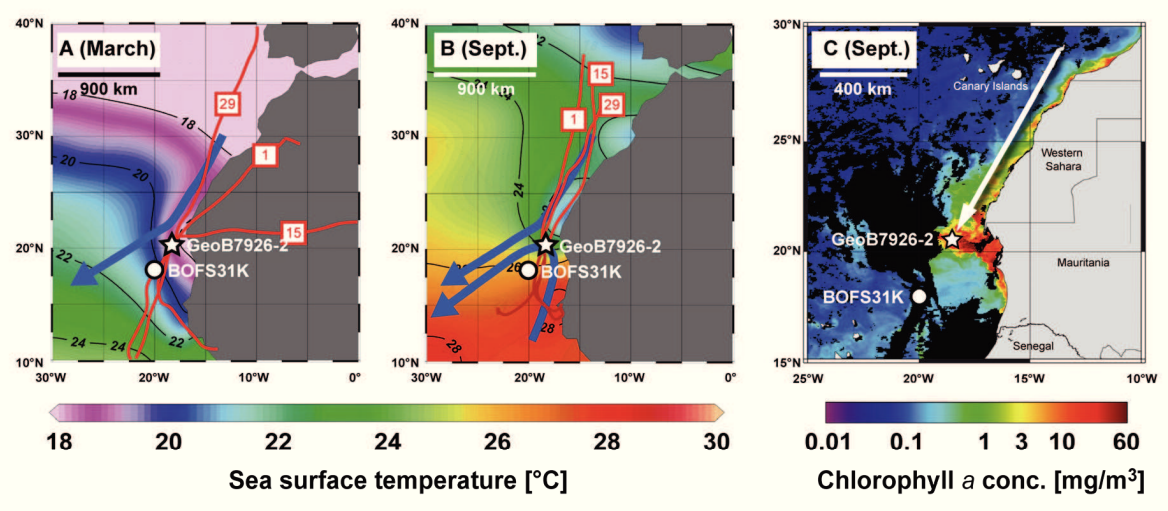

Figure 4.3-2. Map of the study site with simplified atmospheric and oceanographic features. a) Monthly SST during March is shown by color shading [*Locarnini et al.*, 2006]. Red lines show 72h backward (to the north) and forward (to the south) wind trajectories in March moving at 100 m above the study site during the year 2000 (Calculated using the Hybrid single particle Lagrangian Trajectory Model of the National Oceanic and Atmospheric Administration Air resources laboratory; http://ready.arl.noaa.gov/hysplit-bin/trajtype.pl?runtype=archive). Red numbers in boxes indicate respective day of the month. b) same as (a) but for September c) Chlorophyll *a* concentration between 22 and 29 September 2005 (http://oceancolor.gsfc.nasa.gov/).

4.3.3 Material and methods

Sample collection and revised age model

The 1330 cm long gravity core GeoB7926-2 was recovered during R/V *Meteor* Cruise 53/1c [*Meggers and cruise participants*, 2003] at 20°12.8'N, 18°27.1'W at 2500 m water depth. Samples representative for present day were collected from the top centimeter of multicore GeoB 7408-2 at 20°17.4'N, 18°15.0'W, recovered in a water depth of 1935 m, during R/V *Poseidon* cruise 272 [*Meggers et al.*, 2002], less than 13 nm away from the gravity core. Sediment samples were wet-sieved into the two size fractions of 63-150 µm and >150 µm.

The age model of the upper 820 cm is based on 12 Accelerator Mass Spectrometry (AMS) ^{14}C dates on monospecific samples of the planktic foraminifera *G. inflata* and covers approximately the last 24 kyrs. Radiocarbon ages have been previously published [*Romero et al.*, 2008]. We revised the age model, converting radiocarbon ages into calendar years using the Calib Rev 6.1.0 program, with the most recent marine calibration dataset marine09.14c [*Reimer et al.*, 2009]. We acknowledge that the dated species *G. inflata* was possibly exposed to water exceeding the global reservoir age of ~400 yrs. We hence calculated the

calendar age that would be associated with an additional local reservoir age of 197 years (ΔR). This is the local reservoir age further south (http://www.calib.qub.ac.uk/marine/regioncalc.php), where old South Atlantic Central Water is upwelled, likely exhibiting the oldest reservoir age at the study site. In Table 4.3-1, we show calculated calendar ages assuming no reservoir age and in Table 4.3-2 assuming a ΔR of 197 years to show the effect this has on the calculated calendar ages.

Table 4.3-1. Revised age model of sediment core GeoB7926-2, using the ^{14}C dates measured by *Romero et al*. [2008] on *Globorotalia inflata*.

Lab number	Interval [cm]	Age [^{14}C]	± Error [yrs]	Age[a] [cal yrs BP](Δ=0yrs)[b]	1σ range [yrs BP][c]
KIA 24287	8	1170	35	712	670-740 (1.0)
KIA 25812	48	4455	35	4640	4557-4707 (1.0)
KIA 25810	98	8970	45	9629	9542-9681 (1.0)
KIA 24286	173	10050	70	11041	10937-10995 (0.20) 11000-11157 (0.80)
KIA 22417	248	10830	70	12303	12119-12136 (0.05) 12180-12392 (0.79) 12469-12520 (0.16)
KIA 24285	378	12220	70	13662	13517-13528 (0.03) 13578-13777 (0.97)
KIA 29030	418	13050	70	14946	14692-14726 (0.06) 14786-15152 (0.94)
KIA 27310	483	14220	100	16916	16801-17012 (1.0)
KIA 29029	508	14290	60	16956	16850-17044 (1.0)
KIA 22416	553	14670	80	17350	17171-17532 (1.0)
KIA 27309	688	17100	130	19844	19581-19729 (0.38) 19774-20051 (0.62)
KIA 29028	803	20450	160	23956	23742-24218 (1.0)
KIA 24283	868	23650	220-230	28091	27857-28357 (1.0)

Table 4.3-2. Same as table 4.3-1, but with an additional local reservoir age of 197 years

Lab number	Interval [cm]	Age [^{14}C]	± Error [yrs]	Age[a] [cal yrs BP](Δ=197yrs)[d]	1σ range [yrs BP][c]
KIA 24287	8	1170	35	567	530-603 (1.0)
KIA 25812	48	4455	35	4368	4306-4418(1.0)
KIA 25810	98	8970	45	9449	9412-9491 (1.0)
KIA 24286	173	10050	70	10759	10604-10822 (0.86) 10837-10883 (0.14)
KIA 22417	248	10830	70	11945	11754-11797 (0.11) 11840-12092 (0.89)
KIA 24285	378	12220	70	13463	13363-13518 (0.82) 13528-13576 (0.18)
KIA 29030	418	13050	70	14548	14216-14754 (1.0)
KIA 27310	483	14220	100	16763	16660-16889 (1.0)
KIA 29029	508	14290	60	16827	16742-16911 (1.0)
KIA 22416	553	14670	80	17115	16922-17233 (1.0)
KIA 27309	688	17100	130	19684	19445-19605 (0.54)
KIA 29028	803	20450	160	23715	23477-23912 (1.0)
KIA 24283	868	23650	220-230	27872	27602-28250 (1.0)

[a] To convert uncorrected ^{14}C ages into calendar ages, the CALIB REV 6.1.0 program was used [*Stuiver and Reimer*, 1993]. The calibration data set used was marine09.14c [*Reimer et al.,*2009].
[b] Global ocean reservoir correction was used as incorporated in the marine 09.14c calibration data set and is about 400 years [*Reimer et al.*, 2009].
[c] Enclosing 68.3% of the probability distribution. Values in parenthesis are the relative area under probability distribution
[d] An additional local ΔR of 197 years was included, based on the weighted mean of samples between 16.05° and 15.65°N off the West African coast, i.e. samples exposed to upwelling of South Atlantic Central Waters (http://www.calib.qub.ac.uk/marine/regioncalc.php)

Data acquisition

Mg/Ca thermometry

All species were identified following the taxonomy of *Hemleben et al.* [1989]. Most *G. inflata* (d'Orbigny) specimens had four chambers in the last whorl, and had moderately thickened walls. Between 14 and 30 specimens of *G. bulloides*, 14-28 specimens of *G. ruber* (pink) and ~20 specimens of *G. inflata* were gently crushed and cleaned according to the *Barker et al.* [2003] protocol. *G. inflata* sizes were mostly between 400 and 480 µm, while for *G. bulloides* and *G. ruber* (pink) somewhat large size ranges (listed in Table 4.3-S1) were necessary in order to collect enough specimens for analysis. Uncertainties related to these are addressed in the discussion section. Samples were washed seven times with suprapure (18.2 MΩ cm) water, twice with methanol followed by two oxidation steps of 10 min and a weak acid leach in 0.001M TD HNO_3. Samples were dissolved in 0.075M TD HNO_3, centrifuged for 10 min at 6000 rpm, transferred into test tubes and diluted for analysis. Mg/Ca ratios were measured with a Perkin Elmer Optima 3300R Inductively Coupled Plasma Optical Emission Spectrometer (ICP-OES) equipped with an auto sampler and an ultrasonic nebulizer U-5000 AT (Cetac Technologies Inc.) and with an Agilent Technologies 700 Series ICP-OES, at the faculty of Geosciences and the Center for Marine Environmental Sciences, University of Bremen. Verification of the Mg/Ca ratios was achieved against international carbonate reference material ECRM 752-1 [*Greaves et al.*, 2008]. The Mg/Ca ratio of the standard during the analytical sessions for *G. bulloides* and *G. ruber* (pink) was on average 3.84 mmol/mol (n = 21, σ = ±0.02 mmol/mol) and during the analysis of *G. inflata* on average 3.84 mmol/mol (n = 12; σ = ±0.04 mmol/mol). Stability of the Mg/Ca measurements was monitored by analysis of an in-house artificial standard solution with Mg/Ca ratio of 2.95 mmol/mol (n = 35; σ = ±0.02 mmol/mol) during the analytical session for *G. bulloides* and *G. ruber* (pink) and 3.01 mmol/mol (n = 40; σ = ±0.05 mmol/mol) during the analytical session for *G. inflata*. The precision of Mg/Ca measurements on *G. bulloides* and *G. ruber* (pink) was on average 0.09%, based on three replicates (n=120) and the precision of Mg/Ca measurements on *G. inflata* on average 0.22%, based on mostly three (n=111) and few times (n=17) two replicates. In order to correct for small shifts between

analytical sessions, values of individual sessions were normalized to the reported Mg/Ca ratio of 3.75 mmol/mol of the ECRM 752-1 [*Greaves et al.*, 2008].

Samples did not show visible encrustations or dissolution in light microscopic inspection. Core depths with suspiciously high Mg/Ca were resampled for *G. ruber* (pink) and *G. bulloides* and specimens were subjected to SEM inspection, which did not show signs of diagenesis (Figure 4.3-4).

For calculating the Mg/Ca temperatures of *G. bulloides* (equation 4.3-1) and *G. inflata* (equation 4.3-2) the calibration equations of *Elderfield and Ganssen* [2000] were used.

$$T = \ln((Mg/Ca)/0.56))/0.1 \quad (4.3\text{-}1)$$

$$T = \ln((Mg/Ca))/0.49)/0.1 \quad (4.3\text{-}2)$$

For calculating the *G. ruber* (pink) calcification temperature, the equation of *Regenberg et al.* [2009] was used.

$$T = \ln((Mg/Ca)/0.87))/0.056 \quad (4.3\text{-}3)$$

The selection of these equations from a substantial number of calibrations was based on the following considerations. For *G. ruber* (pink) and *G. inflata* these equations gave the most realistic estimates in a sediment trap study just above the core location [*Haarmann et al.*, 2011]. For *G. bulloides*, the use of the *Elderfield and Ganssen* [2000] equation gives a SST of 19.0°C for the most recent sample, in good agreement with the average SST during the times of main flux [*B. Donner, pers. comm.*] at the study site (18.8°C in March and 20.3°C in July).

***G. bulloides* census counts**

Sediment samples were divided into aliquots using a MS-1 microsplitter of ASC scientific and contained at least 300 specimens of planktic foraminifera. *G. bulloides* percentage was then calculated relative to the total fauna.

4.3.4 Results

***G. bulloides* census count**

The relative abundance of *G. bulloides* ranges between 32 % (22.1 kyrs BP) and 4.5 % (2.5 kyrs BP) (Figure 4.3-3b). During the LGM and Heinrich Stadial 1 (HS1) between 23.6 kyrs BP and 15.6 kyrs BP, *G. bulloides* abundances are high and on average 18.4 %. This period is followed by a sharp decrease within about 300 years after HS1. Throughout Bølling-Allerød (B/A), Younger Dryas (YD) and the major part of the Holocene until 3.4 kyrs BP, abundances remain at a moderate level and are on average 12.2 %. After 3.4 kyrs BP until present, values are low and on average 5 %.

Comparison of our results to the study of *Adkins et al.* [2006] shows that the deglacial as well as Holocene values of *G. bulloides* abundances are much lower than in the nearby core ODP 658C (~40 % and ~15 %), with an earlier Holocene decrease than observed in core ODP685C (~5.5 kyrs BP). The *G. bulloides* abundances are closer to values from sediment core GIK 12310-4 [*Diester-Haass et al.*, 1973], which were ~30 % during the last deglacial, and sharply decreased between 10.4 kyrs BP and 9.2 kyrs BP to values of ~20 %.

Mg/Ca paleothermometry

G. ruber* (pink) and *G. bulloides

Mg/Ca ratios of *G. bulloides* range between 2.32 and 6.87 mmol/mol. Using the Mg/Ca temperature calibration of *Elderfield and Ganssen* [2000] this corresponds to temperatures between 14.2°C (16.0 kyrs BP) and 25.1°C (16.8 kyrs BP). No trend is discernable throughout the last 24 kyrs. During the LGM, between 23.2 kyrs BP and 19.1 kyrs BP, temperatures were on average 18.1°C. Between 19.1 kyrs BP and 15.7 kyrs BP, temperatures are slightly higher with two marked temperature maxima at 18.9 kyrs BP (23.7°C) and 16.8 kyrs BP (25.1°C). During the B/A interstadial, no clear temperature trend is observed, while during the YD, SSTs were slightly higher compared to the BA. The average temperature throughout the Holocene was 18°C.

Mg/Ca ratios of *G. ruber* (pink) range between 2.56 and 4.53 mmol/mol. Using the Mg/Ca temperature calibration of *Regenberg et al.* [2009] this corresponds to temperatures between 16.6°C (11.4 kyrs BP) and 25.4°C (16.9 kyrs BP). During the LGM, between 22.8 kyrs BP and 19.1 kyrs BP, temperatures were on average 19.3°C. Between 19.1 and 16.0 kyrs BP, SST

was episodically high with a maximum increase of 7.7°C (25.3°C) compared to the LGM. During the B/A between 13.5 kyrs and 12.8 kyrs BP temperatures reach peak values of 24.9°C and 24.4°C, respectively. A negative anomaly is centered at 11.4 kyrs BP (16.6°C). Throughout the Holocene, temperatures averaged 20°C and varied much less than during the last deglacial (maximal 2.8°C).

G. inflata

The minimum Mg/Ca ratio of *G.inflata* is 1.41 mmol/mol at 1.5 kyrs BP. Using the calibration equation of *Elderfield and Ganssen* [2000], this corresponds to a temperature of 10.6°C. A maximum of 4.08 mmol/mol is reached at 9.9 kyrs BP (21.2°C). Between 23.5 and 22.2 kyrs BP, Mg/Ca ratios sharply decrease from 3.59 mmol/mol to 1.52 mmol/mol (19.9°C to 11.3°C). This is followed by a gradual increase to 4.08 mmol/mol (21.2°C) (9.9kyrs BP). Mg/Ca ratios then decrease again to a value of 1.41 mmol/mol (10.6°C) at 1.5 kyrs BP, before reaching their present day value of 2.25 mmol/mol (15.2°C).

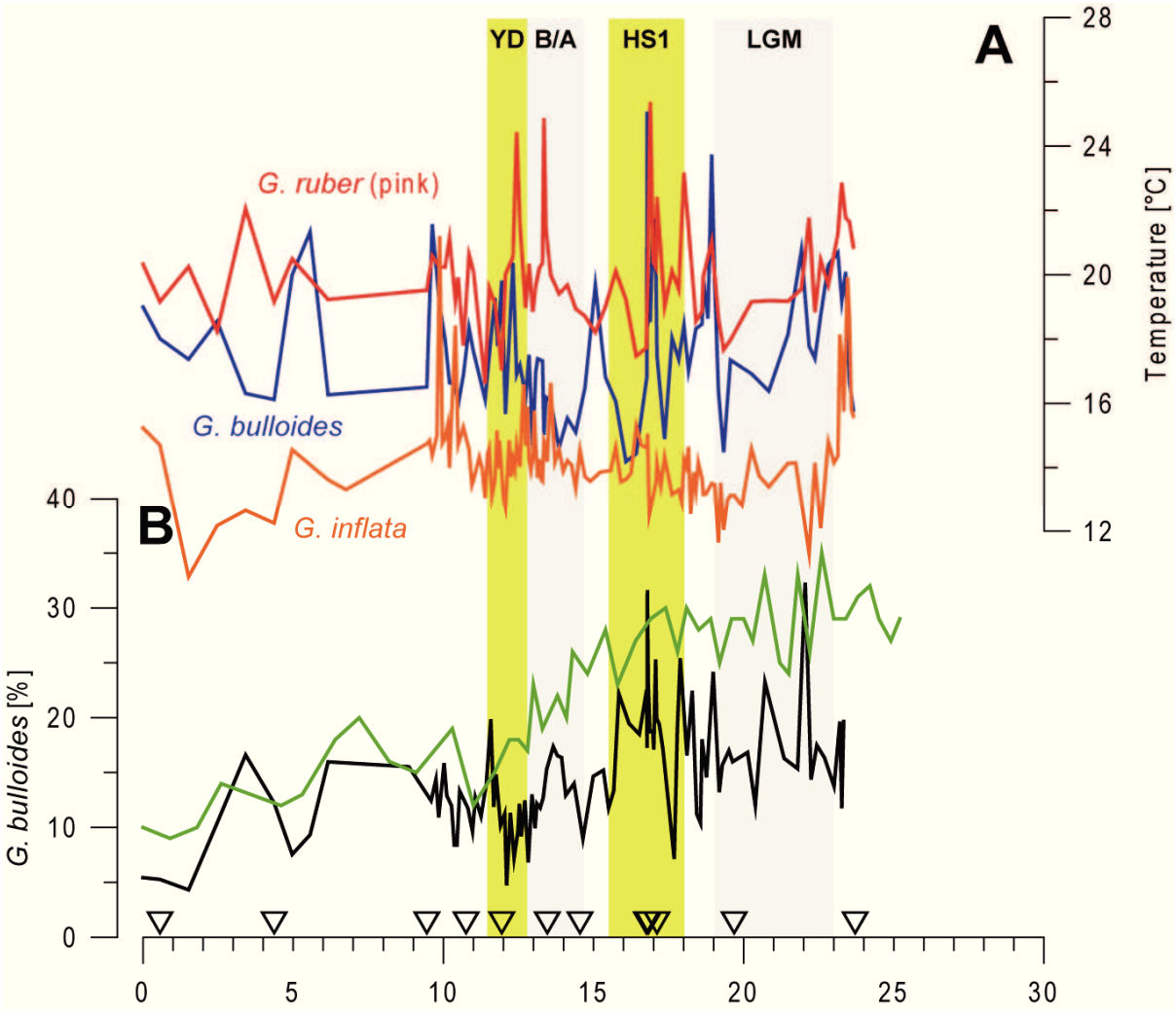

Figure 4.3-3. Upwelling strength and surface and subsurface temperatures reconstructed from sediment core GeoB7926-2 and multicorer GeoB7408-2 off Cape Blanc (NW Africa). a) Red graph: Mg/Ca temperatures of *G. ruber* (pink) calculated using the equation of *Regenberg et al.* [2009]; blue graph: Mg/Ca temperatures of *G. bulloides* calculated using the equation of *Elderfield and Ganssen* [2000]; orange graph: Mg/Ca temperatures of *G. inflata* calculated using the equation of *Elderfield and Ganssen* [2000] b) relative abundance of *G. bulloides* with respect to the total planktic foraminiferal fauna in sediment cores GeoB7926-2 (black line) and BOFS31K (green line, [*Chapman et al.*, 1996]). Triangles on abscissa show ^{14}C age control points, recalculated from ^{14}C ages of *Romero et al.* [2008]. LGM: Last Glacial Maximum, HS1: Heinrich Stadial 1, B/A: Bølling-Allerød, YD: Younger Dryas.

4.3.5 Discussion

G. bulloides abundance

We find high *G. bulloides* abundances, indicative of high nutrient availability, persisting during the LGM and HS1 and lasting until ~15.8 kyrs, after which abundances sharply decreased and remained on a moderate level afterwards (Figure 4.3-3b). This is in contrast to previous assumptions for the study site [*Romero et al.*, 2008] suggesting decreased upwelling strength during the LGM. The variability throughout the past 24 kyrs is higher than in a sediment core BOFS31K some ~200 km southwest of the study site [*Chapman et al.*, 1996], which is ascribed to the

position of the sediment core studies here just below the large upwelling filament. There, a large degree of variability with respect to the offshore export of nutrients is observed on short (daily) as well as long (interannual) timescales [*Gabric et al.*, 1993].

The decrease after ~15.8 kyrs BP coincides with a strong decrease in wind strength between ~16 and 12 kyrs BP reconstructed ~150 km north of the study site [*Martinez et al.*, 1999]. This argues for a control of wind strength on nutrient availability and does not support the assumption of decreased upwelling through an increase of easterly (continental) winds [*Zhao et al.*, 2000]. It is rather in line with previous studies that suggest the strength of northeasterly trade winds controls productivity off Cape Blanc through its influence on the extension of the upwelling cell [*Chapman et al.*, 1996] and a greater offshore movement of upwelled waters by wind-induced advection and diffusion.

Mg/Ca temperatures

Reconstructed Mg/Ca temperatures cannot be clearly assigned to any of the major rapid climatic changes since the LGM. No substantial cooling was reconstructed for the LGM, HS1 or the YD in all species (Figure 4.3-3a) nor reconstructed during the period of strong upwelling as suggested by high *G. bulloides* abundances (Figure 4.3-3b) between the LGM and 15.8 kyrs BP. Rather, high Mg/Ca ratios and consequently high temperatures are recorded by the surface dwelling species during this period and in particular during HS1.

Possible influences on the Mg/Ca ratios

Mg/Ca ratios in foraminifera can be biased by a number of factors other than temperature, that comprise contamination with clay minerals [*Barker et al.*, 2003], dissolution [e.g.; *Benway et al.*, 2003] or secondary calcite addition [e.g.; *Groeneveld and Chiessi*, 2011], size related effects [e.g.; *Elderfield et al.*, 2002] and salinity [e.g. *Ferguson et al.*, 2008; *Kisakürek et al.*, 2008; *Arbuszewski et al.*, 2010].

Clay minerals contain between ~1 and ~10% Mg by weight [*Deer et al.*, 1992], and can therefore bias Mg/Ca determinations towards higher values than that of pristine foraminiferal calcite. Cleaning of the shells was carried out following the well established *Barker et al.* [2003] protocol that included steps for clay removal. Parallel to determination of Mg concentrations, Fe concentrations were measured. In our

method, the calibration range for Fe ranges from 40-200 ppb. The measured concentrations were well below this range and must hence be considered an approximation. During the analytical session for *G. bulloides* and *G. ruber* (pink), Fe concentrations were on average 5.7 ppb ($n = 119$, $\sigma = 4.3$) and during the analysis of *G. inflata* on average 0.9 ppb ($n = 109$, $\sigma = 1.9$). This low concentrations and the lack of a correlation between Fe concentrations and Mg/Ca ratios indicates that cleaning effectively removed clay minerals.

Secondary calcite addition and shell dissolution are further processes that might change the Mg/Ca ratio of foraminiferal calcite. Magnesium is heterogeneously distributed throughout the tests of foraminifera [e.g.; *Hathorne et al.*, 2009] and it enhances the solubility of calcite [*Davis et al.*, 2000]. This results in preferential dissolution of these portions of the foraminiferal test that contain high amounts of Mg [e.g.; *Hathorne et al.*, 2009]. Selective dissolution hence results in decreased Mg/Ca ratios [e.g.; *Regenberg et al.*, 2006; *Dekens et al.*, 2002]. In any case, we did not find indication for dissolution or crust addition in SEM imagery at those depths with exceptionally high Mg/Ca ratios (Figure 4.3-4).

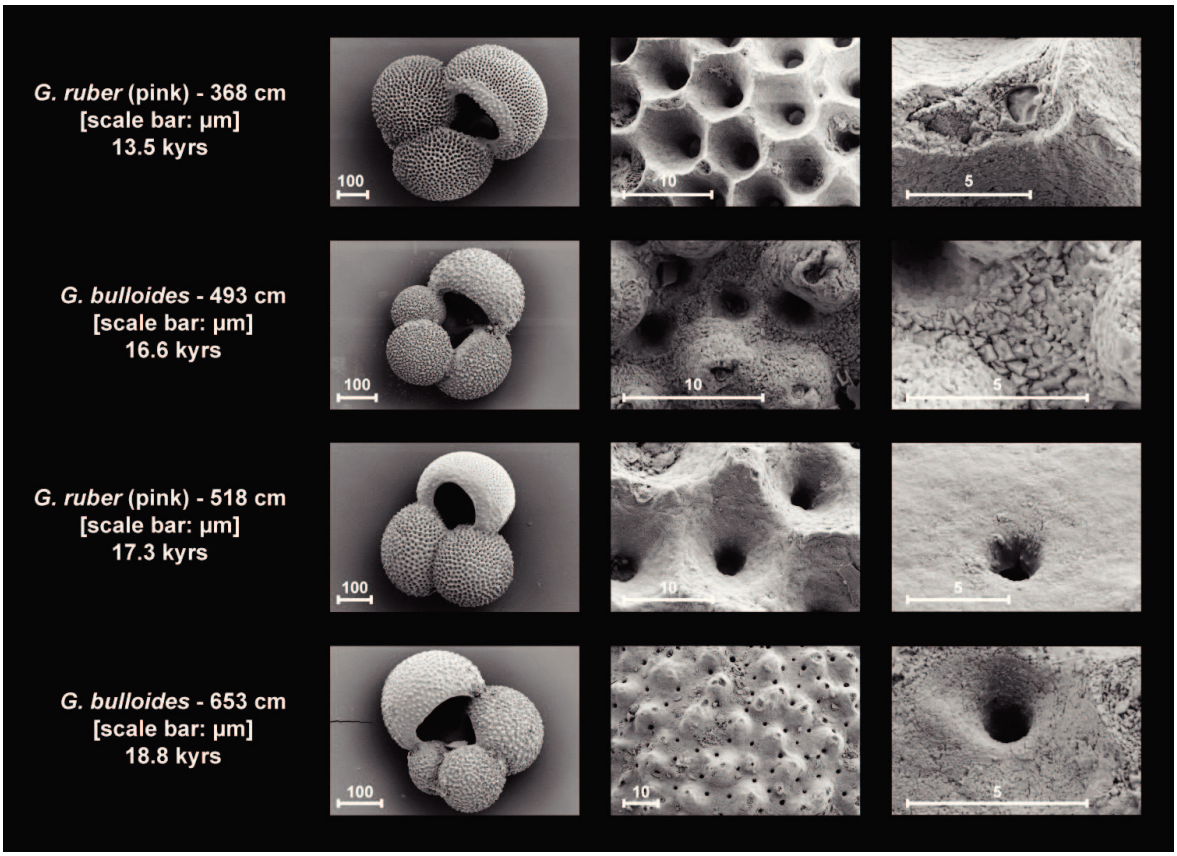

Figure 4.3-4. SEM images of *G. ruber* (pink) and *G. bulloides* from selected depths in sediment core GeoB79262-2.

Limited numbers of specimens within a narrow size fraction forced an occasional inclusion of specimens somewhat larger or smaller than desired (Table 4.3-S1). Foraminifera of different sizes have different Mg/Ca ratios [*Elderfield et al.*, 2002] and this introduces some uncertainty to the temperature estimates. In nearby sediment core BOFS31K, *Elderfield et al.* [2002] report a difference of 0.27 mmol/mol between smallest (212-250 µm) and largest (350-425µm) specimens of *G. bulloides* and of 0.67 mmol/mol between smallest (212 µm) and largest (>500 µm) specimens of *G. ruber* (pink). These are extreme examples from the comparison of very small and very large specimens, which has not been the case in the present study. Our samples were mostly limited to a narrower size fraction. In any case, the Mg/Ca variability and reconstructed temperatures are larger than could be explained by the use of a relatively wide size range.

A recently discussed issue in foraminiferal Mg/Ca thermometry is the influence of salinity [e.g. *Ferguson et al.*, 2008; *Kisakürek et al.*, 2008; *Arbuszewski et al.*, 2010]. For instance, for *G. ruber* (pink) a 18% (±12%)

Mg/Ca increase per psu is reported [*Ferguson et al.*, 2008] and for *G. ruber* (white) and exponential increase of 5% (±3%) [*Kisakürek et al.*, 2008]. Such dependency would affect Mg/Ca temperature determinations at the study site, considering recent studies suggesting a salinity increase of ~2.5 psu along the NW African margin during the LGM [*Huang et al.*, submitted]. Taking the Mg/Ca-salinity relationship of *Ferguson et al.* [2008] at face value, this could account for a ~45% increase of the Mg/Ca ratio in *G. ruber* (pink) during the LGM and HS1. If a substantial advection of salty North Atlantic Central Waters impaired the Mg/Ca ratios of *G. ruber* (pink) and *G. bulloides*, it is then surprising that this did not affect the intermediate depth dwelling species *G. inflata*, which lives in the same water mass. It is therefore assumed that another mechanism must have caused the large variability recorded by the surface dwelling species in contrast to the intermediate depth dwelling species *G. inflata*. We propose that this is the large SST variability at the study site, both on short (daily/weekly) as well as long (interannual) timescales.

Modern SST variability and upwelling strength

Present day satellite observations reveal substantial interannual SST variability at the study site. Figure 4.3-5 shows the range of daily SSTs during November (main flux period of *G. ruber* (pink) and weak upwelling period; conf. section 4.3.2) between 1982 and 2008. SST variability is generally high, while during some years (e.g.; 2000) daily SSTs exhibit a narrow range during November. However, this can be substantially different in the following or preceding years (e.g.; 2001 and 1999 in this example). We note that a change of wind strength/upwelling strength does not influence the overall high SST variability in this example that represents the non-upwelling period (November).

Figure 4.3-5 also shows the range of daily SSTs during July (main flux period of *G. bulloides* and main upwelling period; conf. section 4.3.2). Notably, during the period of weak wind stress, temperatures exhibit a reasonably small range and little variability. With the onset of higher wind stress, temperature variability becomes substantially more pronounced. Most remarkably, higher wind stress does not lead to negative temperature anomalies at the study site, as would be expected through stronger upwelling. Rather, exceptionally high

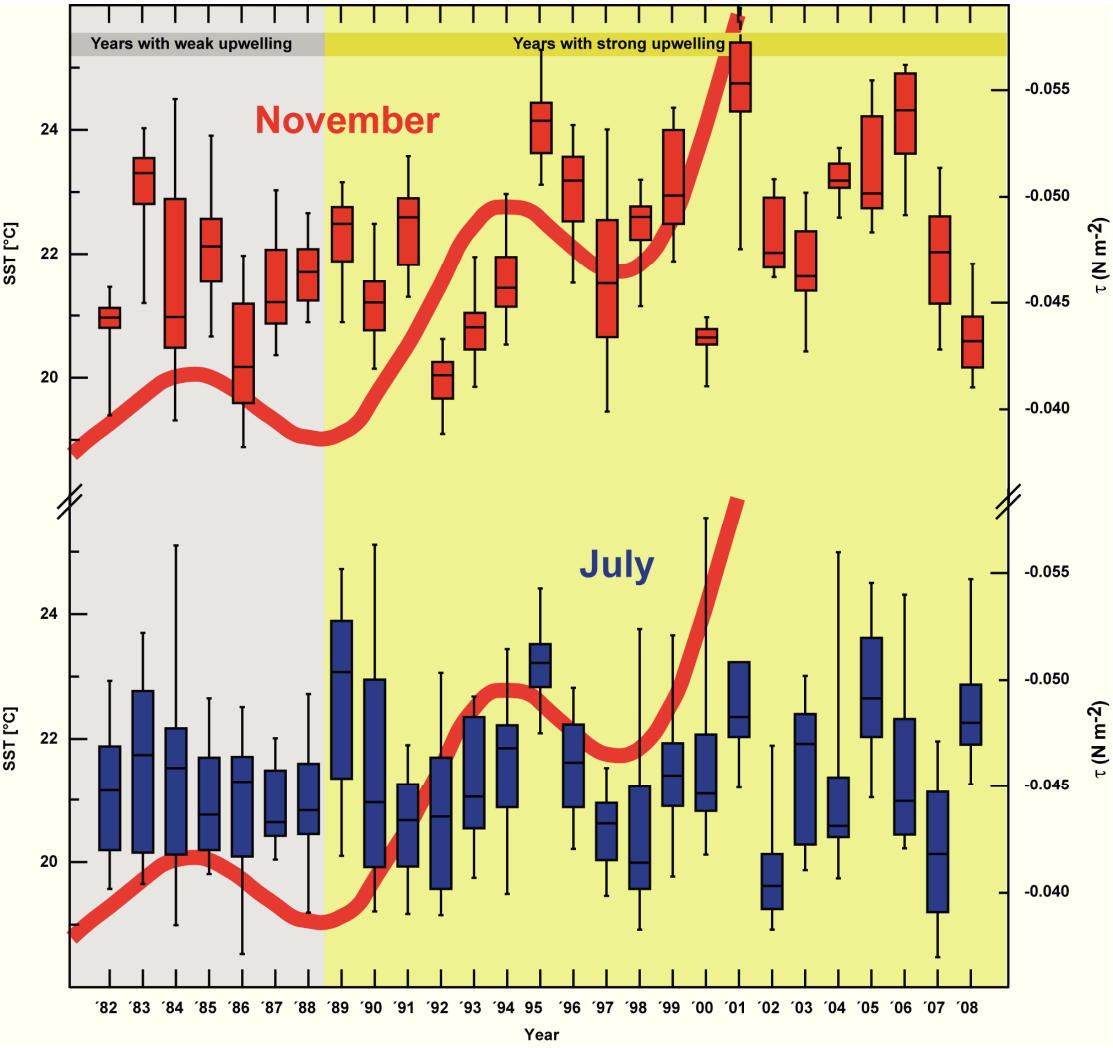

Figure 4.3-5. Monthly SST in November and July off Cape Blanc (20.45°N, 18.41°W) during several years with different upwelling strengths (gray and yellow shading). Each box-whisker plot represents the range of daily SSTs derived from the advanced very high resolution radiometer during November and July (http://www.ncdc.noaa.gov/oa/ncdc.html). The red line shows the annual wind stress off NW Africa in N m^{-2}, calculated by *Narayan et al.* [2010] from the comprehensive ocean atmosphere dataset.

temperatures exceeding 26°C are partly observed, e.g. in 2001.

The warm temperatures are likely the result of warm (>27°C) surface waters [*Nykjær and Van Camp*, 1994 and references therein] advected during summer through a northward compensation flow along the Mauritanian coast. This current is driven by a water mass deficit which is caused by the deviation of the Canary Current to the west [*Mittelstaedt*, 1983; *Gabric et al.*, 1993]. With stronger winds an intensification of this current is to be expected that causes occasionally high SST at the study site. Implications of this high SST variability and its dependency on wind strength/upwelling strength are addressed below.

Influence of large SST variability on Mg/Ca based temperature reconstructions

Planktic foraminifera have short lifespans of a couple of weeks to months [*Bé and Spero*, 1981; *Hemleben et al.*, 1989] and record short termed temperature variations at the study site [*Haarmann et al.*, 2011]. It was demonstrated above that the study site exhibits substantial interannual SST variability, which is particularly pronounced during strong upwelling. Upwelling is perennial at the study site at present [*Mittelstaedt*, 1983; *Barton*, 2001] and even enhanced between 24 and ~16 kyrs BP, implying a large degree of SST variability throughout the past 24,000 years that should be recorded in shell Mg/Ca of surface dwelling species. Contrastingly, intermediate depth dwelling species such as *G. inflata* that live at depths with little seasonal temperature variability [*Haarmann et al.*, 2011] are likely to record less pronounced temperature differences. This seems to be reflected in the Mg/Ca record (Figure 4.3-3a): Both surface dwelling species show a large degree of variability, while *G. inflata* shows only little variability. The highest temperatures and highest temperature variability is observed in *G. bulloides*, while temperature variability is less pronounced in *G. ruber* (pink) and only minor in *G. inflata* (Figure 4.3-3a). At present, *G. bulloides* is most abundant during spring/summer (Figure 4.3-6), reflecting its preference for the main upwelling period (Figure 4.3-1), suggesting that it will be most sensitive to occasionally warm temperatures. Contrastingly, *G. ruber* (pink) prefers warmer temperatures and is less abundant at the study site during the main upwelling period (Figure 4.3-6 and [*Haarmann et al.*, 2011]). The intermediate depth dwelling species *G. inflata* shows very little temperature variability. This reflects the fact that it dwells at a depth (on average ~150 m, [*Haarmann et al.*, 2011]), where temperature changes are only small throughout the year. It is hence not exposed to the pronounced temperature changes as found at the sea surface. Off Cape Blanc, warm temperatures during the LGM have been previously reported [*Zhao et al.*, 2000; *Sicre et al.*, 2001; *Romero et al.*, 2008]. A proposed decrease of upwelling strength [*Zhao et al.*, 2000; *Sicre et al.*, 2001; *Romero et al.*, 2008] linked to this warming is not supported by increased *G. bulloides* abundances in our study.

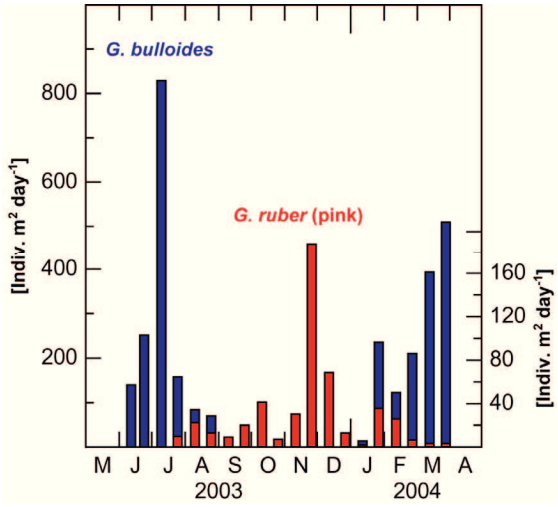

Figure 4.3-6. *G. bulloides and G. ruber* fluxes to sediment trap CBi3-o off Cape Blanc at 20°45'N, 18°41'W [data: *Barbara Donner*]. Blue bars indicate the flux of *G. bulloides*; red bars the flux of *G. ruber* (pink).

Rather, our results support the scenario of invading warm tropical surface waters [*Zhao et al.*, 2000] that caused strong SST variability during the growth seasons of *G. bulloides* and *G. ruber* pink, but no or minor temperature variability at subsurface depth (habitat depth of *G. inflata*). Insignificant temperature variability at subsurface depth compared to surface further negates a control of shifting between SACW and NACW on SST in the study area and suggests that SST and upwelling intensity were controlled mainly by processes confined to the surface ocean and wind system off NW Africa.

4.3.6 Conclusions

In this study, upwelling strength off Cape Blanc (NW Africa) was reconstructed for the past 24,000 years and compared to reconstructed Mg/Ca temperatures of surface- as well as subsurface dwelling species.

In contrast to previous studies [*Romero et al.*, 2008] the present reconstruction does not support a decrease in upwelling strength during the LGM. Rather, upwelling strength was persistently high between the LGM and ~16 kyrs BP and decreased in parallel to a decrease of wind strength reconstructed in previous studies off Cape Blanc. The Mg/Ca temperature records cannot clearly be assigned to any of the major rapid climatic events of the past 24,000 years and show a high degree of variability. Highest variability is recorded in shell Mg/Ca of the surface dwelling species *G. bulloides* and *G. ruber* (pink), while shell Mg/Ca of the intermediate depth dwelling species *G. inflata* shows little variability. Concluded by modern analogy, we explain the high SST variability at the study site during strong upwelling periods of the past 24,000 years with substantial temperature differences at the sea surface: advection of warm tropical surface waters towards the study area caused by a water mass deficit during periods of strong upwelling increased the amplitude and variability of summer and winter SST. Little temperature variability at

subsurface depths suggests negligible contribution of NACW and SACW to SST changes in the study area throughout the past 24,000 years.

Acknowledgements

Sample collection and technical support was provided by The Center for Marine Environmental Sciences (MARUM), University of Bremen. We thank Petra Witte for SEM imaging and Barbara Donner for providing unpublished data. This study was carried out within the International Graduate College EUROPROX, funded by the Deutsche Forschungsgemeinschaft (DFG).

Supplement to: Haarmann, T., M. Mohtadi, J. Groeneveld, and T. Bickert (for submission to Biogeosciences), Upwelling strength off Cape Blanc (NW Africa) during the past 24,000 BP – Effects on the surface and subsurface Mg/Ca temperature records

Table 4.3-S1. Mg/Ca ratios and size fractions of *G. ruber* (pink) and *G. bulloides* specimens sampled from sediment core GeoB7926-2 and top centimeter of multicorer GeoB7408-2

Sediment depth [m]	Species	Mg/Ca [mmol/mol]	Size range [µm]	Individuals analyzed together	Species	Mg/Ca [mmol/mol]	Size range [µm]	Individuals analyzed together
0.00	*G. ruber* (pink)	3.26	320-560	10	*G. bulloides*	3.74	250-400	30
0.08	*G. ruber* (pink)	3.02	320-560	24	*G. bulloides*	3.39	250-400	29
0.18	*G. ruber* (pink)	3.24	320-560	25	*G. bulloides*	3.18	360-440	12
0.28	*G. ruber* (pink)	2.85	320-560	25	*G. bulloides*	3.58	250-360	25
0.38	*G. ruber* (pink)	3.65	360-560	25	*G. bulloides*	2.86	320-560	24
0.48	*G. ruber* (pink)	3.02	360-560	25	*G. bulloides*	2.81	320-560	25
0.58	*G. ruber* (pink)	3.30	320-520	25	*G. bulloides*	4.14	320-520	20
0.68	*G. ruber* (pink)	-	-	-	*G. bulloides*	4.73	400-560	20
0.78	*G. ruber* (pink)	3.04	320-480	25	*G. bulloides*	2.85	400-520	25
0.98	*G. ruber* (pink)	3.09	320-480	25	*G. bulloides*	2.92	320-480	25
1.08	*G. ruber* (pink)	3.32	360-520	25	*G. bulloides*	4.84	400-520	25
1.23	*G. ruber* (pink)	3.24	400-560	25	*G. bulloides*	3.75	440-560	20
1.33	*G. ruber* (pink)	3.24	400-480	25	*G. bulloides*	3.38	400-480	25
1.42	*G. ruber* (pink)	3.44	320-560	23	*G. bulloides*	2.96	400-520	20
1.53	*G. ruber* (pink)	3.03	320-480	28	*G. bulloides*	2.94	320-480	24
1.58	*G. ruber* (pink)	3.18	320-480	19	*G. bulloides*	2.76	320-480	25
1.68	*G. ruber* (pink)	2.77	240-600	16	*G. bulloides*	3.03	360-440	19
1.78	*G. ruber* (pink)	3.32	280-440	6	*G. bulloides*	3.51	400-480	15
1.88	*G. ruber* (pink)	3.21	280-560	23	*G. bulloides*	3.26	360-520	19
2.08	*G. ruber* (pink)	2.56	240-560	8	*G. bulloides*	2.81	360-520	21
2.18	*G. ruber* (pink)	3.11	280-560	17	*G. bulloides*	3.21	400-480	20
2.28	*G. ruber* (pink)	3.01	320-600	25	*G. bulloides*	3.85	360-520	25
2.38	*G. ruber* (pink)	2.86	280-480	17	*G. bulloides*	3.32	360-480	22
2.48	*G. ruber* (pink)	2.63	320-560	19	*G. bulloides*	4.06	360-480	20
2.58	*G. ruber* (pink)	3.19	320-560	22	*G. bulloides*	2.68	400-440	20
2.78	*G. ruber* (pink)	3.31	360-600	26	*G. bulloides*	4.29	400-480	20
2.88	*G. ruber* (pink)	4.26	280-600	22	*G. bulloides*	3.03	360-520	20
2.98	*G. ruber* (pink)	3.53	320-600	15	*G. bulloides*	3.12	360-560	23
3.13	*G. ruber* (pink)	2.99	280-480	20	*G. bulloides*	2.84	320-560	15
3.23	*G. ruber* (pink)	3.26	280-600	24	*G. bulloides*	3.23	320-480	20
3.33	*G. ruber* (pink)	2.96	280-560	23	*G. bulloides*	2.44	360-560	20
3.43	*G. ruber* (pink)	3.12	320-600	25	*G. bulloides*	3.06	400-520	20

Table 4.3-S1 (continued).. Mg/Ca ratios and size fractions of *G. ruber* (pink) and *G. bulloides* specimens sampled from sediment core GeoB7926-2 and top centimeter of multicorer GeoB7408-2

Sediment depth [m]	Species	Mg/Ca [mmol/mol]	Size range [µm]	Individuals analyzed together	Species	Mg/Ca [mmol/mol]	Size range [µm]	Individuals analyzed together
3.53	*G. ruber* (pink)	3.24	400-560	25	*G. bulloides*	-	-	-
3.63	*G. ruber* (pink)	3.27	320-560	22	*G. bulloides*	3.17	440-560	23
3.68	*G. ruber* (pink)	4.38	320-560	25	*G. bulloides*	2.52	320-480	25
3.73	*G. ruber* (pink)	3.51	320-560	23	*G. bulloides*	2.83	400-560	23
3.83	*G. ruber* (pink)	3.19	240-560	24	*G. bulloides*	2.79	360-440	24
3.93	*G. ruber* (pink)	3.07	320-560	30	*G. bulloides*	2.42	400-480	20
4.03	*G. ruber* (pink)	3.13	320-600	25	*G. bulloides*	2.65	400-480	25
4.13	*G. ruber* (pink)	2.98	320-480	18	*G. bulloides*	2.54	320-480	25
4.23	*G. ruber* (pink)	2.94	280-600	17	*G. bulloides*	2.91	320-520	25
4.33	*G. ruber* (pink)	2.84	240-400	8	*G. bulloides*	4.01	360-560	25
4.43	*G. ruber* (pink)	2.99	280-560	13	*G. bulloides*	3.01	360-520	25
4.53	*G. ruber* (pink)	3.22	360-600	24	*G. bulloides*	2.79	360-520	20
4.63	*G. ruber* (pink)	3.04	280-560	22	*G. bulloides*	2.32	320-440	25
4.73	*G. ruber* (pink)	2.71	320-480	13	*G. bulloides*	2.37	320-480	25
4.83	*G. ruber* (pink)	2.75	280-520	9	*G. bulloides*	-	-	-
4.88	*G. ruber* (pink)	-	-	-	*G. bulloides*	3.01	360-520	30
4.93	*G. ruber* (pink)	3.03	440-560	6	*G. bulloides*	6.87 (4.26)	360-560	21
4.98	*G. ruber* (pink)	3.12	320-480	14	*G. bulloides*	3.55	320-480	25
5.13	*G. ruber* (pink)	-	-	-	*G. bulloides*	3.64	360-520	25
5.18	*G. ruber* (pink)	4.53	240-440	6	*G. bulloides*	3.57	360-560	24
5.33	*G. ruber* (pink)	3.28	200-560	20	*G. bulloides*	4.92	360-520	23
5.48	*G. ruber* (pink)	3.24	320-560	30	*G. bulloides*	4.10	440-480	21
5.53	*G. ruber* (pink)	3.73	360-560	27	*G. bulloides*	3.22	440-520	?
5.63	*G. ruber* (pink)	2.99	280-520	25	*G. bulloides*	2.48	400-520	25
5.73	*G. ruber* (pink)	3.22	320-600	25	*G. bulloides*	3.40	360-520	30
5.83	*G. ruber* (pink)	3.10	320-600	30	*G. bulloides*	3.18	320-560	25
5.93	*G. ruber* (pink)	3.92	440-480	3	*G. bulloides*	3.54	360-480	16
6.03	*G. ruber* (pink)	-	-	-	*G. bulloides*	3.07	400-560	25
6.13	*G. ruber* (pink)	3.08	240-520	28	*G. bulloides*	-	-	-
6.18	*G. ruber* (pink)	2.91	360-560	25	*G. bulloides*	3.50	360-440	24
6.33	*G. ruber* (pink)	2.96	280-480	19	*G. bulloides*	3.55	360-520	23
6.38	*G. ruber* (pink)	3.18	280-480	23	*G. bulloides*	4.07	360-560	21

Table 4.3-S1 (continued). Mg/Ca ratios and size fractions of *G. ruber* (pink) and *G. bulloides* specimens sampled from sediment core GeoB7926-2 and top centimeter of multicorer GeoB7408-2

Sediment depth [m]	Species	Mg/Ca [mmol/mol]	Size range [µm]	Individuals analyzed together	Species	Mg/Ca [mmol/mol]	Size range [µm]	Individuals analyzed together
6.48	*G. ruber* (pink)	-	-	-	*G. bulloides*	3.61	400-480	15
6.53	*G. ruber* (pink)	3.41	280-600	23	*G. bulloides*	6.01 (5.03)	360-480	23
6.58	*G. ruber* (pink)	-	-	-	*G. bulloides*	4.03	400-560	20
6.63	*G. ruber* (pink)	2.92	360-560	19	*G. bulloides*	2.88	360-520	23
6.73	*G. ruber* (pink)	2.74	320-480	22	*G. bulloides*	2.38	320-480	25
6.83	*G. ruber* (pink)	2.80	280-480	12	*G. bulloides*	3.17	360-520	24
6.98	*G. ruber* (pink)	3.02	320-480	25	*G. bulloides*	3.04	320-480	25
7.08	*G. ruber* (pink)	3.03	320-560	25	*G. bulloides*	2.88	400-520	25
7.18	*G. ruber* (pink)	3.03	320-480	25	*G. bulloides*	3.44	320-480	25
7.28	*G. ruber* (pink)	3.10	280-600	25	*G. bulloides*	4.46	360-560	25
7.33	*G. ruber* (pink)	3.58	320-480	25	*G. bulloides*	3.32	320-480	25
7.38	*G. ruber* (pink)	2.96	360-560	25	*G. bulloides*	3.19	360-560	25
7.43	*G. ruber* (pink)	3.29	320-480	26	*G. bulloides*	3.65	320-480	25
7.48	*G. ruber* (pink)	3.13	360-560	25	*G. bulloides*	4.27	360-520	25
7.58	*G. ruber* (pink)	3.47	320-560	27	*G. bulloides*	4.43	400-520	24
7.68	*G. ruber* (pink)	3.85	360-600	30	*G. bulloides*	3.81	400-480	24
7.78	*G. ruber* (pink)	3.58	400-600	30	*G. bulloides*	4.18	360-520	25

V. SUMMARY AND OUTLOOK

5.1 Summary

This thesis investigated the potential of single foraminiferal shells for recording short-term temperature variations and for reconstructing the water column stratification off NW Africa in the oceanographic past. Recent studies suggest that interspecimen Mg/Ca and $\delta^{18}O_c$ differences resemble the seasonal range of temperatures at the sea surface [*Sadekov et al.*, 2008; *Wit et al.*, 2010]. This was tested for two surface-dwelling species (*G. ruber* (white) and *G. ruber* (pink)) collected in a sediment trap off Cape Blanc. The past water column stratification at this site was assessed for the past 24,000 years through the analysis of single specimen $\delta^{18}O_c$ of the subsurface-dwelling species *G. inflata*. Hypotheses of unexpectedly warm sea surface temperatures (SST) at the study site, due to decreased upwelling of cold subsurface waters [*Romero et al.*, 2008] were tested, using the relative abundance of *G. bulloides* and Mg/Ca analyses of *G. ruber* (pink), *G. bulloides* and *G. inflata*.

In a sediment trap study (**Manuscript I**), it was demonstrate that single specimens of *G. ruber* (pink) are suitable in the upwelling region off Cape Blanc for tracking the seasonal amplitude of SST, when the Mg/Ca temperature equation of *Regenberg et al.* [2009] is used. Mg/Ca ratios of single *G. ruber* (white) shells do not track the seasonal SST and best SST estimates are obtained when using the *Elderfield and Ganssen* [2000] Mg/Ca temperature equation. Mg/Ca ratios of *G. inflata* do not exhibit seasonality and temperature estimates correspond to calcification depths between the surface and ~400 m water depth, when using the equation of *Elderfield and Ganssen* [2000]. The measured present day variability allowed to calculate that changes in the range between highest and lowest Mg/Ca ratios are indicative of changes of the calcification temperature range, when the changes are ≥0.80 mmol/mol (*G. ruber* (pink)) or ≥0.34 mmol/mol (*G. inflata*). Single specimens were cleaned prior to analysis using a flow-through system, in order to prevent sample loss. The previously installed system was further developed during this PhD project in order to allow for the cleaning of freshly sedimented shells; however the cleaning of sedimentary shells remains problematic.

For the reconstruction of calcification temperatures from single sedimentary shells, a new approach recently proposed by *Ganssen et al.* [2011] was used. In collaboration with the

Section Marine Biogeology at the Vrije Universiteit in Amsterdam (VUA), the calcification temperature range of single sedimentary *G. inflata* specimens was reconstructed for the past 22,000 years by combining conventional Mg/Ca analysis with single specimen $\delta^{18}O_c$ measurements (**Manuscript II)**. It was found that temperature estimates (12.7 to 17.8°C) agree well with the temperature estimates from the sediment trap study (11.4 to 20.3°C). Also, the calcification depth range (0-420 m) calculated by comparison of $\delta^{18}O_c$ with $\delta^{18}O_{eq}$ agrees well with the sediment trap study. In order to test the applicability of single *G. inflata* specimens for reconstructing past water column stratification, single specimens from seven time slices between the near present and 22,000 years before present were analyzed from a sediment core retrieved at the same site. The calcification temperature range was significantly reduced off Cape Blanc during the last deglaciation as compared to the Last Glacial Maximum and the Holocene. Comparison to water temperatures predicted by a climate model suggests that the habitat range of *G. inflata* was narrower during the last deglaciation as a response to increased thermal stratification of the water column.

At the study site, previous studies found unexpectedly warm sea surface temperatures, which were attributed to decreased upwelling strength [*Romero et al.*, 2008]. Upwelling strength was reconstructed for the past 24,000 years (**Manuscript III**) and high upwelling strength found between 24,000 and 16,000 years before present, contradicting this hypothesis. Mg/Ca temperature reconstructions using the species *G. ruber* (pink) and *G. bulloides* showed a generally high variability throughout the record, in contrast to Mg/Ca temperatures reconstructed from *G. inflata*. Inspection of daily SSTs between 1982 and 2008 shows a high degree of local SST variability and substantially increased local SSTs during years with high wind strength, likely through a northward advection of warm southerly waters towards the study site. It is presumed that this mechanism might have also caused high SST variability at the study site in the past.

It was shown in **Manuscript I** that *G. ruber* (pink) is likely to record short-term SST variability. The high variability observed in the downcore *G. bulloides* record suggests that this is also true for *G. bulloides*. This could be tested in future studies by quantifying the present day Mg/Ca variability between individual specimens of this species collected from a sediment trap as it was done for *G. ruber* (pink) in **Manuscript I**. In the light of substantial present day SST variability at the study site, it is further desirable to constrain

SST extrema in the past. This could be achieved through analysis of single *G. ruber* (pink) and *G. bulloides* specimens, using combined multispecimen Mg/Ca and single specimen $\delta^{18}O_c$ analysis. More directly the observed variability could be constrained through Mg/Ca analysis of single shells. This however requires a reliable cleaning of single sedimentary shells prior to analysis. During this thesis, considerable effort was put into the further development of the flow-through system, in order to allow for such cleaning. This work was carried out in collaboration with Dr. Ed C. Hathorne and Dr. Jeroen Groeneveld and further experiments are still required. Below, the present state of the art during the time of completion of this thesis is summarized.

5.2 Outlook

Cleaning of sedimentary shells requires a technique that also removes clay contaminants, which are abundantly found in sedimentary shells and contain 1-10% Mg by weight [*Deer et al.*, 1992]. These cannot be removed using the previously introduced cleaning technique. The procedure was therefore modified as follows.

1. As in the previous cleaning, specimens were placed on PTFE filters with a mesh width of 0.45µm (to hold back clay minerals)
2. Cleaning reagents were applied as listed in Table 5.2-1
3. After cleaning, specimens were kept on the filter and
4. dissolved in a constant flow of acid (mix of 1 M HNO_3 pumped at 0.45ml min^{-1} with suprapure water pumped at 0.1 ml min^{-1})
5. The solution was collected in cleaned (soaked for several days in 10% HNO_3) PTFE beakers
6. The solution was then evaporated to a small rest (done by Dr. Ed C. Hathorne in clean labs of the IFM-GEOMAR, Kiel) which was finally
7. redissolved in 2 ml 0.075 M HNO_3 for analysis

For testing this cleaning procedure, single specimens of *G. inflata* were used, since this species has a relatively high shell mass (~30µg) that was expected to provide high enough concentrations in the final solution for Mg/Ca determination on an ICP-OES. The shells were collected from sediment core GeoB7926-2 at depth intervals (273 and 498 cm), for which the range of single *G. inflata* calcification temperatures is well known (conf.

manuscript II). This allowed for excellent control, if the calculated Mg/Ca temperatures are within a reasonable range.

Element/Ca ratios were determined on a Perkin-Elmer Optima 3300R ICP-OES equipped with an ultrasonic nebulizer U-5000 AT (Cetac Technologies Inc.) housed at the faculty of Geosciences, University of Bremen. A solution of international carbonate reference material ECRM 752-1 was analyzed before and after the samples. Its Mg/Ca ratio was on average 3.90 mmol/mol (n = 5; σ = 0.11 mmol/mol), in acceptable agreement with the reported Mg/Ca ratio of 3.75 mmol/mol [*Greaves et al.*, 2008].

Table 5.2-1. Cleaning program used for cleaning and dissolving single sedimentary foraminifer shells

Duration [min]	Reagent	Pump speed [ml/min]	Reagent	Pump speed [ml/min]	Destination
Lines below: preconditioning steps for cleaning lines					
2	-	-	1 M HNO_3	3	Waste
3	H_2O	3	-	-	Waste
Lines below: dissolution and collection of single specimens					
20	H_2O_2	4	-	-	Waste
16.6	H_2O	4	-	-	Waste
2	H_2O	0.45	1 M HNO_3	0.1	Waste
30	H_2O	0.45	1 M HNO_3	0.1	Collect
2	H_2O	4	-	-	Waste

The average Al/Ca ratio of 0.40 mmol/mol (n = 5; σ = 0.05 mmol/mol) was within the reported Al/Ca ratio of 0.65 (±0.34) mmol/mol and the average Fe/Ca ratio of 0.10 mmol/mol (n = 5; σ <0.00 mmol/mol) slightly lower than the reported Fe/Ca ratio of 0.17 (±0.03) mmol/mol.

It must be noted that the Al concentrations (on average ~10 ppb) and Fe concentrations (on average ~5 ppb) were below the calibration range of the ICP-OES for these elements (40-200 ppb) and should therefore be interpreted with caution and considered an approximation of the true ratios.

Table 5.2-2 summarizes the results of the analysis and additionally provides Mg/Ca ratios which are considered realistic, based on the temperature range calculated previously (conf. manuscript II). As can be seen from Table 5.2-2, the following difficulties are noted.

1. Filling of the beakers varied strongly
2. Ca concentrations in the sample solutions were low (0.4-24.8 ppm)
3. Al/Ca ratios are partly high (e.g. 25.58 mmol/mol)
4. Given the expected Mg/Ca ranges, it is noted that only two samples are within these ranges, while the other samples give values that are higher than expected.

Table 5.2-2. Element/Ca ratios and Ca concentrations of 0.075 M HNO_3 solutions in which single *G. inflata* shells were dissolved using the FT. Cleaning and dissolution was done according to the procedure given in Table 5-1. The PTFE collecting beakers were not filled equally and the filling level and Ca concentration of the solution is provided. Mg/Ca ratios of multispecimen analysis and estimated temperature ranges are given as calculated in manuscript II. The expected Mg/Ca range was calculated from these temperatures using the equation of *Elderfield and Ganssen* [2000]). Mg/Ca ratios within a reasonable range based on this estimate are underlined.

Sample	Beaker filling [%]	Ca [ppm]	Mg/Ca [mmol/mol]	Al/Ca [mmol/mol]	Mg/Ca multispecimen [mmol/mol]	Estimated temp. range [°C]	Estimated Mg/Ca range [mmol/mol]
273 cm	100	6.2	5.58	2.99			
273 cm	20	7.3	2.72	1.55			
273 cm	70	16.6	<u>2.31</u>	0.45			
273 cm	60	11.2	3.15	1.20	1.91	12.1-16.1	1.64-2.45
273 cm	50	7.0	3.87	1.91			
273 cm	70	6.9	2.86	1.88			
273 cm	20	4.5	<u>2.12</u>	1.96			
273 cm	80	13.7	2.64	0.61			
498cm	90	5.2	5.22	3.48			
498cm	40	7.7	3.94	1.44			
498cm	30	7.9	3.18	1.12			
498cm	90	5.9	6.59	4.69	2.19	12.9-17.4	1.78-2.79
498cm	70	7.4	4.36	3.72			
498cm	60	0.4	17.83	25.58			
498cm	1	0.4	15.81	5.45			
498cm	20	24.8	3.12	0.48			

During purely oxidative cleaning (conf. manuscript I), no unequal flow was observed. It thus appears to result from the simultaneous operation of two pumps; however the definite cause could not yet be fully constrained.

Ca concentrations in the final solution are lower than expected (~37.5 ppm) from the dissolution of *G. inflata* shells (~30 µg), suggesting that the shells were either not entirely dissolved or that not all Ca was completely flushed out of the system and into the collecting beakers. Both could be addressed in future utilizations of the flow-through system by longer dissolution intervals and/or higher acid strength.

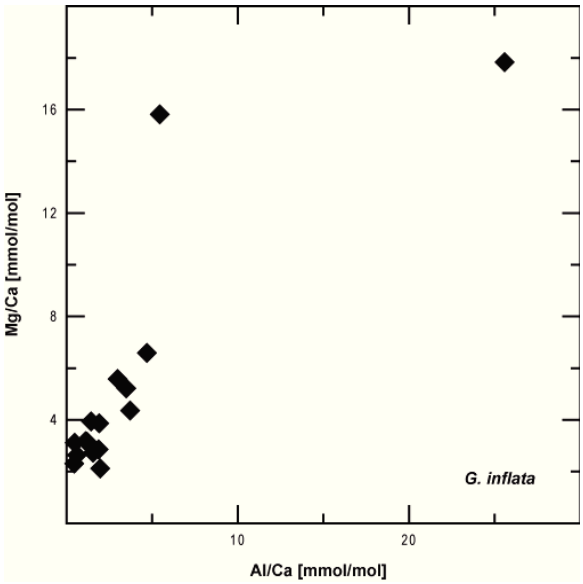

Figure 5.2-1. Mg/Ca ratios vs. Al/Ca ratios of 0.075 M HNO_3 solutions in which single *G. inflata* specimens were dissolved.

Elemental analysis found that Mg/Ca ratios increased parallel to Al/Ca ratios (Figure 5.2-1), suggesting contamination with clay minerals. This is surprising, since clay minerals should principally not be able to pass the PTFE filters and reach the collecting beakers. Several experiments were therefore run in order to identify the source of the contamination (Table 5.2-3). The experiments showed that highest Al and Fe concentrations are measured, when the system is exposed to HNO_3 and that Al and Fe concentrations decreased with increasing operation time. Possibly, clay minerals were attached to the walls of the tubes and became mobile during subsequent HNO_3 rinse. In any case, this underlines the need for a very thorough rinsing of the flow-through system, when working with sedimentary shells and when HNO_3 is used.

Table 5.2-3. Experiments carried out in order to identify the source of Al and Fe contamination of the flow-through system and the attached tubes/beakers.

Possible source of contamination	Test strategy	Al concentration [ppb]	Fe concentration [ppb]	Remarks/ observations
		Session 1		
Test tubes	H_2O (18.2 MΩ cm) poured straight into test tubes	23.4-22.9	below detection limit	Test tubes are the same as used in standard analyses and have additionally been filled for several days with QD HNO_3
Contamination of hoses/cleaning lines	H_2O (18.2 MΩ cm) pumped through all lines and collected in test tubes	23.9-9.9 (no trend relatable to specific lines)	8.7 – below detection limit (decreasing with time)	Test tubes are the same as used in standard analyses and have additionally been filled for several days with QD HNO_3
Contamination of PTFE beaker	0.3 M QD HNO_3 poured straight into PTFE vials	14.4-12.0	2.0-1.6	PTFE beaker have been repeatedly washed with QD HNO_3
Removal of accumulated contaminants by acid/MilliQ mixture	0.3 M QD HNO_3 + H_2O (18.2 MΩ cm) pumped through lines 2A-2E and collection in PTFE vials	629.3-44.8 (decreasing with increasing time)	1280-58.6 (decreasing with increasing time)	Substantial removal of Al and Fe
		Session 2 (7 days later)		
Acid pump	0.3 M QD HNO_3 pumped and collected	5.3	25.1	Moderate removal of Fe
PP filter (cleaned with QD HNO_3)	H_2O (18.2 MΩ cm) pumped through filer	20.9	0.9	PP filters were tested as an alternative to PTFE filters
Release of contaminants by acid from PP filter (cleaned with QD HNO_3)	0.3 M QD HNO_3 pumped through PP filter and collected	0.0	2.7	Reduced removal of Al and Fe
		Session 3 (15 days later)		
Release of contaminants by H_2O_2	1% H_2O_2 pumped through PP filter and collected	15.2	20.6	-

VI. REFERENCES

Abrantes, F. (2000), 200,000 yr diatom records from Atlantic upwelling sites reveal maximum productivity during LGM and a shift in phytoplankton community structure at 185,000 yr, *Earth Planet. Sc. Lett.*, *176*(1), 7-16.

Adkins, J., P. deMenocal, and G. Eshel (2006), The "African humid period" and the record of marine upwelling from excess 230Th in Ocean Drilling Program Hole 658C, *Paleoceanography*, *21*(4), PA4203.

Anand, P., and H. Elderfield (2005), Variability of Mg/Ca and Sr/Ca between and within the planktonic foraminifers *Globigerina bulloides* and *Globorotalia truncatulinoides*, *Geochem. Geophys. Geosyst.*, *6*(11), Q11D15.

Anand, P., H. Elderfield, and M. H. Conte (2003), Calibration of Mg/Ca thermometry in planktonic foraminifera from a sediment trap time series, *Paleoceanography*, *18*(2), 1050.

Antonov, J. I., R. A. Locarnini, T. P. Boyer, A. V. Mishonov, and H. E. Garcia (2006), World Ocean Atlas 2005, Volume 2: Salinity, in *NOAA Atlas NESDIS 62*, edited by S. Levitus, U.S. Government Printing Office, Washinton D.C., 182 pp.

Arbuszewski, J., P. deMenocal, A. Kaplan, and E. C. Farmer (2010), On the fidelity of shell-derived δ^{18}Oseawater estimates, *Earth and Planetary Science Letters*, *300* (3-4), 185-196.

Arhan, M., A. Colin De Verdiére, and L. Mémery (1994), The Eastern Boundary of the Subtropical North Atlantic, *Journal of Physical Oceanography*, *24*(6), 1295-1316.

Bakun, A. (1990), Global Climate Change and Intensification of Coastal Ocean Upwelling, *Science*, *247*(4939), 198-201.

Barker, S., M. Greaves, and H. Elderfield (2003), A study of cleaning procedures used for foraminiferal Mg/Ca paleothermometry, *Geochem. Geophys. Geosyst.*, *4*.

Barton, E. D. (2001), Canary and Portugal Currents, *University of Wales Academic Press*.

Bé, A. W. H. (1960), Ecology of recent planktonic foraminifera: Part 2 - Bathymetric and seasonal distribution in the Sargasso Sea off Bermuda, *Micropaleontology*, *6*, 373-392.

Bé, A. W. H., and W. H. Hamlin (1967), Ecology of Recent Planktonic Foraminifera: Part 3: Distribution in the North Atlantic during the Summer of 1962, *Micropaleontology*, *13*(1), 87-106.

Bé, A. W. H. (1977), An ecological, zoogeographic and taxonomic review of recent planktonic foraminifera, in *Oceanic Micropaleontology*, edited by A. T. S. Ramsay, Academic Press, London, pp. 1-100

Bé, A. W. H., and H. J. Spero (1981), Shell regeneration and biological recovery of planktonic foraminifera after physical injury induced in laboratory culture, *Micropaleontology*, *27*(3), 305-316.

Bemis, B. E., H. J. Spero, J. Bijma, and D. W. Lea (1998), Reevaluation of the oxygen isotopic composition of planktonic foraminifera: Experimental results and revised paleotemperature equations, *Paleoceanography*, *13*(2), 150-160.

Benway, H. M., B. A. Haley, G. P. Klinkhammer, and A. C. Mix (2003), Adaptation of a flow-through leaching procedure for Mg/Ca paleothermometry, *Geochem. Geophys. Geosyst.*, *4*.

Bijma, J., J. Erez, and C. Hemleben (1990), Lunar and semi-lunar reproductive-cycles in some spinose planktonic foraminifers, *Journal of Foraminiferal Research*, *20*(2), 117-127.

Billups, K., and H. J. Spero (1996), Reconstructing the stable isotope geochemistry and paleotemperatures of the equatorial Atlantic during the last 150,000 years: Results from individual foraminifera, *Paleoceanography*, *11*(2), 217-238.

Boyle, E. A. (1981), Cadmium, zinc, copper, and barium in foraminifera tests, *Earth Planet. Sc. Lett.*, *53*(1), 11-35.

Caron, D. A., O. Roger Anderson, J. L. Lindsey, J. W. W. Faber, and E. E. Lin Lim (1990), Effects of gametogenesis on test structure and dissolution of some spinose planktonic foraminifera and implications for test preservation, *Mar. Micropaleontol.*, *16*(1-2), 93-116.

Chapman, M. R., N. J. Shackleton, M. Zhao, and G. Eglinton (1996), Faunal and alkenone reconstructions of subtropical North Atlantic surface hydrography and paleotemperature over the last 28 kyr, *Paleoceanography*, *11*(3), 343-357.

Chiessi, C. M., S. Ulrich, S. Mulitza, J. Pätzold, and G. Wefer (2007), Signature of the Brazil-Malvinas Confluence (Argentine Basin) in the isotopic composition of planktonic foraminifera from surface sediments, *Mar. Micropaleontol.*, *64*(1-2), 52-66.

Clarke, F. W., and W. C. Wheeler (1922), The inorganic constituents of marine invertebrates, *USGS Prof. Pap.*, *124*, 55.

Cléroux, C., E. Cortijo, J.-C. Duplessy, and R. Zahn (2007), Deep-dwelling foraminifera as thermocline temperature recorders, *Geochem. Geophys. Geosyst.*, *8*.

Cléroux, C., E. Cortijo, P. Anand, L. Labeyrie, F. Bassinot, N. Caillon, and J.-C. Duplessy (2008), Mg/Ca and Sr/Ca ratios in planktonic foraminifera: Proxies for upper water column temperature reconstruction, *Paleoceanography*, *23*, PA3214.

Curry, W. B., R. C. Thunell, and S. Honjo (1983), Seasonal changes in the isotopic composition of planktonic foraminifera collected in Panama Basin sediment traps, *Earth and Planetary Science Letters*, *64*(1), 33-43.

Davis, K. J., P. M. Dove, and J. J. De Yoreo (2000), The Role of Mg2+ as an Impurity in Calcite Growth, *Science*, *290*, 1134-1137.

Dekens, P. S., D. W. Lea, D. K. Pak, and H. J. Spero (2002), Core top calibration of Mg/Ca in tropical foraminifera: Refining paleotemperature estimation, *Geochem. Geophys. Geosyst.*, *3*(4).

Dekens, P. S., A. C. Ravelo, M. D. McCarthy, and C. A. Edwards (2008), A 5 million year comparison of Mg/Ca and alkenone paleothermometers, *Geochem. Geophys. Geosyst.*, *9*.

Deer, W. A., R. A. Howie, and J. Zussman (1992), *An introduction to the Rock Forming Minerals* (second edition), Longman Reading, Mass.; 712 pp.

Deuser, W. G., E. H. Ross, C. Hemleben, and M. Spindler (1981), Seasonal changes in species composition, numbers, mass, size, and isotopic composition of planktonic foraminifera settling into the deep sargasso sea, *Palaeogeography, Palaeoclimatology, Palaeoecology*, *33*(1–3), 103-127.

Diester-Haass, L. (1973), Absolute abundance pf particles and planktic foraminifera in sediment core GIK12301-4, Cape Barbas, North-West Africa, *PANGAEA* data repository.

Elderfield, H., and G. Ganssen (2000), Past temperature and delta-^{18}O of surface ocean waters inferred from foraminiferal Mg/Ca ratios, *Nature*, *18*, 442-445.

Elderfield, H., M. Vautravers, and M. Cooper (2002), The relationship between shell size and Mg/Ca, Sr/Ca, δ^{18}O, and δ^{13}C of species of planktonic foraminifera, *Geochem. Geophys. Geosyst.*, *3*.

Emiliani, C. (1955), Pleistocene Temperatures, *The Journal of Geology*, *63*(6), 538-578.

Erez, J., and S. Honjo (1981), Comparison of isotopic composition of planktonic foraminifera in plankton tows, sediment traps and sediments, *Palaeogeogr. Palaeocl.*, *33*(1-3), 129-156.

Fairbanks, R. G., P. H. Wiebe, and A. W. H. Be (1980), Vertical Distribution and Isotopic Composition of Living Planktonic Foraminifera in the Western North Atlantic, *Science*, *207*, 61-63.

Fairbanks, R. G., M. Sverdlove, R. Free, P. H. Wiebe, and A. W. H. Be (1982), Vertical distribution and isotopic fractionation of living planktonic foraminifera from the Panama Basin, *Nature*, *298*, 841-844.

Farmer, E. C., A. Kaplan, P. B. de Menocal, and J. Lynch-Stieglitz (2007), Corroborating ecological depth preferences of planktonic foraminifera in the tropical Atlantic with the stable oxygen isotope ratios of core top specimens, *Paleoceanography*, *22*(3), PA3205.

Farmer, E. J., M. R. Chapman, and J. E. Andrews (2010), North Atlantic *Globorotalia inflata* coretop Mg/Ca calibrations and temperature reconstructions over Termination I, *IOP Conf. Ser.: Earth Environ. Sci.*, *9*, 1-7.

Ferguson, J. E., G. M. Henderson, M. Kucera, and R. E. M. Rickaby (2008), Systematic change of foraminiferal Mg/Ca ratios across a strong salinity gradient, *Earth and Planetary Science Letters*, *265*(1-2), 153-166.

Filipsson, H. L., O. E. Romero, J.-B. W. Stuut, and B. Donner (2011), Relationships between primary productivity and bottom-water oxygenation off northwest Africa during the last deglaciation, *Journal of Quaternary Science*, *26*(4), 448-456.

Fischer, G., B. Donner, V. Ratmeyer, R. Davenport, and G. Wefer (1996), Distinct year-to-year particle flux variations off Cape Blanc during 1988-1991: Relation to $\delta^{18}O$-deduced sea-surface temperatures and trade winds, *Journal of Marine Research*, *54*(1), 73-98.

Fischer, G., G. Ruhland, and cruise participants (2008), Report and preliminary results of Poseidon cruise 344, Leg 1 & Leg 2, Las Palmas -Las Palmas, *Berichte, Fachbereich Geowissenschaften*, *259*, 47.

Freudenthal, T., H. Meggers, J. Henderiks, H. Kuhlmann, A. Moreno, and G. Wefer (2002), Upwelling intensity and filament activity off Morocco during the last 250,000 years, *Deep Sea Research Part II: Topical Studies in Oceanography*, *49*(17), 3655-3674.

Gabric, A. J., L. Garcia, L. Van Camp, L. Nykjaer, W. Eifler, and W. Schrimpf (1993), Offshore export of shelf production in the Cape Blanc (Mauritania) giant filament as derived from coastal zone color scanner imagery, *J. Geophys. Res.*, *98*, 4697-4712.

Ganssen, G., and M. Sarnthein (1983), Stable-isotope composition of foraminifers: the surface and bottom water record of coastal upwelling, in *Coastal Upwelling: Its Sedimentary Record*, edited by J. Thiede and E. Suess, Plenum, New York, pp. 99-121.

Ganssen, G. M., and D. Kroon (2000), The isotopic signature of planktonic foraminifera from NE Atlantic surface sediments: implications for the reconstruction of past oceanic conditions, *J. Geol. Soc. London*, *157*(3), 693-699.

Ganssen, G. M., F. J. C. Peeters, B. Metcalfe, P. Anand, S. J. A. Jung, D. Kroon, and G. J. A. Brummer (2011), Quantifying sea surface temperature ranges of the Arabian Sea for the past 20 000 years, *Clim. Past*, *7*(4), 1337-1349.

Gastrich, M. D. (1987), Ultrastructure of a new intracellular symbiotic alga found within planktonic foraminfera, *J. Phycol.*, *23*, 623-632.

Greaves, M., et al. (2008), Interlaboratory comparison study of calibration standards for foraminiferal Mg/Ca thermometry, *Geochem. Geophys. Geosyst.*, *9*(8), Q08010.

Groeneveld, J., and C. M. Chiessi (2011), Mg/Ca of Globorotalia inflata as a recorder of permanent thermocline temperatures in the South Atlantic, *Paleoceanography*, *26*(2), PA2203.

Haarmann, T., E. Hathorne, M. Mohtadi, J. Groeneveld, M. Kölling, and T. Bickert (2011), Mg/Ca ratios of single planktonic foraminifer shells and the potential to reconstruct the thermal seasonality of the water column, *Paleoceanography*, *26*, PA3218.

Hagen, E., and R. Schemainda (1987), On the annual distribution of South Atlantic Central Water (SACW) along a section off Cape Blanc, Northwest Africa, *Oceanol. Acta*, *19*, 61-70.

Hagen, E. (2001), Northwest African upwelling scenario, *Oceanol. Acta*, *24* (Suppl. 1), 113-128.

Haley, B. A., and G. P. Klinkhammer (2002), Development of a flow-trough system for cleaning and dissolving foraminiferal tests, *Chem. Geol.*, *185*, 51-69.

Hammer, Ø., D. A. T. Harper, and P. D. Ryan (2001), PAST: Paleontological Statistics software package for education and data analysis, *Palaeontologia Electronica*, *4*(1), 9.

Haslett, S. K., and C. W. Smart (2006), Late Quaternary upwelling off NW Africa: new micropaleontological evidence from ODP hole 658C, *J. Quaternary Sci.*, *21*(3), 259-269.

Hastings, D. W., S. R. Emerson, J. Erez, and B. K. Nelson (1996), Vanadium in foraminiferal calcite: Evaluation of a method to determine paleo-seawater vanadium concentrations, *Geochim. Cosmochim. Ac.*, *60*(19), 3701-3715.

Hathorne, E. C., R. H. James, and R. S. Lampitt (2009), Environmental versus biomineralization controls on the intratest variation in the trace element composition of the planktonic foraminifera *G. inflata* and *G. scitula*, *Paleoceanography*, *24*, PA4204.

Hecht, M. W., and H. H. Hasumi (Eds.) (2008), *Ocean Modeling in an Eddying Regime*, Geophys. Monogr. Ser. (vol. 177), AGU, Washington, D.C.

Helmke, P., O. Romero, and G. Fischer (2005), Northwest African upwelling and its effect on offshore organic carbon export to the deep sea, *Global Biogeochem. Cycles*, *19*(4), GB4015.

Hemleben, C., M. Spindler, and O. R. Anderson (1989), *Modern Planktonic Foraminifera*, Springer-Verlag, New York, 363 pp.

Henderiks, J., T. Freudenthal, H. Meggers, and S. Nave (2002), Glacial-interglacial variability of particle accumulation in the Canary Basin: a time-slice approach, *Deep Sea Research II*, *49*, 3675-3705.

Huang, E., S. Mulitza, A. Paul, J. Groeneveld, S. Steinke, and M. Schulz (submitted), Response of the eastern tropical Atlantic central waters to thermohaline circulation changes during the Last Glacial Maximum and Heinrich Stadial 1.

Khider, D., L. D. Stott, J. Emile-Geay, R. Thunell, and D. E. Hammond (2011), Assessing El Niño Southern Oscillation variability during the past millennium, *Paleoceanography*, *26*(3), PA3222.

Killingley, J. S., R. F. Johnson, and W. H. Berger (1981), Oxygen and carbon isotopes of individual shells of planktonic foraminifera from Ontong-Java plateau, equatorial pacific, *Palaeogeography, Palaeoclimatology, Palaeoecology*, *33*(1-3), 193-204.

Kim, S.-T., and J. R. O'Neil (1997), Equilibrium and nonequilibrium oxygen isotope effects in synthetic carbonates, *Geochim. Cosmochim. Ac.*, *61*(16), 3461-3475.

King, A. L., and W. R. Howard (2005), δ18O seasonality of planktonic foraminifera from Southern Ocean sediment traps: Latitudinal gradients and implications for paleoclimate reconstructions, *Mar. Micropaleontol.*, *56*(1-2), 1-24.

Kisakürek, B. A., A. Eisenhauer, F. Böhm, D. Garbe-Schönberg, and J. Erez (2008), Controls on shell Mg/Ca and Sr/Ca in cultured planktonic foraminiferan, *Globigerinoides ruber* (white), *Earth Planet. Sc. Lett.*, *273*(3-4), 260-269.

Koutavas, A., P. B. deMenocal, G. C. Olive, and J. Stieglitz-Lynch (2006), Mid-Holocene El Niño-Southern Oscillation (ENSO) attentuation revealed by individual foraminifera in eastern tropical Pacific sediments, *Geology*, *34*(12), 993-996.

Kučera, M. (2007), Planktonic foraminifera as tracers of past oceanic environments, in *Proxies in Late Cenozoic Paleoceanography*, edited by Hillaire-Marcel, C. and de Vernal, A., Developments in Marine Geology (vol.1), Elsevier, Amsterdam, pp. 213-262

Kuhlmann, H., T. Freudenthal, P. Helmke, and H. Meggers (2004), Reconstruction of paleoceanography off NW Africa during the last 40,000 years: influence of local and regional factors on sediment accumulation, *Marine Geology*, *207*(1-4), 209-224.

Lachkar, Z., and N. Gruber (2011), What controls biological production in coastal upwelling systems? Insights from a comparative modeling study, *Biogeosciences*, *8*(10), 2961-2976.

Lea, D. W., and E. A. Boyle (1991), Barium in planktonic foraminifera, *Geochim. Cosmochim. Ac.*, *55*(11), 3321-3331.

Lea, D. W., T. A. Mashiotta, and H. J. Spero (1999), Controls on magnesium and strontium uptake in planktonic foraminifera determined by live culturing, *Geochimica et Cosmochimica Acta*, *63*(16), 2369-2379.

Lea, D. W., D. K. Pak, and H. J. Spero (2000), Climate impact of Late Quaternary Equatorial Pacific sea surface temperature variations, *Science*, *289*, 1719-1724.

Leduc, G., L. Vidal, O. Cartapanis, and E. Bard (2009), Modes of eastern equatorial Pacific thermocline variability: Implications for ENSO dynamics over the last glacial period, *Paleoceanography*, *24*.

Liu, Z., et al. (2009), Transient Simulation of Last Deglaciation with a New Mechanism for Bølling-Allerød Warming, *Science*, *325*(5938), 310-314.

Locarnini, R. A., A. V. Mishonov, J. I. Antonov, T. P. Boyer, and H. E. Garcia (2006), World Ocean Atlas 2005, Volume 1: Temperature, in *NOAA Atlas NESDIS 61*, edited by S. Levitus, p. 182, U.S. Government Printing Office, Washington, D.C.

Lohmann, G. P. (1995), A model for variation in the chemistry of planktonic foraminifera due to secondary calcification and selective dissolution, *Paleoceanography*, *10*(3), 445-457.

Lončarić, N., F. J. C. Peeters, D. Kroon, and G.-J. A. Brummer (2006), Oxygen isotope ecology of recent planktic foraminifera at the central Walvis Ridge (SE Atlantic), *Paleoceanography*, *21*(3), PA3009.

Marr, J. P., J. A. Baker, L. Carter, A. S. R. Allan, G. B. Dunbar, and H. C. Bostock (2011), Ecological and temperature controls on Mg/Ca ratios of *Globigerina bulloides* from the southwest Pacific Ocean, *Paleoceanography*, *26*(2), PA2209.

Martinez, P., P. Bertrand, G. B. Shimmield, C. Karen, F. J. Jorissen, J. Foster, and M. Dignan (1999), Upwelling intensity and ocean productivity changes off Cape Blanc (northwest Africa) during the last 70,000 years: geochemical and micropalaeontological evidence, *Marine Geology*, *158*(1-4), 57-74.

Merkel, U., M. Prange, and M. Schulz (2010), ENSO variability and teleconnections during glacial climates, *Quaternary Science Reviews*, *29*(1-2), 86-100.

Meggers, H., M. Bergenthal, and C. participants (2002), Report of R/V *Poseidon* cruise POS 272, Las Palmas-Las Palmas, 1.4.-14.4.2001, *Berichte, Fachbereich Geowissenschaften*, *197*, 19.

Meggers, H., and cruise participants (2003), Report and preliminary results of METEOR Cruise M53/1, Limassol - Las Palmas - Mindelo, 30.03.2002 - 03.05.2002, *Berichte, Fachbereich Geowissenschaften, Universität Bremen*, *214*, 81.

McConnell, M. C., and R. C. Thunell (2005), Calibration of the planktonic foraminiferal Mg/Ca paleothermometer: Sediment trap results from the Guaymas Basin, Gulf of California, *Paleoceanography*, *20*, PA2016.

McKenna, V. S., and W. L. Prell (2004), Calibration of the Mg/Ca of *Globorotalia truncatulinoides* (R) for the reconstruction of marine temperature gradients, *Paleoceanography*, *19*(2), PA2006.

Mittelstaedt, E. (1983), The upwelling area off Northwest Africa - A description of phenomena related to coastal upwelling, *Progress In Oceanography*, *12*(3), 307-331.

Mohtadi, M., S. Steinke, J. Groeneveld, H. G. Fink, T. Rixen, D. Hebbeln, B. Donner, and B. Herunadi (2009), Low-latitude control on seasonal and interannual changes in planktonic foraminiferal flux and shell geochemistry off south Java: A sediment trap study, *Paleoceanography*, *24*., PA1201.

Mulitza, S., W. Dürkoop, W. Hale, and G. Wefer (1997), Planktonic foraminifera as recorders of past surface-water stratification, *Geology*, *24*(4), 335-338.

Mulitza, S., T. Wolff, J. Pätzold, W. Hale, and G. Wefer (1998), Temperature sensitivity of planktonic foraminifera and its influence on the oxygen isotope record, *Mar. Micropaleontol.*, *33*, 223-240.

Mulitza, S., B. Donner, G. Fischer, A. Paul, J. Pätzold, C. Rühlemann, and M. Segel (2004), The South Atlantic oxygen isotope record of planktic foraminifera, in *The South Atlantic in the Late Quarternary: Reconstruction of Material Budgets and Current Systems*, edited by G. Wefer, S. Mulitza and V. Ratmeyer, Springer, Berlin, pp. 121-142.

Narayan, N., A. Paul, S. Mulitza, and M. Schulz (2010), Trends in coastal upwelling insensity during the late 20th century, *Ocean Science*, *6*, 815-823.

Nürnberg, D., J. Bijma, and C. Hemleben (1996), Assessing the reliability of magnesium in foraminiferal calcite as a proxy for water mass temperatures, *Geochim. Cosmochim. Ac.*, *60*(5), 803-814.

Nykjær, L., and L. Van Camp (1994), Seasonal and interannual variability of coastal upwelling along northwest Africa and Portugal from 1981 to 1991, *J. Geophys. Res.*, *99*(C7), 14197-14207.

Okai, T., A. Suzuki, S. Terashima, M. Inoue, M. Nohara, H. Kawahata, and N. Imai (2004), Collaborative analysis of GSJ/AIST geochemical reference materials JCp-1 (Coral) and JCt-1 (Giant Clam), *Chikyukagaku*, *38*, 281-286.

Pastor, M. V., J. L. Pelegrí, A. Hernández-Guerra, J. Font, J. Salat, and M. Emelianov (2008), Water and nutrient fluxes off Northwest Africa, *Continental Shelf Research*, *28*(7), 915-936.

Pelegrí, J. L., J. Arístegui, L. Cana, M. González-Dávila, and A. Hernández-Guerra (2005), Coupling between the open ocean and the coastal upwelling region off northwest Africa: water recirculation and offshore pumping of organic matter, *J. Marine Syst.*, *54*, 3-37.

Pérez-Rodríguez, P., J. L. Pelegrí, and A. Marrero-Díaz (2001), Dynamical characteristics of the Cape Verde frontal zone, *Sci. Mar.*, *65*, 241-250.

Pierre, C., A. Vangriesheim, and E. Laube-Lenfant (1994), Variability of water masses and of organic production-regeneration systems as related to eutrophic, mesotropic and oligotrophic conditions in the northeast Atlantic Ocean, *J. Marine Syst.*, *5*(2), 159-170.

Reimer, P. J., et al. (2009), IntCal09 and Marine09 radiocarbon age calibration curves, 0 – 50,000 years cal BP, *Radiocarbon*, *51*(4), 1111-1150.

Rashid, H., and E. A. Boyle (2007), Mixed-Layer Deepening During Heinrich Events: A Multi-Planktonic Foraminiferal $\delta^{18}O$ Approach, *Science*, *318*(5849), 439-441.

Ravelo, A. C., R. G. Fairbanks, and S. G. H. Philander (1990), Reconstructing tropical Atlantic hydrography using planktonic foraminifera and an ocean model, *Paleoceanography*, *5*, 409-431.

Regenberg, M., S. Steph, D. Nürnberg, R. Tiedemann, and D. Garbe-Schönberg (2009), Calibrating Mg/Ca ratios of multiple planktonic foraminiferal species with $\delta^{18}O$-calcification temperatures: Paleothermometry for the upper water column, *Earth Planet. Sc. Lett.*, *278*(3-4), 324-336.

Romero, O. E., J.-H. Kim, and B. Donner (2008), Submillennial-to-millennial variability of diatom production off Mauritania, NW Africa, during the last glacial cycle, *Paleoceanography*, *23*, PA3218.

Rosenthal, Y., M. P. Field, and R. M. Sherrell (1999), Precise determination of element/calcium ratios in calcareous samples using sector field inductively coupled plasma mass spectrometry, *Analytical Chemistry*, *71*(15), 3248-3253.

Russell, A. D., and H. J. Spero (2000), Field Examination of the Oceanic Carbonate Ion Effect on Stable Isotopes in Planktonic Foraminifera, *Paleoceanography*, *15*(1), 43-52.

Sadekov, A., S. M. Eggins, P. De Deckker, and D. Kroon (2008), Uncertainties in seawater thermometry deriving from intratest and intertest Mg/Ca variability in Globigerinoides ruber, *Paleoceanography*, *23*(1), PA1215.

Sautter, L. R., and R. C. Thunell (1991), Seasonal Variability in the $\delta^{18}O$ and $\delta^{13}C$ of Planktonic Foraminifera from an Upwelling Environment: Sediment Trap Results from the San Pedro Basin, Southern California Bight, *Paleoceanography*, *6*(3), 307-334.

Sautter, L. R., and C. Sancetta (1992), Seasonal associations of phytoplankton and planktic foraminifera in an upwelling region and their contribution to the seafloor, *Marine Micropaleontology*, *18*(4), 263-278.

Schemainda, R., P. Nehring, and S. Schulz (1975), *Ozeanologische Untersuchungen zum Produktionspotential der nordwestafrikanischen Wasserauftriebsregion*, Nationalkomitee für Geodäsie und Geophysik bei der Akademie der Wissenschaften der Deutschen Demokratischen Republik, Berlin 88 pp.

Schmidt, G. A., G. R. Bigg, and E. J. Rohling (1999), Global Seawater Oxygen-18 Database, http://data.giss.nasa.gov/o18data/.

Shackleton, N. J. (1967), Oxygen isotopic analyses and Pleistocene temperatures re-assessed, *Nature*, *215*, 15-17.

Shackleton, N. J. (1974), Attainment of isotopic equilibrium between ocean water and the benthonic foraminifera genus *Uvigerina*: isotopic changes in the ocean during the last glacial, *Cent. Nat. Rech. Sci. Colloq. Int.*, *219*, 203-209.

Shapiro, S. S., and M. B. Wilk (1965), An analysis of variance test for normality (complete samples), *Biometrika*, *52*, 591-611.

She, J., J. L. Høyer, and J. Larsen (2007), Assessment of sea surface temperature observational networks in the Baltic Sea and North Sea, *J. Marine Syst.*, *65*(1-4), 314-335.

Siegel, D. A., T. C. Granata, A. F. Michaels, and T. D. Dickey (1990), Mesoscale eddy diffusion, particle sinking, and the interpretation of sediment trap data, *J. Geophys. Res.*, *95*(C4), 5305-5311.

Sicre, M.-A., Y. Ternois, M. Paterne, P. Martinez, and P. Bertrand (2001), Climatic changes in the upwelling region off Cap Blanc, NW Africa, over the last 70 kyear: a multi-biomarker approach, *Organic Geochemistry*, *32*(8), 981-990.

Spero, H. J., and D. F. Williams (1990), Evidence for Seasonal Low-Salinity Surface Waters in the Gulf of Mexico Over the Last 16,000 Years, *Paleoceanography*, *5*(6), 963-975.

Speth, P., H. Detlefsen, and H.-W. Sierts (1978), Meteorological influences on upwelling off Northwest Africa, *Dt. Hydrogr. Z.*, *31*(3), 98-104.

Spindler, M., C. Hemleben, U. Bayer, A. W. H. Bé, and O. R. Anderson (1979), Lunar periodicity of reproduction in the planktonic foraminifer *Hastigerina pelagica*, *Marine Ecology Progress Series*, *1*, 61-64.

Steph, S., M. Regenberg, R. Tiedemann, S. Mulitza, and D. Nürnberg (2009), Stable isotopes of planktonic foraminifera from tropical Atlantic/Caribbean coretops: Implications for reconstructing upper ocean stratification, *Mar. Micropaleontol.*, *71*, 1-19.

Stouffer, R. J., et al. (2006), Investigating the Causes of the Response of the Thermohaline Circulation to Past and Future Climate Changes, *Journal of Climate*, *19*(8), 1365-1387.

Stuiver, M., and P. J. Reimer (1993), Calib Rev. 6.1.0. Calib Radiocarbon Calibration Program *Radiocarbon*, *35*, 215-230.

Takahashi, K., and A. W. Bé (1984), Planktonic foraminifera: factors controlling sinking speeds, *Deep-Sea Res.*, *31*, 1477-1500.

Tang, C. M., and L. D. Stott (1993), Seasonal Salinity Changes during Mediterranean Sapropel Deposition 9000 Years B.P.: Evidence from Isotopic Analyses of Individual Planktonic Foraminifera, *Paleoceanography*, *8*(4), 473-493.

Tedesco, K., R. Thunell, Y. Astor, and F. Muller-Karger (2007), The oxygen isotope composition of planktonic foraminifera from the Cariaco Basin, Venezuela: Seasonal and interannual variations, *Mar. Micropaleontol.*, *62*(3), 180-193.

Thornalley, D. J. R., H. Elderfield, and I. N. McCave (2009), Holocene oscillations in temperature and salinity of the surface subpolar North Atlantic, *Nature*, *457*(7230), 711-714.

Thunell, R. C., W. B. Curry, and S. Honjo (1983), Seasonal variation in the flux of planktonic foraminifera: time series sediment trap results from the Panama Basin, *Earth Planet. Sc. Lett.*, *64*(1), 44-55.

Thunell, R., E. J. Tappa, C. Pride, and E. Kincaid (1999), Sea-surface temperature anomalies associated with the 1997–1998 El Niño recorded in the oxygen isotope composition of planktonic foraminifera, *Geology*, *27*(9), 843-846.

Tomczak, M., and J. S. Godfrey (1994), *Regional oceanography: An introduction*, Pergamon, Oxford, 422 pp.

van Raden, U. J., J. Groeneveld, M. Raitzsch, and M. Kucera (2011), Mg/Ca in the planktonic foraminifera *Globorotalia inflata* and *Globigerinoides bulloides* from Western

Mediterranean plankton tow and core top samples, *Marine Micropaleontology*, *78*(3-4), 101-112.

Waelbroeck, C., L. Labeyrie, E. Michel, J. C. Duplessy, J. F. McManus, K. Lambeck, E. Balbon, and M. Labracherie (2002), Sea-level and deep water temperature changes derived from benthic foraminifera isotopic records, *Quaternary Science Reviews*, *21*(1-3), 295-305.

Wang, L. (2000), Isotopic signals in two morphotypes of *Globigerinoides ruber* (white) from the South China Sea: implications for monsoon climate change during the last glacial cycle, *Palaeogeography, Palaeoclimatology, Palaeoecology*, *161*(3-4), 381-394.

Weichart, G. (1980), Chemical changes and primary production in upwelled water off Northwest Africa, *Ocean Dynamics*, *33*(5), 192-198-198.

Wilke, I., T. Bickert, and F. J. C. Peeters (2006), The influence of seawater carbonate ion concentration [CO_3^{2-}] on the stable carbon isotope composition of the planktic foraminifera species *Globorotalia inflata*, *Mar. Micropaleontol.*, *58*(4), 243-258.

Wilke, I., H. Meggers, and T. Bickert (2009), Depth habitats and seasonal distributions of recent planktic foraminifers in the Canary Islands region (29°N) based on oxygen isotopes, *Deep-Sea Res. Pt. 1*, *56*(1), 89-106.

Williams, D. F., A. W. H. Be, and R. G. Fairbanks (1979), Seasonal Oxygen Isotopic Variations in Living Planktonic Foraminifera off Bermuda, *Science*, *206*, 447-449.

Wit, J. C., G. J. Reichart, S. J. A Jung, and D. Kroon (2010), Approaches to unravel seasonality in sea surface temperatures using paired single-specimen foraminiferal $\delta^{18}O$ and Mg/Ca analyses, *Paleoceanography*, *25*(4), PA4220.

Yeager, S. G., C. A. Shields, W. G. Large, and J. J. Hack (2006), The low-resolution CCSM3, *J. Clim.*, *19*, 2545-2566.

Yu, J., H. Elderfield, Z. Jin, and L. Booth (2008), A strong temperature effect on U/Ca in planktonic foraminiferal carbonates, *Geochimica et Cosmochimica Acta*, *72*(20), 4988-5000.

Žarić, S., B. Donner, G. Fischer, S. Mulitza, and G. Wefer (2005), Sensitivity of planktic foraminifera to sea surface temperature and export production as derived from sediment trap data, *Mar. Micropaleontol.*, *55*(1-2), 75-105.

Zhao, M., G. Eglinton, S. K. Haslett, R. W. Jordan, M. Sarnthein, and Z. Zhang (2000), Marine and terrestrial biomarker records for the last 35,000 years at ODP site 658C off NW Africa, *Organic Geochemistry*, *31*(9), 919-930.